Mid-air Deployment Safety Assessment Method for a Morphing UAV

Muhammad Ridho Said

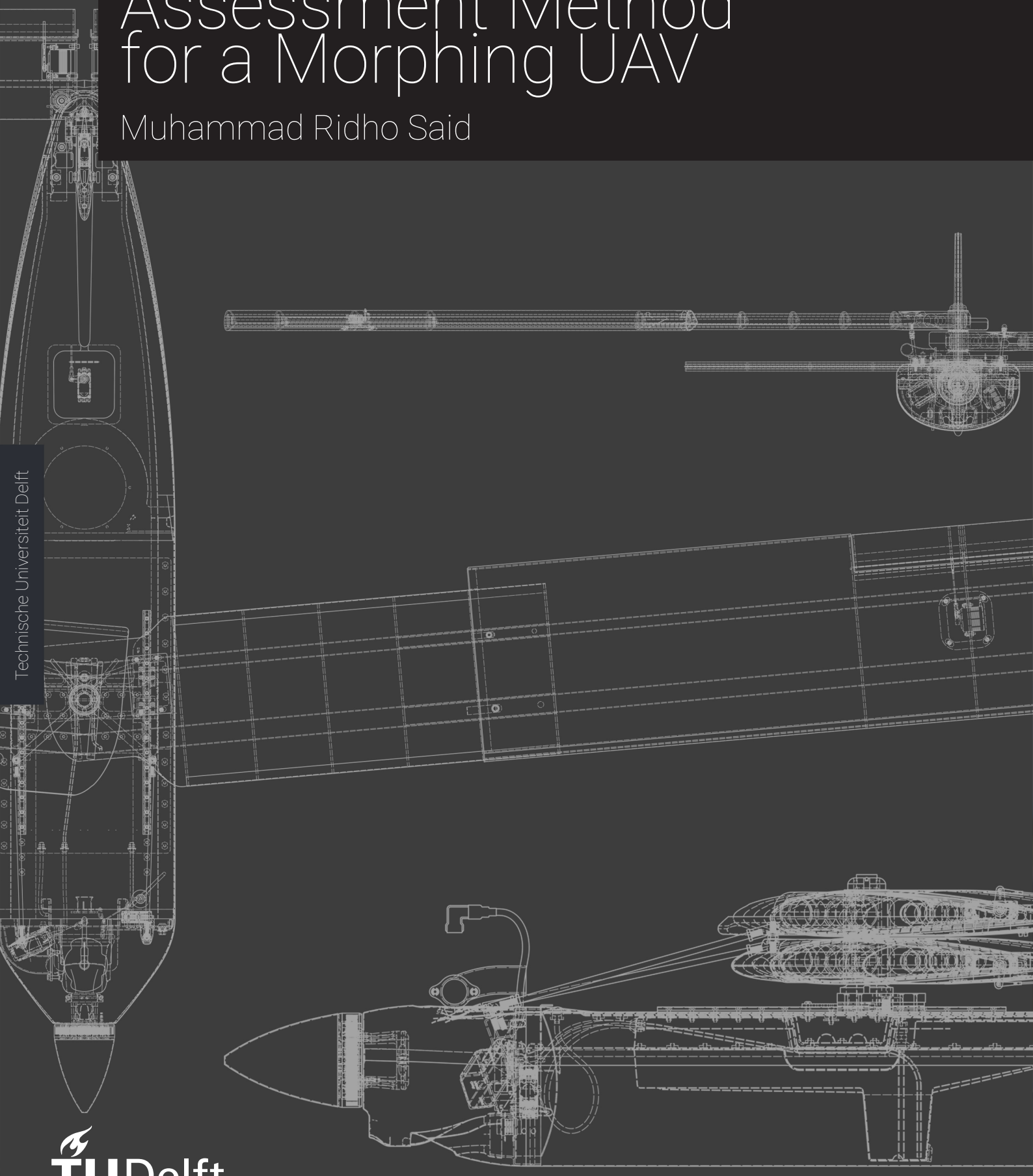

Technische Universiteit Delft

TU Delft

Mid-air Deployment Safety Assessment Method for a Morphing UAV

by

Muhammad Ridho Said

to obtain the degree of Master of Science

at the Delft University of Technology,

to be defended publicly on Thursday November 29, 2018 at 14:30.

Student number:	4616197	
Project duration:	December 1, 2017 – October 31, 2018	
Thesis committee:	Dr. ir. M. Voskuijl ,	TU Delft, supervisor
	Prof. dr. ir. L. L. M. Veldhuis ,	TU Delft, chairman
	Dr.ir. S. Hartjes,	TU Delft

This thesis is confidential and cannot be made public until December 31, 2022.

TU Delft

Acknowledgements

What a wonderful year it has been! Beginning in November of 2017, I approached Mark and asked him about the possibility of doing a thesis with UAVs. Along with other projects, he proposed the project of an analysis of the deployment of a morphing UAV, which caught my eye and I decided to adopt as my graduation project. It has been an honor to be a part of the team involved in working with the Dash-X aircraft. Although facing some hurdles on the way, the project is finally completed in the end and I am proud to be able to present my work in front of the graduation committee. This report thus marks the end of a phase in my life, a phase which I will never forget, a phase where I have learned a lot both in my work life and my private life.

This thesis would not be complete without the support of various individuals with whom I stayed in contact and exchange information. First and foremost, I would like to thank my thesis supervisor, Prof.dr.ir. Mark Voskuijl, who has been of great assistance in the times I am up and the times I am down during the completion of this thesis project. His guidance and support plays a big role in my work and how I am able to complete it. I also would like to thank Jessie as my contact person in the University of South Carolina, whom I frequently contacted when I have problems regarding the project. In addition to that, I also would like to thank Blin Richards as a representative of VX Aerospace, the company who help build and fly the Dash-X aircraft, for supporting me with information regarding the aircraft. All of your support will not be forgotten.

I also would like to thank my family, whom I have not met for two and a half years and whose indirect support has brought me to the level I am in right now. Thank you to my father Said Abubakar Hassan, my mother Seha Habiba and my two brothers Esaam Hassan and Mazen Hassan.

My life in Delft will not be completed if it wasn't for my friends and families here. To my dearest friends of the Flight Performance & Propulsion track, I thank you for being the friends I need in my most desperate times. We have together experienced the sweetness and bitterness of the master student life of the faculty of aerospace of the TU Delft. This journey has shaped me and make me stronger. I hope it also does to you all.

To my beloved friends Indonesian student friends here in Delft whom I cannot state their names one by one, I thank you for all the support that you gave me both intentionally and unintentionally. My life in Delft wouldn't be the same without you all.

To Uswatun Hasanah, my life companion. Special thanks to you for lifting me up when I am down and giving color to the final phases of my life in Delft. Whether you know it or not, your existence in my life has been of great importance and impact in shaping me to be the person I am right now. I am tremendously grateful to have you by my side as I face and struggle through this phase in life.

In the end, I also would like to thank LPDP for granting me the scholarship to finance my studies and life here in Delft. This experience has been an unforgettable one and one which is not possible without your support.

Muhammad Ridho Said
Delft, November 2018

Abstract

Deployable morphing aircraft are gaining popularity in the academic and industrial world. Their deployability offer the possibility to be stored and takes less space. This is advantageous in volume limited applications like space explorations, where every cubic centimeter is important. Another field where this aircraft is increasingly used is the military field. Deploying it in the battlefield directly from a carrier aircraft opens endless possibility to the operation of such aircraft. However, mid-air deployment is subjected to several internal and external factors that could lead to the failure of the deployment.

In this study, a method to assess the safety of deployment of a deployable morphing UAV is constructed. To do this, an aircraft test case is taken and a corresponding model of the aircraft is made using the Multibody dynamics approach. This model is then verified and validated by two different methods. First, a comparison of the stability derivatives of the created model and an off-the-shelf aerodynamic solver is performed. Secondly, the response of the created model is compared with actual flight test data, where the test case aircraft performs a maneuver. For both validation methods used in this study, the created model is able to resemble the output from the off-the-shelf aerodynamic solver and the flight test data. The validated model is then used as to test the method developed in this study.

The method developed starts with the definition of a safe deployment of a deployable morphing aircraft, where three different safety concerns are considered. The definition of a safe deployment also helps in deriving different categories of deployment which includes safe and various unsafe deployment depending on what causes the deployment to be unsafe. This method is tested on two different deployment scenarios.

By using the method developed in this study, safety deployment spaces are constructed from the range of input parameters determined for the two different scenarios. It is revealed from this safety deployment space what combination of input parameters is favorable for a safe deployment, and what causes the different unsafe deployments. Unsafe deployments are also categorized to understand which of the safety concern causes the deployment to be unsafe.

Contents

List of Figures

List of Tables

List of Symbols

Symbols

α	Angle of Attack	kgm^2
α	Angle of Attack	deg
β	Sideslip angle	deg
δ_a	Aileron Deflection	deg
δ_e	Elevator Deflection	deg
δ_r	Rudder Deflection	deg
ϕ	Roll attitude	deg
ψ	Yaw attitude	deg
ρ	Air density	kg/m^3
τ	Moment experienced by body	Nm
θ	Pitch attitude	deg
b	Wingspan	m
b_{strip}	Strip Width	m
c	Chord length	m
c_D	Drag coefficient	-
c_L	Lift coefficient	-
c_l	Roll Moment coefficient	-
c_m	Pitch Moment coefficient	-
c_n	Yaw Moment coefficient	-
D	Drag Force	N
h	Aircraft altitude	m
I	Body inertia	kgm^2
K_a	Aileron Gain	-
K_e	Elevator Gain	-
K_r	Rudder Gain	-
L	Lift Force	N
l_h	Distance between main wing & horizontal tail aerodynamic centres	m
l_v	Distance between main wing & vertical tail aerodynamic centres	m

l_a	Fuselage aft section length	m
l_f	Fuselage forward section length	m
m	Aircraft total mass	kg
M_∞	Freestream Mach number	-
n	Load Factor	-
p	Roll rate	deg/s
q	Pitch rate	deg/s
r	Yaw rate	deg/s
Re	Reynolds Number	-
V_{NE}	Aircraft never exceed speed	m/s
x_m	Fuselage midpoint distance from nose tip	m
X_{ref}	Distance between aircraft centre of gravity to wind-tunnel measurement point	m

Subscripts

0	Initial Values
FT	Flight Test Data
HT	Horizontal Tail
max	Maximum allowable value
min	Minimum allowable value
$Model$	Data Obtained from Model Results
MW	Main Wing
$oper$	Design operational value
t	Trimmed control surface deflection angles
VT	Vertical Tail

1 Introduction

1.1. Background

The development of morphing aircraft has seen a sharp increase in the past few decades. The current trend suggest that there is room to improve with regard to aircraft size, flying range and flight performance envelope [2]. The ability of changing a large portion of the aircraft's geometry has been proven to benefit users in a lot of ways. Flight envelopes, which are generally treated as the operation limits of an aircraft, can be potentially extended due to morphing technologies [3]. Unlike the conventional way of thinking that an aircraft is created for a specific purpose/role only, now a single aircraft can have multiple roles and performs different missions due to its airframe being reconfigurable. This technology is also useful to reduce the storage capacity or the overall mass of an aircraft [4]. When not operating, the aircraft can be contained in a smaller space and stored and later be deployed when needed. In particular UAV designers are fond of utilizing morphing technology to further reduce the size of the already small aircraft that they created. In such cases, morphing is not used to extend the flight envelope, but rather to trim the amount of space the aircraft takes when unused.

Either by varying their sweep angle, dihedral angle, sectional airfoil camber, wing twist, or by even using inflatable structures, all morphing aircraft can be said to have at least two configurations. This statement is also true for morphing aircraft which are only used to reduce storage spaces, since they have a configuration before operation and another during operation. This means that all morphing aircraft undergo a certain transformation. When a morphing aircraft is not undergoing any transformation, the manoeuvres that it performs can easily be analyzed by treating the aircraft as a single rigid body [5]. However, the interesting part of morphing aircraft is its dynamics when transforming from one configuration to another and this analysis cannot be performed by the method above. Here, multiple factors contribute to the dynamics of the aircraft and all of them needs to be addressed simultaneously since the changes in parameters are interrelated. For example during wing morphing, a shape change in the wing causes a change in the aerodynamics forces which again could cause a deformation in the structure, therefore again changing the shape of the wing.

Emerging as a new and promising technology, currently morphing aircraft have been used mostly in two very demanding fields, space exploration and the military. The challenges in both fields requires designers and engineers to turn their heads and look for out-of-the box concepts that can only be provided by reconfiguring the aircraft. In the field of space exploration, a concept for a Mars exploration aircraft was proposed to bridge between the low resolution but wide coverage data from Mars satellites and high resolution but narrow coverage data of the Mars rovers [6]. This is the idea behind the Mars ARES (Aerial Regional-scale Environmental Survey) aircraft and the concept was to transport a capsule containing the folded aircraft to Mars atmosphere, reduce the speed of the capsule inside Mars atmosphere by means of a parachute, and release the aircraft mid-air so that the aircraft can unfold itself and directly operate [7]. However, the Mars ARES aircraft project was not favoured over the MAVEN satellite project by NASA [8]. Other than using morphing aircraft technologies to increase the compactness of an aircraft during transportation, hypersonic re-entry

vehicles have also tried to utilize morphing aircraft technology to increase overall lift-to-drag ratio during descend in Earth's atmosphere. This is highly beneficial as compactness during re-entry is desired but during descend, a relatively high lift-to-drag ratio is preferred to accommodate the aircraft to fly slowly for the landing approach [9].

Similar to the field of space exploration, the military has also been experimenting with morphing aircraft technologies for a while now. Two of the most distinct implementation of morphing aircraft technologies can be seen in the Bell Boeing V-22 Osprey tiltrotor or the variable-sweep wing of the General Dynamics F-111 Aardvark aircraft. However, these aircraft are manned, and with the recent trend of unmanned aerial systems, the military is also looking for possibilities of incorporating morphing technologies to unmanned aircraft designs. Unmanned aircraft are generally, but not necessarily, small in size and are used for either reconnaissance or to perform attacks on the battlefield. Since they are unmanned, UAVs are more expandable and they are not bounded by the pilot's physical and mental limitations that a manned aircraft is limited to. Thus, more radical designs are possible and wild transformations can be implemented. Several examples have been proposed and are currently under development to test the feasibility of morphing UAVs, some of which are intended to be deployed in hostile zones by first transporting the UAVs in carrier aircraft. An example of this type of UAV is the DARPA's ambitious Gremlin program [10], in which the aircraft designed will be deployed from a C-130 aircraft and, after performing their mission, can autonomously return to the carrier aircraft and dock back for further missions. Another example is the Dash-X aircraft which has high morphing rates and multiple morphing control surfaces.

Deployable morphing aircraft which are to be launched from carrier aircraft can be deployed in various ways. No matter how different the deployment scheme is, there is still so much to investigate regarding the dynamics of the aircraft during and after deployment. This is because different parameters of the deployment may lead to different results of how the deployment will pan out. The dynamics of these aircraft are interesting as they are unorthodox compared to conventional aircraft. Such an aircraft is also subjected to sudden forces during transformation, since their deployments are generally quick to allow the aircraft to be operational as soon as possible. But this also implies that the high morphing rates during the unfolding process of the aircraft may influence the success of the deployment itself. And bearing in mind the field that these aircraft are being used, there should not be any room for errors. Hence, a certainty that a deployment is successfully performed and that it leads to a controllable flight is necessary. This means that the morphing process needs to be quantified and analyzed properly before allowing the aircraft to be operated in the field.

To do this, a study that focuses on analyzing the safety of a deployable morphing aircraft needs to be conducted. The study should be able to quantify which parameters are influential in the deployment of morphing aircraft and what different causes might impact the different results in both successful and fail deployment. Classification on different safety deployment types will also needs to be made, which can later be used as a reference for further studies. The method developed here should also not only be limited to a specific deployment scheme, but should be universal enough to be used on various deployment schemes. Thus, a review should also be made to correctly select and define the scenarios of deployment schemes to be assessed with the method. This study will also allow designers and engineers to be more aware of the flight dynamic limitations of a morphing aircraft and can help them test morphing aircraft designs before production.

1.2. Research Scope & Objectives

1.2.1. Research Scope

Deployable UAVs are seen as smart solutions in two main fields, which are space exploration and the military field. Its ability to be folded to reduce storage space opens a whole new spectrum of possibilities. In the current market, various deployment schemes are available and the extent to which these schemes can be modeled are limitless. In this research however, to limit the scope, the phases of deployment being considered focuses only from the time the aircraft starts to unfolds itself, until the time the aircraft is fully unfolded and is able to control itself. This applies to all the deployment schemes considered in this research.

The methodology selected for this research considering available time and expense as well as safety is numer-

ical. First, a test case will be selected and a corresponding model of the aircraft will be created. The decision of using a test case here is to give the possibility to later validate the created model with available data and make sure that the model actually represents the dynamics of a real aircraft. The validated model will then be simulated in different deployment scenarios to check the behaviour of the aircraft when different deployment parameters are used in a deployment scheme. The selection of the various schemes will be performed with the help of a literature review.

For this research, the test case selected is the Dash-X aircraft, further explained in Chapter 3. At the time this report was formulated, the first phase of the project has been completed. This phase includes the design and construction of the aircraft. Flight tests of the aircraft have also been done to check its stability. However, this tests does not include the deployment scheme, and is solely performed to check the performance of the aircraft itself. The deployment comes in phase 2 of the project, and this is where this research comes in. Before conducting experiments on the deployment and performing flight tests, this study is conducted to give an overview of the allowable combination of deployment parameters which will result in a controllable flight. The research here can also serve as a basis to select the deployment velocity, altitude, attitudes, etc. used for the later flight tests, which will include the deployment of the aircraft.

1.2.2. Assumptions & Limitations

As with any other researches, this research has some limitations on its own, which are mainly caused by the assumptions made in the model creation and execution of the deployment safety assessment. Below are a few assumptions made that indirectly limits the scope of this research:

1. The lifting surfaces of the aircraft is considered to be rigid and not flexible during and after the deployment.
2. Each lifting surface of the model is divided into a finite number of strips with a uniform distribution.
3. The relationship between the additional lift and the control surface deflection angle is linear, and is based on empirical data [11, 12].
4. The engine of the aircraft is represented by a point force.
5. Deployment actuator dynamics is not considered.
6. The deployment sequence of the lifting surfaces of the aircraft is predefined and not varied in this research.
7. Aerodynamic interaction between lifting surfaces are not considered in the created model.
8. Aircraft weight reduction due to the burning of fuel is neglected.
9. Simulation is run with the aircraft at maximum payload.

1.2.3. Research Objective & Questions

Reflecting on the research background and the necessary work to be done, the research objective here is **to develop a method to assess the safety of deployment of a deployable morphing aircraft by testing a validated model of a deployable morphing aircraft with varying deployment parameters in different deployment schemes.**

Following the research objective, several research question can be derived as follows:

1. What is the definition of a safe deployment of a deployable aircraft?
2. What different possible deployment results might appear from a deployment of a deployable aircraft?
3. Which input parameters are most/least critical to the safety of deployment?
4. For the case considered here, within what boundaries will the deployment of the aircraft result in a safe deployment?

1.3. Outline

This study starts with Chapter 1, which explains the background of the research as well as the definition of the research scope and objectives. Then a chapter regarding the literature review follows, where the writer explains the different important aspects of the research and what other researchers have been doing in the same or similar field. The proceeding chapter introduces the test case used for this research, along with the aircraft's specifications and intended deployment scheme. Next comes the chapters that focuses on the three main parts of the study, namely: model creation, model validation and deployment assessment. Each parts is represented with Chapter 4, 5 and 6. After presenting the methods and ways to perform the study, results of the studies are shown in Chapter 7 and finally, conclusions are drawn in Chapter 8.

2

Literature Review

In this section, the literature review performed as a prerequisite before starting this research is presented. Here, a recapitulation of similar and contributing research done by other researchers is first shown, and the chapter is concluded with a synthesis section, which describes the tools and methods selected in this research and its reasons. The 4 main aspects investigated through a literature study here are the morphing aircraft modeling, the aerodynamic model suitable for representing the aerodynamics of the morphing aircraft and validating the created aircraft model, the various deployment schemes used in similar deployment cases, and the method of assessing the safety of deployment.

2.1. Morphing Aircraft Modeling

Unlike a conventional aircraft, the configuration of a morphing aircraft experiences major shape change for a specific purpose. This means that a morphing aircraft cannot be regarded as a single rigid body floating in space [13**?** –15]. Generally, a morphing aircraft has multiple major components that are stowed prior to operation. For the case considered here, an important difference between the Dash-X aircraft and most morphing aircraft research found in the literature is that the Dash-X aircraft utilizes both rotational & telescopic wing deployment to unfold its lifting surfaces (main wing, vertical & horizontal tail). This is a big challenge as the modelling is not only specific to one component, but to several components that may also interact during the deployment. And unlike most deployable aircraft that deploys only the main wings, the Dash-X aircraft has to deploy all of its lifting surfaces. This is also problematic because for most deployable wing aircraft, the vertical and horizontal tail are used for counteracting the sudden forces and moment generated during the wing deployment.

Due to that, new concepts of modelling the aircraft is needed. Santoni & Gasbarri[16] investigated the case of a deployable wing aircraft to support human landing on Mars and their focus was on the pull-up manoeuvre after deployment of the aircraft in Martian atmosphere . Their method here is to derive equations of motion of the aircraft and incorporating the swing-wing equations into it. With it, they created a cost function which is related with the load factor of the aircraft, and optimized it. The aim here is to find the set of parameters which result in the lowest possible load factor generated at the end of the pull-up manoeuvre. Hence, the focus is at the end of the manoeuvre and any excessive load factor during the manoeuvre is not considered. Here, the modelling is done by an analytic approach and optimizing the cost function created. However, their research only considers the translational motion of the aircraft (angle of attack is assumed to be preserved during pull-up) and the parameters being optimized only takes into account the time-frame between deployment to steady level flight.

Kuchta et al.[9] took a different approach and tested models of multiple re-entry vehicles which transform to increase overall lift-to-drag ratio inside a static subsonic wind tunnel. They then uses this experimental data to estimate the dynamic stability of the vehicles and also run a piloted computer simulation to come up

with the stability & performance analysis of different morphing re-entry vehicles. With their method, they are able to observe that one of the aircraft experienced a pitch up moment during forward sweep motion. This moment combined with a large increase in lift causes a flight path disturbance of considerable magnitude which persists for several minutes due to it being lightly damped.

An et al.[13, 15] investigates the dynamic response of aircraft to variable sweep geometry in different morphing rates. Both forward sweep motion and also backward sweep motion is investigated here. They defined the relation between sweep angle change and the change of the aircraft aerodynamic characteristics by a hysteresis basis. This means that the aerodynamic characteristics and aircraft responses is based on the time history of the corresponding aircraft parameters. The investigation concludes that higher morphing rates causes the dynamic response of the aircraft to settle longer. The response of the aircraft investigated is also sensitive to sweep change rate and therefore the need for an autopilot is inevitable to make adjustments in different sweep change rates. The research also underlines that the backward shift in centre of gravity due to the change in wing position improves the aerodynamic characteristics of the aircraft.

Different to the researches above, Prabhakar et al.[16–18] initially computes the static stability derivatives of a variable span, variable sweep aircraft by generating multiple meshes of the aircraft's step-by-step sweep and span change and simulating it in a medium fidelity off-the-shelf aerodynamic analysis tool. The solver used here is called SURFACES, which is Vortex Lattice Method based solver developed by Flight Level Engineering [19]. They then create a function which correlates the aerodynamic derivatives of the aircraft with the aircraft's span and/or sweep change. However, this means that the data obtained is only a function of the position of the wing, and not a function of deployment rate of the wing. Once the aerodynamic values for different morphing configurations have been obtained, it is used along the dynamic modelling tool to predict the response of the aircraft during morphing. The aircraft is both simulated in an open and closed loop manner and the aircraft stability is determined by checking the root locus plots of the system. The research also incorporates the development of a controller to regulate the transient response due to morphing.

Niksch et al.[20] focuses on the creation of a simulation tool which is able to simulate a flying wing, where the morphing degrees of freedom can be selected from the various set provided. The morphing degrees of freedom here includes the span, dihedral, sweep, twist, and even the airfoil's camber, thickness, etc. Modelling the aircraft is done by deriving the equation of motions of the aircraft, which incorporates different morphing parameters. The aircraft is assumed to be a point mass object, where forces and moments are imposed upon and the along with the aircraft's mechanical properties, the aircraft's response can be calculated. These forces includes the aerodynamic forces, the propulsion forces as well as the body forces (gravitational). Unlike the method used in other papers, in this paper the changes in forces distribution due to morphing is calculated in the aerodynamic model, which is the emphasis of the work. This allows more allocation of computational power to the aerodynamic section of the solver, since the dynamic model only calculates the equation of motion of a point mass object.

Another team of researchers that have published extensive research that focuses on modeling and analyzing the dynamics of deployable wing aircraft is Fujita et al. The team adopted Multibody dynamics to both easily model different components of the aircraft and assign relationship between them. Although their research case is the deployment of a Mars aircraft, the sequence and method of deploying is similar to the Dash-X aircraft with an exception on the morphing method being an out-of-plane morphing. Their papers started with a parametric study of a deployable wing aircraft for Mars, where they ended up with a design of the aircraft [21]. Then continued with an analysis of the dynamics of the folded-wing aircraft during deployment. Here they noticed that a pitching moment is generated during the out-of plane wing deployment and causes either a positive or negative pitching to the aircraft depending on the deployment angle [22]. Later on, the research continued with the development of an analysis method to quantify the most sensitive/critical parameter during the deployment of the aircraft [6]. Successful deployment criteria are initially defined and the simulation takes the time-frame between the nose-dive motion of the aircraft and the time when the aircraft reaches a positive flight path angle value into account.

After being able to determine which parameter is most sensitive during the deployment of the folded-wing aircraft, the research by Fujita et al. focuses on investigating the robustness of the deployment [5]. The two sensitive parameters considered here is the wing unfolding torque and the difference in deployment time between the right and the left wing. Here, the interaction of flows between bodies are ignored and the method

used to compute the robustness level is a modified sensitivity analysis, which based its deployment assessment on the six-sigma principle. The deployment variables are monitored throughout the simulation and compared with the allowable limits prescribed before. Then the margin between these variables with its limits is calculated and from this, a sigma value which acts as a form of confidence rating is calculated for the variable for that specific run. Multiple simulation is run by varying the drop velocity, surrounding gust, initial pitch angle and the deployment height of the deployment. This investigation also is directly followed by the research to minimize the amount of actuator torque needed to fully deploy the wing by varying the wing folding axis in both the pitch and the yaw direction [23, 24].

Other than Fujita et al., Multibody dynamics is also quite popularly used by other researchers in this field. **Yue et al.** utilizes it as the basis for modelling of their morphing aircraft. In their research, a clear division is made between the dynamic response during and after morphing of a tailless aircraft with an out of plane morphing. The investigation concludes that higher morphing rates causes more violent oscillation of the parameters observed and the dynamic response of the parameters did not deteriorate. Tong & Ji[25] also modelled their aircraft with Multibody dynamics to investigate the possibility of using asymmetric variable sweep for roll control. They used Kane's method and deriving equations of motion of the aircraft. However, the research neglects the shift in centre of gravity of the system and the coupling effect of roll and yaw is also not considered.

Pons & Cirak[26] created a simulation model that effectively model a 3-parameter morphing aircraft (dihedral, incidence angle and sweep) . Multibody dynamics is also used to model the motion of the aircraft. The research also incorporates the Goman-Khabrov stall model[27] to accommodate for the 360 degree movement capability of the incidence angle. Finally, to demonstrate that the aircraft is capable of multiple manoeuvres, the aircraft is simulated to do multiple profiles including the Pogachev's cobra.

Shi & Wan[14] investigated the flight dynamics of a large-scale morphing aircraft. On the contrary to most researchers that uses Multibody dynamics, their method is to relax the rigidity by making the centre of gravity and inertia functions of the morphing parameters. The case being evaluated here is a morphing aircraft that have multiple configurations, including high-lift, cruise, climb, loiter and high-speed manoeuvre. Nonetheless, the simulation only evaluates longitudinal dynamics of the aircraft. In a way, it can be said that Shi & Wan took the opposite approach from Niksch et al[20], who in their work, instead of varying the aircraft mechanical properties, updates the aerodynamic calculation during morphing.

Samareh et al. developed a quick analysis integrated tool that incorporates the aerodynamics, structural and dynamics of a morphing aircraft [28]. Their methodology is to use off-the-shelf tools for the aerodynamics, dynamics and the structural analysis tools, and make it loosely coupled so that it can be easily improved and interchanged. For the aerodynamics, the potential flow aerodynamic code CMARC[29] program is used. Virtual Lab & DYMORE [30] (Finite-element-based tool to analyze non-linear Multibody systems) are used for the dynamic analysis. The analysis starts with the parameterization of the wing shape and later connecting the different analysis tools together in a single framework. Here, Multibody dynamics is used to compute the dynamics of the aircraft and a finite element method is used to compute the amount of deformation and forces distribution in the aircraft's structure. During evaluation of the tool with 3 different morphing flying wing aircraft, the morphing rate is taken to be much lower than the flow of the air around the aircraft.

An investigation on the aerodynamics forces generated during span extension is investigated by Fincham et al. [31]. The main focus of the the paper is to analyze the axial forces generated during span extension and whether or not it is possible to use it for a quick actuated roll control. The investigation is performed by using AVL[**?**], which is a vortex lattice method based solver, & OpenFoam[**?**], an open source CFD software where RANS calculations is possible to be performed. Both medium and high fidelity aerodynamic analysis tools are used here to see the impact of the high-rate span extending wings on the aircraft, which is shown to be negligible as compared to the lift & drag forces produced by the wing.

2.2. Aerodynamic Model

For a deployable aircraft which has to deploy its lifting surfaces as soon as possible, the aerodynamics of the aircraft needs to be evaluated differently from an aircraft at a steady level flight. A deployable aircraft under-

goes unfolding at mid air and during this short but critical time, the aircraft can experience sudden moments and forces which may lead the aircraft to an uncontrollable state. Thus, the modelling of the aerodynamics is critical as this will determine whether or not the transient effects of the aerodynamics are considered and whether or not the forces generated are in the right value, times, and magnitude.

In the literature found, there are a lot of researchers that uses the quasi-steady assumption for the aerodynamics of the lifting surfaces [14], and for most of it, the assumption is justified by the low morphing rate of the wings. In some cases, even steady aerodynamic models are also used with the assumption that the wing morphs slower compared to the flow of air running over the wing [28**?**]. As demonstrated by Fincham et al. by using a high-fidelity unsteady RANS aerodynamic analysis tool, there exist transient behaviour of the aerodynamic forces at high morphing rates (deployment time : 0.875s). The case investigated here is the span extension and it is observed that the aerodynamic forces generated took some time before reaching a steady-state. It is also concluded here that the force in the span-wise direction is negligible compared to the lift and drag forces, and thus implementing high speed actuators to extend the span of the wings is possible. Another research team that uses a high-fidelity unsteady aerodynamic analysis tool are Han et al, who also stated that quasi-steady model undermines the forces generated [32]. In their research the team stated that there is a significant difference between the forces during forward sweeping and backward sweeping motion.

Important to bear in mind is that to model the aerodynamics, the lifting surfaces needed to be finitely divided into strips/panels. Pons & Cirak[26] did this by incorporating the Goman-Khabrov dynamic stall model[27] into the generalized blade element model in their 3-parameter morphing wing aircraft. The blade element model used divides the main wing of the aircraft into several panels and for an efficient division of the lifting surfaces. Niksch et al. also explained the division of the lifting surface in their paper [20]. Cosine spacing of the lifting surface division is implemented to increase the effectiveness of the surface division. As the flow is more dynamic at the wing root and tip, more panels are placed at these positions. The research utilizes potential flow elements (constant strength source doublet) and validates the result of this method with an existing software (TRANS3DNS) that was home-built. The model assumes that the flow is inviscid and incompressible (aircraft flying slower than Mach 0.3) and therefore, to get the profile drag forces, DATCOM is used. In a technical report by W.J. Vink[33] which focuses on the evaluation of strip theory and doublet-lattice aerodynamics, it is concluded that the plunge mode aerodynamic lift distribution of both methods outputs very little difference in result at low frequencies. However, the results are significantly different at high frequencies. The strip theory method here has been supplemented by a representation for unsteady aerodynamic effects in the form of Theodorsen (Wagner) and Sears (Küssner) functions. These comparisons are done in symmetrical conditions with a Fokker 100-like aircraft model with rigid & flexible wings.

Other researchers also tried different methods to model the aerodynamics of the morphing aircraft. An et al. self derived the unsteady aerodynamics equation based on the distribution of the unsteady vortex rings on the lifting surfaces of the aircraft [13, 15]. Fujita et al. uses experiment data of a flat plate and treated the lifting surfaces of the aircraft as flat plates [5, 6, 21–24, 34]. This method is also efficient and computationally inexpensive. Kuchta et al. estimates the dynamic stability derivatives from subsonic wind tunnel data of the aircraft. Vortex Lattice method is also used by several researchers to compute the aerodynamic characteristics of their morphing aircraft cases [17, 18].

However, as the emphasis of this research is on testing the proposed method to evaluate the safety of deployment of a morphing aircraft, the selection of the aerodynamic model here is mainly backed by its simplicity, easiness to incorporate and its low computational power & time requirement. This is essential as the flight dynamics model created will be used in multiple cases and run thousands of times. Thus a selection of a simple aerodynamic model that sufficiently represents the response of the aircraft is highly preferred than the selection of a sophisticated model that accurately predicts the aerodynamic behaviour of the aircraft but requires a lot of computing power. In other words, a low fidelity aerodynamic solver is favored than a high fidelity one.

A comparison will also be made here between the performance of the aerodynamic model selected for the model and the performance of the morphing UAV, modeled in a different aerodynamic solver. This comparison will serve as a validation of the aerodynamic model selected. However, it is difficult and time consuming if the validation process is to be done by comparing the dynamic parameters of the aircraft during its deployment. Hence, the decision is to compare the flight dynamics properties of the aircraft during steady level

flight. This decision is also made considering not all solvers are able to evaluate a morphing aircraft during its morphing process. In other words, not all solvers is able to calculate the transient effects of the morphing by means of a dynamic mesh. Unlike the method used by Prabhakar et al [17, 18], which evaluates the dynamic properties of the aircraft for every timestep of morphing statically, in this research the comparison will be done to show that the model here is representative enough of the real aircraft.

In the market right now, there exist several off-the-shelf aerodynamic solvers which can be selected and used for the validation process. Some of the solvers are listed below:

ANSYS Fluent[1] is a Computational Fluid Dynamics (CFD) tool that is capable of simulating various fluid flow problems, with various fluid models available. To use the software, a mesh needs to be created which will define the space by which the flow problem is going to be simulated. Then, boundary conditions and fluid model will need to be specified before running the software. Generally, taking into account that the fluid flow model used is appropriate for the problem, results from CFDs are accurate but computationally expensive. This is the trade off that will needs to be made when using a CFD tool assess the dynamics of an aircraft. Other CFD tool that are also available in the market includes OpenFoam[2], which is an open source CFD tool with a lot of open source backing from its community.

Athena Vortex Lattice[3] (AVL) is a vortex lattice method based solver which is able to calculate aerodynamic forces as well as static & dynamic stability derivatives as well as control derivatives of the aircraft evaluated. The solver is considered to use little computational power, though this depends highly on the panel density in the aircraft case file. It is also a windows-command-prompt-based software and thus is very easy to integrate with general mathematical solver such as MATLAB.

Digital DATCOM[4] is an USAF program which in essence is a database of empirical data of various aircraft configurations. The program calculates static stability, high lift & control, and dynamic derivatives of various aircraft configurations. Since the validation of the flight dynamics of the UAV considered here will only be evaluated after it is fully deployed, DATCOM could be an option. This is because after it has unfolded, the UAV generally has a conventional shape and could be its flight dynamics properties could be predicted with an empirical database like DATCOM.

2.3. Deployment Schemes

To show that the method proposed in this research is not specific to one case only, several other deployment schemes are considered to be simulated. Here, the literature review focuses on the available deployment schemes of other morphing deployable UAVs, which are frequently used.

ALTIUS[5] (Air-Launched, Tube Integrated, Unmanned Systmes) as a project by Area-I, is a high endurance airframe that is initially stored and launched from the Air Force's Common Launch Tube. Its main purpose is to conduct Information, Surveillance and Reconnaissance missions. The deployment of the the aircraft is similar to the Dash-X aircraft, but is different in one way. The carrier aircraft here is a rotorcraft which carries the UAV to mid-air, where it will be deployed. However, since the UAV is deployed from a rotorcraft which flies in a low altitude, the UAV will need to be launched and not dropped from the carrier aircraft [35]. Thus, the UAV here will experience an initial launch velocity during its discharge from the carrier aircraft.

A study by Hurst et al. [36] which focuses on the design, testing and analysis of a canister-launched mini UAV shows a UAV which has a deployment scheme that is very similar to the Dash-X aircraft. Only the main wings are initially stowed but the vertical and horizontal tail are not.

DARPA (Defense Advanced Research Project Agency) is also involved in the business of developing deployable UAVs. Called project Gremlins [10], the reusable morphing aircraft used here is a deployable morphing

[1] https://www.ansys.com/products/fluids/ansys-fluent
[2] https://www.openfoam.com/
[3] http://web.mit.edu/drela/Public/web/avl/
[4] http://www.pdas.com/datcom.html
[5] https://areai.aero/aircraft/altius-air-launched-tube-integrated-unmanned-system/

UAV which deploys from a carrier aircraft and is planned to also be able to return to the carrier aircraft autonomously. In their design, the aircraft is planned to be deployed by various schemes, i.e. from under the wing of the carrier aircraft or can be treated as a bomb and dropped from the bomb bay of a bomber aircraft. In this case, the initial velocity of the aircraft will be of that of the carrier aircraft and no additional launcher will be necessary. This also means that the carrier aircraft might have to fly a bit higher from the operational altitude of the UAV to compensate for the altitude drop due to the deployment.

Plans have also been made to arm AFSOC (Air Force Special Operations Command) C-130 gunships with air-launch UAVs [37] to extend the capabilities of manned platforms. Treated as the carrier aircraft, the C-130 aircraft is equipped with the Coyote UAV[6] by Raytheon which can be air launched from various different platforms. In another project, the Raytheon's Coyote UAV is used to demonstrate swarming technologies in deployable UAVs. Here, instead of launching the UAV mid-air, the ground platform used to launch the vehicle is used. The vehicle unfolds itself almost instantly to its launch and due to its low weight, it is capable to operate by a such ground-to-air deployment scheme.

A concept of a gun launched micro-air vehicle is also proposed by Gnemmi & Haertig [38]. The UAV here is a lightweight rotary wing UAV which is propelled from a ground station. In this case, due to the low weight of the UAV, the aircraft is able to hover quickly after reaching peak altitude, where it will unfolds its rotor and operate.

2.4. Stability Assessment Method

For a deployable UAV like the Dash-X aircraft, it is necessary to make sure that the deployment and unfolding of the aircraft is performed successfully. To do this, the aircraft needs to be modelled correctly and an evaluation of multiple deployment parameters needs to be conducted.

Although it is not common to research the success of deployment of an aircraft, several researchers have come up with ways to make sure that an aircraft will be stable during or after the deployment. Tong et al. used the Lyapunov stability theorem to confirm the stability of an asymmetric variable sweep aircraft [**?**]. Another method is to assess the stability of the vehicle during shape change by inspecting the eigenmodes of the aircraft as done by Prabhakar et al. and Beaverstock et al. [3, 18]. Beaverstock et al. in particular investigated span morphing dynamics. They used a pre-developed framework of software to assess the morphing aircraft. Shi & Wan derives the condition of stable morphing and assess the flight stability based on Hurwitz rules. Unfortunately, these assessment are mostly focused on the stability of the aircraft with low-rate shape changes and not directly related to deployable wing aircraft like the Dash-X aircraft.

An interesting method is proposed by Fujita et al. to assess the robustness of deployment by using a sigma level method. Basically, the method combines a sensitivity analysis of the variables deemed critical to change with an assessment of the deployment likelihood to success. The assessment is based on the six-sigma principle, where each deployment simulated will be given a certain value to state how confident is the method that the deployment at the specified conditions will result in a safe deployment. A definition of safe deployment is defined at the beginning and simulations is run several times with varying deployment parameters. The variables which are stated in the definition of a safe deployment are compared with its allowable upper & lower limits for every timestep. When a variable goes over the limits, the simulation stops and the deployment is deemed unsafe.

Another method by Santoni & Gasbarri is to create a cost function and have the values necessary for an effective deployment. Unlike the methods from other researchers, these methods by Fujita et al. and Santoni & Gasbarri is focused on the deployment of the vehicle and not morphing during steady level flight.

For the criteria of safe deployment, Fujita et al. listed several important points. However, for the lack of aerodynamic data of angle of attack & sideslip angle, the team decided to treat this as one of the limits of the simulation. In other words, if the simulated deployment goes into a state where the angle of attack goes beyond the available data, the simulation stops and the deployment is considered a not successful one. This is

[6] https://www.raytheon.com/capabilities/products/coyote

not necessarily true and therefore, further investigation needs to be done before placing a cap on the simulation due to the lack of data. Other than that, the criteria for deployment also considers the altitude drop of the aircraft from the deployment, whether or not the wing is deployed and stays deployed, structural limits and the aircraft's load factor. Santoni & Gasbarri listed the load factor of the aircraft as the parameter to minimize in their work, and incorporated it in their cost function.

The assessments here are of an open loop system, where there are no correction by a Stability Augmentation System in the aircraft. However, if it is known that the aircraft is most likely to fail and there is only a small window of successful flight for the open loop system, a control augmentation to assist in the safe deployment of the vehicle should be considered. Stoica & Yaesh investigated the control necessary for a deployable wing aircraft which is launched from a carrier aircraft [39]. The goal of the control system is to have zero angle of attack change during the transformation. In this case, the aircraft morphs only on the main wing and the tail section is able to correct for the changes in pitching moment caused by the motion of the wing. This research only takes the longitudinal axis into account. The research focuses on a creation of a Jump-Markovian controller to compensate for the sudden forces and moment created by rapid motion of the wing.

Sensitivity analysis in general is a promising method to be used to test different deployment schemes with different varying parameters of the aircraft or the deployment condition. Such method is also able to assess the amount of influence a parameter has on the output of the deployment, as well as how interactions between factor might arise and impact the output considerably. By using sensitivity analysis, the input variables could be varied at a range specified by the user and, in stochastic processes,a probability distribution of the input variables can also be defined beforehand. In essence, the method will find how much an output parameter vary when one or more input parameter is changed. Based on the book by Saltelli et al.[40], there are various methods of sensitivity analysis available, each with its benefits & drawbacks. Saltelli et all.[40] classified sensitivity analysis into 2 different groups, namely the local and global method. Generally, these methods require the model to be run multiple times, which causes them to be computationally expensive. However there are also less computationally expensive methods, with the precision of the result as the trade-off. Thus, a correct selection of the sensitivity analysis method will determine how accurate the results are and how long will it takes to obtain a result.

To evaluate the safety of deployment for various parameters, with ranges of values for each parameter, a lot of computing time is needed. Sensitivity analysis however is able to reduce the computational time needed for the evaluation of a deployment scheme by identifying the number of influential parameters to the safety of deployment. Once known, the simulation can only be made to vary the influential parameter. This reduction of parameters to vary can be done by using the screening method of sensitivity analysis.

In general, there exist multiple screening methods. Morris's method [41] for global sensitivity analysis is one where each input parameter is varied individually where other parameter is kept constant. The result is that the change in output will be only due to the variable that is varied. Thus, a relation can be made between the change in input parameter and the change in the output parameter. This method is also able to identify the effect of interaction with other parameter, though not identifying which parameter the interaction is with. Cotter [42] proposed a method where the number of runs to determine the influential parameter is equals to 2k+2 runs, with k as the number of parameter. In the method, each parameter will be varied once to its maximum value and once to its minimum value, while the other parameters are kept constant. Then a run with all the parameter at their maximum value and one with all parameter at their minimum value will also be performed. The catch here is that the method then ranks the importance of all the parameters. However, with this method, an important factor may still remain undetected since the response of the factor might cancel out in the end. Then there is also the Iterated Fractional Factorial Design method [43] by Andres and Bettonvil's Sequential Bifurcation [44] which are more advanced, but are not easy to implement in all cases. Both of these methods cluster the parameters into several groups and checks which group output the most extreme result. This extreme result directly corresponds to the importance of the parameter within that group. Later the group is split the division of the group which still result in an extreme result is considered to be the group with the influential parameter. The same process is repeated until the influential parameters are identified in the last groups with only several parameters.

2.5. Synthesis

After having reviewed the available literature to date, a decision needs to be established on how the research is to be conducted. Unlike previous research, which focuses only on the morphing aircraft dynamics during flight, this research has its emphasis on the deployment scheme of the morphing aircraft. The method developed here could also serve as a basis for the safety assessment of other morphing aircraft during different kinds of deployment which are not stated here, be it rocket-powered deployment, hand launched, etc. The only difference will be on the modelling part of the aircraft, whereas the evaluation of the deployment stability with the method developed here could be used universally in different cases. However, since the Dash-X aircraft is the aircraft being considered here, the choice of modelling and simulation method, and also the method to evaluate the deployment stability of the aircraft will be focused on the this type of airframe.

To tackle the problem, the writer has decided that a simulation of the deployment scheme of the Dash-X aircraft will be constructed. The method is chosen as it is not-time consuming and also risk-free as compared to experimenting with the deployment of the aircraft without having a good understanding of what is going to happen. The simulation can later also be used to improve the design and observe how the aircraft will respond when changes are made to the design, etc. The construction of the simulation will be based on the modelling of the aircraft. Reflecting to the literature being reviewed above, a lot of researchers rely on the robustness and easiness of Multibody dynamics. This method not only is able to model the moving components of a morphing aircraft, but also is quite sophisticated that it also can takes into account the damping, stiffness and other mechanical properties of bodies and joints. It is easy to use as the method is quite straightforward and is available in the form of off-the-shelf programs or toolboxes in software that are familiar in the academia world like MATLAB.

In this research, a suitable aerodynamic model is also selected that can correctly represent the aerodynamics during the deployment of the aircraft's lifting surfaces. However, taking into account the increase in computational time that rises with the complexity of aerodynamic models, a simple strip theory is selected instead and later will be validated. The validation here is performed by checking the correspondence of the aerodynamics model with the result of a proven aerodynamic solver. In addition to that, the performance of the model will also be evaluated with actual flight test data of the aircraft, where the aircraft performed maneuvers and the instant response of the aircraft and model will be compared. The main focus of the paper is to develop a deployment stability assessment method, and thus the aerodynamic model created here will have a lower importance. In future work, a more sophisticated aerodynamic model may be selected and tested to increase the fidelity of the overall simulation. However, for this phase the strip theory method will be used.

For the selection of the aerodynamics solver, AVL has been chosen considering its accuracy and easiness to integrate with the medium where the whole research is being conducted, i.e. MATLAB. The method is a based on a medium-fidelity solver and the result of the model will later be compared with this tool. The comparison will be made on the static and dynamic stability derivatives of the aircraft.

As to the selection of the deployment schemes for this research, it is decided that 2 mid-air deployment scenarios will be tested with the method developed here. The selection is made considering the frequency and trend of UAV deployment in the field of aviation today. Since the case selected here is the Dash-X aircraft, the case of deploying the aircraft from a canister that is slowed down mid-air by a parachute will definitely be selected as deployment scenario 1. Deployment scenario 2 will be of the deployment from under the wing of a carrier aircraft. Considering the scope of this research, the deployment from the bomb bay of a bomber aircraft can also be treated as deployment scheme 2.

To perform the stability assessment, a definition on what a stable deployment is, should be made beforehand, as done in the works of Fujita et al.[5, 6, 21–24, 34]. This includes the determination of what the safety concerns are and what the deployment parameters that describes this safety concerns are. Then, a selection will be made on which of the available assessment method is most suitable for the case of the Dash-X aircraft deployment. Reflecting on the papers available, a very promising method is to use the screening method of sensitivity analysis. Bearing in mind that the deployment simulation constructed is highly influenced by different operational parameter of the aircraft, this method will also be used to identify which parameters has a higher impact and which parameter is less-influential in the safety of deployment of the aircraft. Sensitivity analysis itself is time consuming, and a for methods which are not, the accuracy of the results is sacrificed.

Thus only the screening method of sensitivity analysis will be used here. Considering the straightforwardness and easiness to implement, the one-at-a-time method by Morris is selected to be screening method in this research. The method is intuitive and the results of the method can be easily traced back and understood. However, a modified version of the method needs to be made considering the output being evaluated here will only result in a binary value (either "safe" or "unsafe" deployment). Further description of the method will be presented in Chapter 6.

After obtaining information on which parameter is less influential, the next step is to perform multiple runs to the model to obtain a safety deployment space of the aircraft in the evaluated deployment scheme. The aim here is to visualize the safety deployment space of the aircraft considered in this research, which is a combination of different influential parameters which either can result in a safe or unsafe deployment. Thus, during operation, the aircraft can minimize having an unsuccessful deployment by referring to the safety deployment space obtained in this research.

Table 2.1: Project synthesis

Component	**Method**
Morphing Aircraft Dynamics	• Multibody dynamics
Aerodynamics	• Simple strip theory • Validated with off-the-shelf aerodynamic solver • Validated with flight test data
Deployment Schemes	• Deployment from a canister slowed down by a parachute • Deployment from under the wing of a carrier aircraft
Stability Assessment	• One-at-a-time screening method • Multiple runs of model with varying inputs

3

Case: Dash-X Project

In this research, the Dash-X project as a collaboration project between VX Aerospace, the University of South Carolina and the University of North Carolina is taken as the test case[45]. The project is initiated in 2016 and is projected to be market-ready by the year 2023. The first phase of the project, which is the design, construction and flight testing of the aircraft has been performed successfully. However, the flight test performed does not include the deployment of the aircraft as intended in the operations of the aircraft. The deployment testing will be done in the second phase of the project and before performing actual deployment of the aircraft, the mechanics during the deployment will be predicted with this study. The following sections presents a more in depth description on the Dash-X aircraft.

3.1. Aircraft Deployment Scheme

The aircraft is unmanned and is to be contained inside a modified munitions dispenser (generally used for dispensing cluster bombs) and later deployed from a carrier aircraft. The canister, which is brought to an altitude by the carrier aircraft, is let go at its drop altitude and then free falls until a certain altitude and is slowed down by deploying a parachute. Upon reaching the UAVs deployable altitude, the canister opens, the UAV slides out of the canister and is released. The folded UAV then unfolds itself by spreading its main wing, horizontal tail and its vertical tail which are originally stowed inside the fuselage. After unfolding itself, the aircraft finds a steady state and then operates. The deployment scheme is illustrated in Figure 3.1, which is similar to the proposed deployment mechanism of the proposed Mars ARES aircraft [7].

In order for the the aircraft to attain a safe deployment, after the transformation process, it is necessary to make sure that all of the stages are performed correctly and successfully. Therefore, a study needs to be performed on the different stages to deploy the aircraft. An interesting aspect here is the dynamics that the aircraft will experience in each stage, especially when the aircraft unfolds itself after being released from the canister. Here, different factors like the velocity of deployment, the altitude of deployment as well as the attitude in which the canister releases the aircraft and other factors will play a role in leading to the final condition of the aircraft. All this calls for a complete understanding of the behaviour of the aircraft during deployment, which is a challenge on its own.

3.2. Aircraft Design & Specifications

The Dash-X aircraft is a fixed wing aircraft which is different with ordinary fixed wing aircraft in one single way. It is a morphable aircraft which has its lifting surfaces stowed initially around the fuselage of the aircraft and can be unfolded prior to operation. The aircraft is designed in such a way that its deployment is considered as a major part of the aircraft overall design. The goal here is to deploy the aircraft from another carrier aircraft,

Figure 3.1: Stages of deployment of the Dash-X aircraft (Developed from the Dash-X presentation

Figure 3.2: Dash-X aircraft (i)before & (ii)after unfolding

which brings the aircraft into its operating environment inside a canister. The Dash-X aircraft is contained inside a standard munitions dispenser, and therefore the geometrical design follows the available space of the dispenser. The folded and unfolded configuration of the aircraft is shown in Figure 3.2.

The munitions dispenser is in the form of a hollow cylinder, and hence the aircraft should be designed to be carried inside this narrow space. As the main lifting surfaces are generally the components which require a lot of storage space, these are the components that needed to be relocated. The solution implemented by the engineer here is to initially place the lifting surfaces around the fuselage, to reduce the amount of space needed to store the aircraft when it is not in operation. A pivot mechanism with springs as actuators is used to deploy the main wing, horizontal and vertical stabilizer when the aircraft is to be used in operation. This mechanism allows the orientation of the lifting surfaces to be altered when stored inside the canister, which significantly reduces the space needed of the overall aircraft to be stored. This also applies for the horizontal and vertical tail. Moreover, for the vertical tail, a storage chamber needs to be cut out in the fuselage. Table **??** shows the specification of the Dash-X Aircraft.

This geometrical limitation indirectly also affects one important aircraft parameter which is the wingspan. Since the space inside the munitions dispenser is limited, even when the main wing is reoriented by the pivot mechanism, the wingspan of the aircraft is still capped. A workaround to this problem by the engineers is to not only make the wing rotates around a pivot in the fuselage during unfolding, but also to make the wing telescopic. This elegant solution is implemented in extending the geometry of the main wing, which also helps to reduce the wing loading of the aircraft.

Parameter	Value	Unit
b	3.607	m
MAC	0.308	m
l_h	1.036	m
l_v	0.888	m
m	26.182	kg
Airfoils	NACA 2415, NACA 0012	-
V_{ne}	55.05	m/s
n_{max}	3.8	-
n_{min}	−1.52	-
h_{oper}	±5000	ft

Another thing to consider here is that the design of the aircraft is asymmetric. As a result of the wing deployment mechanism, the right wing plane of the aircraft is slightly above the left wing plane. This means that there should also be differences in the forces generated in the right side of the aircraft to the left to compensate for this asymmetry. Furthermore, the asymmetry of the aircraft also result in coupling between the longitudinal and the lateral axis of the aircraft. Therefore a 3D analysis of the aircraft involving not only longitudinal but also the lateral and directional axis is necessary in this study.

4

Morphing Aircraft Modeling

This chapter presents information related to the modeling part of the morphing aircraft. As presented before, the modeling of the aircraft is one of the three main parts of this research project, which is directly followed by the validation of the model, presented in the following chapter. In this section, the theory behind the method selected to model the aircraft will first be presented, followed by the components of the model and the types of models used in this research. Several model types are created in this research due to their different uses, which will be further explained in section 4.3.

4.1. Theory

Since the aircraft being considered in this research is a morphing UAV, two main aspects of modeling the aircraft needs to be determined, which are the modeling of the morphing process of the aircraft, and the modeling of the aerodynamics of the aircraft. Unlike a conventional aircraft, a morphing aircraft cannot be represented by a point mass floating in space. Representing the aircraft as a simple rigid body floating in space is also not an option since the aircraft will need to change its shape during operation, and this means the body properties as well as the aerodynamic properties of the aircraft will change when morphing. Thus a more suitable and sophisticated approach of modeling the aircraft is required. The modeling of the aerodynamics of the aircraft on the other hand will be described in further detail in Section 4.2.

Based on the literature study conducted previously, the modeling technique adopted to model the morphing aircraft is multibody dynamics. Multibody dynamics is proven to be robust, reliable and easy to use and therefore the techniques is selected in this project. Bearing in mind that the modeling is just one part of the project, the quickness and easiness of learning the method as well as implementing it is treated as a major consideration in the techniques selection. Also, by using multibody dynamics, the equation of motion of the aircraft is directly calculated with the method.

A multibody body system is a combination of a number of rigid or flexible bodies connected together by means of joints, which can be externally excited by external forces from springs, dampers or other forms of actuators. The masses of the bodies are also possible to be varied, but in this study, masses of the bodies are kept constant throughout the simulation. The equation of motions of a multibody system are generally written in the form of a second order system of ordinary differential equation as follows [46]:

$$M(q)\ddot{q} = f(q,\dot{q}) \Leftrightarrow \begin{cases} \dot{(q)} = u \\ \dot{u} = \tilde{f}(q,u) = M^{-1}(q)f(q,u) \end{cases} \tag{4.1}$$

This equation holds for a system that is not mechanically constrained in any of its degree of freedom. However, most multibody dynamic system includes joints, which are treated as constrained to one or more of

the degree of freedom between two bodies. When these joints/constraints are included in the system, additional algebraic constraints are introduced in the equations of motion and the system is then represented by a differential-algebraic equation (DAE) which is represented by Equations 4.2 to 4.4 [47]:

$$\dot{q} = u \tag{4.2}$$

$$M(q)\dot{u} = f(q,u) - G^T(q)\lambda \tag{4.3}$$

$$g(q) = 0 \tag{4.4}$$

In Equations 4.2 to 4.4, q are the generalized positions, u are the generalized velocities, $M(q)$ are the mass matrix which is a function of the position of the object, $g(q)$ are the algebraic constraints which defines the limitations to the degrees of freedom (DOF) of the link between two bodies, λ are the Lagrange multiplier and $G(q)$ the constraint matrix which is given by the Jacobian of $g(q)$. In essence, in multibody dynamics, to identify the configuration of a body in space, six coordinates is required [48]. The relation between two bodies in which no constraints/joints are imposed on are totally free to move from one another. Every two bodies have 6 degrees of freedom that connects them. However, with the introduction of joints, since the motion might be constrained in one or more axis, the mobility of the two bodies can be less than 6. This of course depends on the type of joint/constraints that is used to define the motion between the two bodies.

The equations above includes both the kinematics as well as the dynamics of a multibody system. By using computers to solve these equations numerically for every timestep and using time-integration methods, the movement as well as other parameters of a multibody dynamic system can be calculated. This simple theory that backs the multibody dynamics approach is used in this study. For the numerical solver, Simulink, as a software environment that is quite frequently used in the academic world is used. More specifically, the Simscape Toolbox in Simulink, which uses the method of solving DAEs of systems is used. The toolbox comes in two different variants and the one chosen in this research is the Simscape Multibody First Generation Toolbox, where the bodies, joints and sensors modules are treated as Simulink blocks. The Simscape Multibody First Generation Toolbox is a very straightforward toolbox to model dynamic systems, and is very suitable to model the morphing process of the aircraft considered here.

In the Simscape Multibody First Generation Toolbox, a multibody system is composed of several important components. As the name states, an important component is the body, which is treated as a single body which may be connected to other bodies in the assembly by means of joints. Then, external forces and moments or even motions can also be exerted into the assembly at different location by the use of actuators. The forces may be imposed either on the body or the joints of the system. These external forces creates motions in the system and wherever required, sensors which measures the forces, moments, motions or the change in location of a specific point can be included into the system. With these few blocks, a system can be created, tested and analyzed in with the toolbox used.

4.2. Modeling Components

For the model to correctly represent the dynamics of the morphing aircraft, the model is divided into several components that each represent an individual system in the aircraft. The division is mainly done by considering what function a component has to the whole aircraft. Movables due to the morphing technologies are also treated as individual bodies and connected by means of joints. Each of the part modeled are represented by a single block, where, if necessary, consist of multiple sub-blocks that represents the different sub-functions of the sub-blocks in it. In addition to the individual components that represent the physical parts of the aircraft, 7 additional supporting blocks is created which helps in defining the simulation and logging the simulation data.

For a multibody system, the number of degrees of freedom of the whole system is directly related to the number of bodies as well as the number of joints and their types. In the case of this study, to model the aircraft, 1 body is required to model the fuselage, 4 bodies to model the main wing, 2 bodies to model the horizontal tail and one body to model the vertical tail, there exists 8 bodies in total. By using the mobility formula/Kutzbach criterion [48] as shown in Equation 4.5, the number of degrees of freedom of the system can be found.

$$DOF = 6 \times N_{BODIES} - N_{CONSTRAINT.EQUATIONS} \tag{4.5}$$

The inboard part of the main wing rotates about a pivot on the fuselage. A revolute joint is used to model this pivot. Then, to model the extension of the main wing, a prismatic joint is used to define the relation between the inboard and outboard section of the main wing. Since the horizontal tail and vertical tail only rotates about a pivot on the fuselage, revolute joints are used to model their motion. Since there are 8 bodies in total for the multibody assembly, and since for every revolute or prismatic joint 5 constraint equations are needed, thus by referring to the Kutzbach criterion, the total number of degrees of freedom in the assembly is $(8 \times 6) - (5 \times 7) = 13$ DOFs.

For the simulation to be defined properly, initial conditions are also applied to the aircraft before deploying. These conditions are imposed a starting attitudes as well as starting velocities and rates of the aircraft. Other than that, for this study, since the actuator dynamics of the deployment mechanism has been neglected, an imposed motion has been applied to every joint in the aircraft which specifies when the lifting surface will be deployed and how fast it is deployed. In other words, instead of specifying the amount of moment or force is exerted on a joint, an acceleration profile is imposed on it along with the relative velocities and positions of the two reference frames which are connected by the joint.

4.2.1. Aircraft Components Blocks

The design of the Dash-X aircraft possesses challenges that needs to be handled properly. Unlike other deployable UAVs where only the main wings are stowed initially, the Dash-X aircraft has its main wing, horizontal stabilizer and vertical stabilizer in a stowed position inside a canister. This means that during the deployment of the main wing, there will be no control surfaces that can be used to provide a counteracting moment to the moment generated by the deployment of the main wing. When released from the canister mid-air, these aircraft unfolds itself by sweeping the main wing forward and also extending the span of the wing by means of springs as actuators. A similar mechanism is also implemented in the horizontal & vertical stabilizer of the aircraft. The engine of the aircraft is positioned in the forward section of the fuselage. In the end, to model the aircraft, each of the components described above is represented by individual blocks. These blocks include the fuselage block, the main wing block, the horizontal & vertical tail block & the engine block. According to the complexity of the components modeled these blocks may have sub-blocks inside them which is required to represent the internal mechanics of the main component block, like the main wing block, which consist of the inboard wing block, outboard wing block as well as the telescopic joint block.

Fuselage

The fuselage block is where all of the components of the aircraft are assembled. This block is used to define the geometry of the aircraft, which is defined by the coordinate systems in the fuselage. Another important function of this fuselage block is to determine where the reference frames of the most influential components are and also the inertia matrix of the fuselage. This block also serves as the block which defines how each connected component of the fuselage is oriented with respect to the fuselage. Initial attitudes of the aircraft are also defined in this block to accommodate for the limitations of the 6-DOF joint block in the environment settings block, where only initial conditions of the linear joints are able to be specified.

In addition to the fuselage block, a fuselage forces block is also added to the model. Since the fuselage block is only a body block where all other components are connected to and no real calculation of the fuselage forces & moments are done, the addition of this fuselage forces block accommodates this issue. The calculation of the fuselage forces is based on papers provided by the IHS ESDU Aerodynamics series [1, 49–53], where the data are obtained from experimental testings. These forces and moments are a direct relation to the angle of attack and angle of sideslip by which the fuselage experiences. The reference point taken here is the midpoint along the longitudinal axis of the fuselage. Figure 4.1 shows a body representation of a fuselage and its forces along with the convention of the signs considered in the papers .

The papers also comes with a online solver [49] where the user can input design parameters of the fuselage

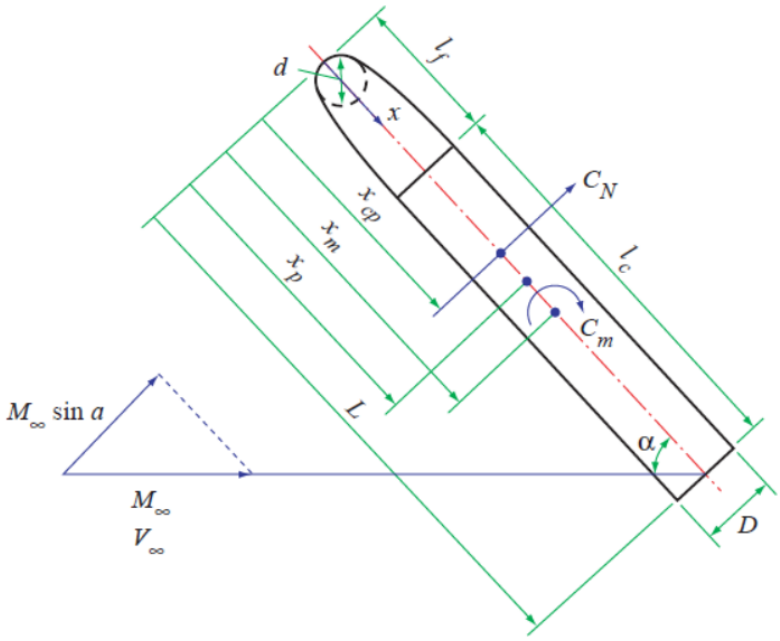

Figure 4.1: Fuselage forces & moments representation and sign convention [1]

and get the normal and pitching moments coefficient of the fuselage being evaluated here. Since the method is limited to fuselages with a circular cross section, several assumptions to use the software needs to be made. Table 4.1 shows the online solver inputs parameters used and some remarks on the choice of the variables.

Parameter	Value	Unit	Remarks
Forward Fuselage Body Type	x	-	Resembles the fuselage forward shape of the aircraft considered
D	x	m	Equivalent fuselage diameter
l_f	x	m	Measured
L	x	m	Measured
l_a	x	m	Measured
β	x	°	Measured
M_∞	x	-	Assumed
Re	x	-	Calculated
x_m	x	m	Measured

Table 4.1: Aircraft fuselage parameters

Main Wing

The main wing of the aircraft is composed of two separate bodies. The inboard part of the main wing is the one connected to the fuselage by means of the revolute joint, whereas the outboard part of the main wing is connected to the inboard part by a prismatic joint. The choice of these joints are based on the type of motion the real aircraft has when unfolding. Initially, both parts of the main wing are stowed around the fuselage. Then, during deployment, the main wing rotates 85 degrees to its operational position by an actuator. However, in this simulation, since the actuator dynamics has been neglected, the motion of the main wing is initiated with an imposed motion defined in the simulation. This motion is described inside the revolute joint sub-block inside the main wing block. After the main wing rotates, it will extend itself. The mechanism here is represented in the simulation by the prismatic joint which connects the inboard and outboard wing bodies. The translation is done until the length of one wing is equal to the semispan

of the aircraft. To control the timing of the deployments of different components of the main wing, a delay is imposed for both the rotational and telescopic motion of the main wing. The imposed motion here is described inside the prismatic joint sub-block inside the main wing block.

In the deployment modelling of the aircraft, due to the lack of actuator data, it is decided that an imposed motion will be implemented to unfold the aircraft from its folded state. To do this, several parameters regarding the unfolding mechanism needs to be predefined. These values are assumed reflecting on the available literature of deployable wing aircraft and will not be varied throughout this research.

Parameter	Value	Unit
Wing Delay Time (Rotation)	1	s
Wing Deployment Time (Rotation)	0.5	s
Wing Delay Time (Telescopic)	1	s
Wing Deployment Time (Telescopic)	0.5	s
Horizontal Tail Delay Time	0.5	s
Horizontal Tail Deployment Time	0.5	s
Vertical Tail Delay Time	1.2	s
Vertical Tail Deployment Time	0.5	s

Table 4.2: Predefined set of deploying parameters of lifting surfaces

Table 4.2 presents the different delays and deploying times of the different lifting surfaces of the morphing aircraft, which defines the sequence and length of deployment for the different lifting surfaces of the aircraft. The parameters "delay times" describes from which point in time in the simulation will the corresponding lifting surfaces starts to deploy itself. The parameters described as the "deployment time" on the other hand describes how long will the the unfolding motion of the corresponding lifting surfaces will take.

In this research, it is decided that the lifting surfaces on the empennage of the aircraft should deploy first, as they are the ones that will counteract the moments during the deployment of the main wing, which is significantly larger in size. The first lifting surface to deploy is the horizontal tail. This is due to the design of the aircraft which stores the vertical tail inside a chamber within the fuselage, and can only be deployed without hitting the horizontal tail after the horizontal tail has moved out of the way. After the deployment of the horizontal tail, he vertical tail still cannot be deployed as the main wing is still on the way. Thus, the main wing rotational joint is deployed second. After the rotational motion of the main wing, the vertical tail then deploys with a slightly later time than the main wing. This is then followed by the telescopic motion of the main wing, which concludes the deployment of the aircraft. The deployment times between the lifting surface of the empennage and the main wing is taken as the same. In further researches however, it is possible to use the model created here to tweak the design parameters as the actuator parameters and find the impact it has on the overall deployment of the aircraft.However, for this research the values are predefined.

Since we have decided in the previous chapter to use simple strip theory for the aerodynamics of the aircraft, the main wing is divided into several strips. This is also important to model the deploying process since the outboard wing of the aircraft will experience a higher local velocity compared to the inboard wing. The main wing is divided into 10 strips, with 6 strips to represent the inboard wing and 4 strips to represent the outboard wing. Each strip is positioned by defining a reference frame in the bodies of the inboard and outboard wing. Figure 4.2 shows the Simscape representation of the morphing aircraft after being fully deployed.

$$L = \frac{1}{2}\rho V^2 c_L b_{strip} c \tag{4.6}$$

$$D = \frac{1}{2}\rho V^2 c_D b_{strip} c \tag{4.7}$$

$$M = \frac{1}{2}\rho V^2 c_m b_{strip} c^2 \tag{4.8}$$

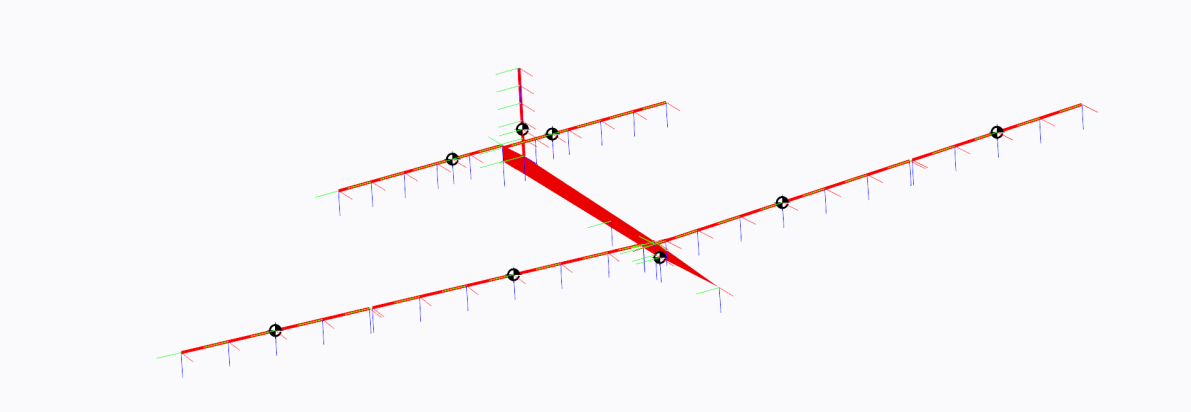

Figure 4.2: Simscape model visualization of the morphing aircraft after being fully deployed

For each strip, a body sensor is placed to measure the local velocities experienced by the strips in their respective positions. This velocity measurement can then be converted into the local angle of attack angle and local sideslip angle. The measured parameters will then be used to calculate the aerodynamic forces and moments experienced by the strip. In this research, a simple aerodynamic equation to calculate the forces and moments are used as expressed in Equations 4.6 to 4.8. Wind tunnel airfoil data are gathered and used to get the values of the coefficients for the angle of attack and angle of sideslip experienced by the strip. These forces and moments values are then feedbacked to the reference frame of the body where the strip is defined. With this method, the magnitude of the aerodynamic forces can be calculated and the response of the overall aircraft due to the aerodynamic forces can be seen. The process of incorporating aerodynamic forces calculation in the model is shown in Figure 4.3.

From the control surfaces point of view, the main wing of the aircraft considered here has ailerons located in the outboard section of the wing. Referring to the papers in IHS ESDU about control surfaces [**? ?**], a linear relation between the control surface deflection and the additional lift is calculated. This correlation is calculated for the NACA2415 and implemented in the model. The input for the control surfaces are described in the Virtual Pilot block and sent via a "Goto" block to the strip of the main wing where the aileron is present.

Horizontal Tail

The horizontal & vertical tail are also deployed by the same actuation system as the main wing, although they both only rotate about an axis to unfold unlike the main wing that rotates and also extends itself in translating manner. This means that one body to model each lifting surface is sufficient. Each unfolding lifting surface is also connected with a joint to the fuselage, which is also actuated. However, again, due to the lack of actuator data, the actuator dynamics have been neglected here and an imposed motion as described in Table 4.2 have been incorporated.

The horizontal tail of the aircraft is divided into 5 strips, considering its length. The elevator is present throughout the length of the elevator and the same procedure to get the relation between the control surface deflection angle and the additional lift in the airfoil as the main wing is used here. The calculation of the aerodynamic forces and moments and how they are feedbacked to the airframe is the same as the main wing, and is shown in the form of a flowchart in Figure 4.3. Again here, the input of the elevator deflection is specified in the Virtual Pilot Block.

Vertical Tail

Unlike the deployment of the main wing or the horizontal tail, the axis of rotation of the vertical tail is along the lateral axis of the vehicle. The vertical tail is also deployed later than the horizontal tail due to the design restriction. The unfolding here is also directed by the imposed motion, with which values of delays and deployments are described in Table 4.2. The calculation of the aerodynamic forces and moments are also

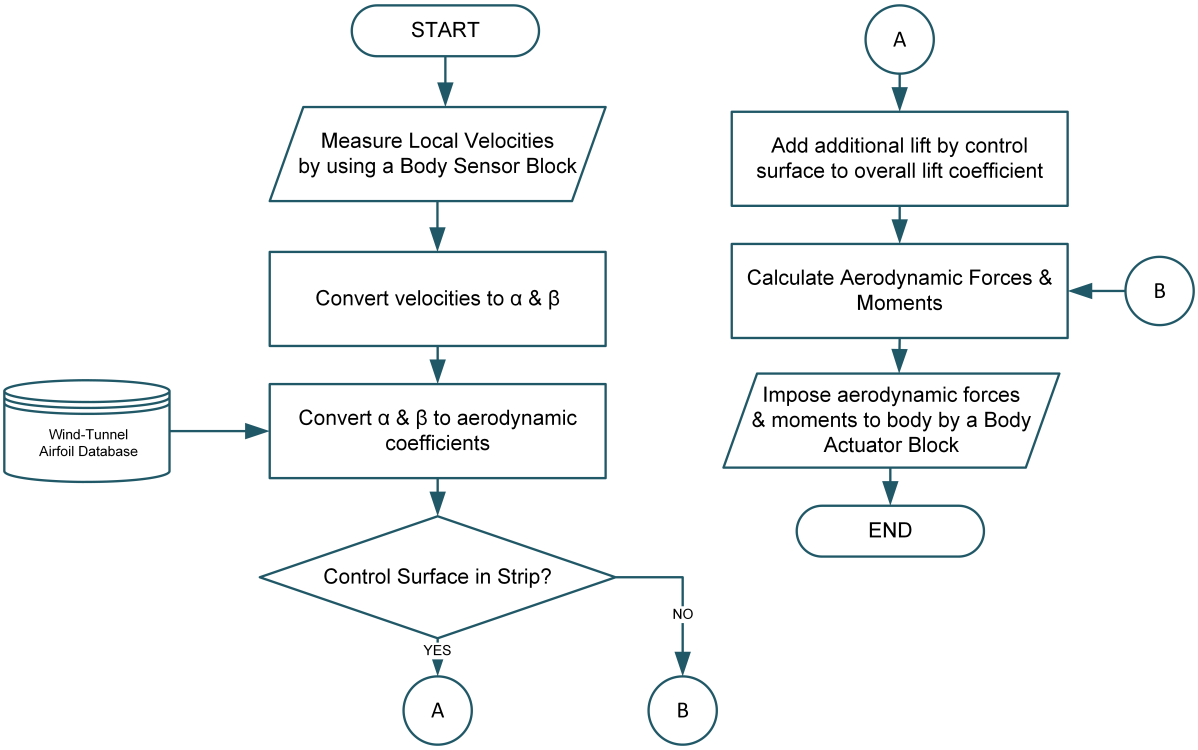

Figure 4.3: Process of calculating & including aerodynamic forces & moments in the model

similar to that of the other lifting surfaces, expressed in Figure 4.3.

The rudder here is modeled by an increase in lift force due to the control surface deflection whose signal is directed from the Virtual Pilot Block. Since the airfoil of the horizontal tail and the vertical tail are the same, the linear relation between the control surface deflection and the additional lift is the same with the horizontal tail.

Engine

The engine for the aircraft is represented by a single point force. The force here is capped to the maximum thrust capable of being produced by the engine. The amount of newtons for the engine is determined by the output of the Virtual Pilot block.

4.2.2. Supporting Blocks

After describing the model components that is directly related to the aircraft, in this section the blocks that acts as supporting components will be described. The functions of these blocks vary per block, and their presence is essential in running the simulation and gathering information from the simulation. Not all of the supporting blocks described here will be present in all of the model and the contents can also differ from one model type to another. The supporting blocks in the models are listed below:

Environment Settings Block

In the environment block, the relation between the aircraft and the world frame is specified. For the model created in this study, the default joint chosen is the 6-DOF joint, although this also varies on the type of model used, later described in Section 4.3. Another candidate would be the bushing joint. However, in Simscape Multi body, the bushing joint is prone to gimbal lock problem, in which two prismatic joints are aligned with each other. Thus the 6-DOF joint is used instead.

The 6-DOF joint is not perfect on its own. The problem with this joint is that the initial condition that can be specified is for the three linear axis, whereas no initial attitude and angular rate can be specified for the rotational axis. Thus, a workaround is made to accommodate for the issue by specifying the initial attitude in the fuselage block and initial rates with the initial rates block.

Virtual Pilot Block

The virtual pilot block represents a pilot which directs the motion of the aircraft by specifying the input values to the engine or control surfaces of the aircraft. There are four different input parameter specified, which corresponds to the four controls of the aircraft, namely the engine, the elevator deflection, the aileron deflection and the rudder deflection. Depending on the type of model being evaluated, the contents of this block may differ. Further information regarding the types of model will be explained in section 4.3.

Sensors Block

The sensors block is where information regarding the raw parameters of the flight is converted into meaningful information that satisfy the aerospace convention. Within the sensors block, values of the aircraft as a whole throughout the simulation is measured, prepared and visualized. These values includes the aircraft's speed, attitude, linear and angular rates, position, accelerations, load factor and angles. There are 2 links that connects the sensor block and the fuselage block of the aircraft. These links are each connected to separate body sensors, which measures the values described above in the world and the body reference frames. For both body sensors, the reference point on the aircraft by which the values are measured is in the CG of the aircraft.

Atmosphere Block

The Atmosphere block defines the properties of the air and surroundings of the aircraft throughout the simulation. Since during the simulation the altitude of the aircraft changes, the properties of the air at that specific altitude needs to also be constantly updated. For instance the density of the air at low altitudes is different from the air at higher altitudes and this will have an impact on many of the aircraft performance and trim values. Thus the inclusion of this block is necessary. The input of this block is the current altitude of the aircraft and the outputs are the the air density, temperature, pressure and speed of sound at that particular altitude. The calculation of the atmosphere is based on a built in block in Simulink, which is called the ISA Atmosphere model, which bases its calculation on the U.S. Standard Atmosphere 1976 Paper [54].

Data Logger Block

To be able to work with the results of the simulation, it is not rare that the output of the simulation need to be opened in a different software environment. Thus the storage or logging of the data of the simulation run is necessary. The data logger block here serves this function and stores the timeseries values of selected parameters of the flight to the MATLAB workspace, which can later be saved or worked with. Some of the values logged include the input values of the virtual pilots, the aircraft flight parameters calculated and measured in the sensors block, the values of the parameter blocks and the triggers by which the simulation is stopped in the Simulation Stopping Criteria Block.

Simulation Stopping Criteria Block

The Simulation Stopping Criteria Block is one where the upper and lower limits of the safety deployment parameters is being monitored throughout the simulation. In the model, the simulation is prematurely stopped once a variable is observed to have crossed either its upper or lower limits. On the other hand, the simulation is let to run until the prescribed endtime if no observed variable crosses its limits. Further information on what the evaluated variable are will be discussed in Chapter 6.

Each observed value is given a designation number, which can be tracked later to check which values triggers the stop of the simulation. This is useful in the analysis phase, where a simulation might even be stopped due to the crossing of 2 variables at the same time. With this method, the reason for stopping the simulation can be understood and in the future, steps can be taken to prevent it from happening.

Initial Rates Block

The addition of this block in the model is to accommodate the limitations of the joint used to connect the aircraft to the world axis. Since the 6-DOF joint is used, the initial condition that can be specified here is that of the 3 linear axis. Unfortunately it is not possible to specify joint initial condition for the 3 rotational axis. Thus, this block is added as another method to specify the initial rotational rates of the aircraft.

$$\tau = I\alpha \tag{4.9}$$

Inside the joint, a body sensor is used to impose an instant moment to the aircraft. As shown by Equation 4.9 ,based on Newton's second law of motion for rotational motion, the inertia of the body can be determine once the moment applied to it and the angular acceleration is known. By imposing a random value of moment to the model at the first time step and knowing the value of the timestep as well as measuring the rate generated due to the motion, one can reversely calculate the inertia of the body due to the moment in a single axis. This method is performed for the three rotational axis and the inertia of the aircraft before unfolding for the three rotational axis can be determined. Once determined, the same formula can be used again to determine what initial rate should the aircraft has at the beginning of the simulation.

4.3. Models Types

In this research, three types of the model are created which each will be used for a specific purpose. The main model here is the deployment model, which will includes the deployment dynamics of the aircraft, whereas in the free-flight model and the wind-tunnel model, the simulation begins with the lifting surfaces of the aircraft already deployed. The modeling of the aerodynamics in all the models are the same, however minor changes exist. Other than that, several basic differences also exist between the model and their uses. Thus, in this section, an explanation on the differences and uses of the models will be described. Table 4.3 shows an overview of what the differences the three types of models are.

Free-flight Model	Wind-tunnel Model	Deployment Model
· Aircraft initially unfolded · Aircraft allowed to fly freely · 6-DOF joint used to connect to world frame · For validating with flight test data	· Aircraft initially unfolded · Aircraft grounded to base · Welded joint used to connect to world frame · For validating with AVL results	· Aircraft initially folded · Aircraft deployed · 6-DOF joint used to connect to world frame · For simulating deployment

Table 4.3: Differences between model types

4.3.1. Free-flight Model

The free flight model is used to simulate the aircraft by specifying the initial airspeed and flight path angle of the vehicle. The term free-flight here is used to differentiate between the other model types and to emphasize that the model has no direct link to the world. This is due to the joint used here to relate the aircraft with the world frame is the 6-DOF joint. The free flight model is also used to test the response of the aircraft to basic inputs, and to check the dynamic stability of the aircraft. To do this, two types of free flight models are created, which both focuses on obtaining the stability derivatives of the Simscape model.

The piloted free flight model is one where control strategy is included into the model. The aim of including this control strategy is so that the aircraft can be trimmed in a flight condition specified at the beginning of the simulation. In other words, a trim routine is added by adding a simple controller ahead of the plant of the aircraft and errors between the reference and actual values are corrected with this controller. For this study, since the control strategy included is only for trimming purposes, a simple PID controller is used for all the 4 control inputs to the aircraft, namely the force generated by the aircraft engine, the deflections of the elevator, the aileron and the rudder. The aircraft being considered here does not have any high lift surfaces but the addition of such in another case is possible. The piloted model free flight model is run for 150 seconds just to make sure that the parameters of the flight have converged and is not oscillating when the final values of the control inputs to the aircraft are taken as the trim values.

After obtaining the values necessary to trim the aircraft in steady level flight or steady climb, the unpiloted free flight model is used to check the correctness of the model. Basically, the output values that have converged after running the piloted free flight model is taken as constants that will be included as control inputs to the unpiloted free flight model. This value, along with the final aircraft world speeds, attitudes, altitude and speed are altogether treated as initial conditions of the unpiloted free flight model. Running the unpiloted free-flight model with these values should give out a trimmed steady level flight, which is used for verification purposes.

Other than that, the unpiloted free flight model is the model that is used to check the stick-fixed responses of the aircraft upon the introduction of various control inputs on top of the trim values obtained before. The main purpose of creating a free-flight model is for the validation of the Simscape model with the flight test data, which will be done in Chapter 5.

4.3.2. Wind-tunnel Model

The second type of model created in Simscape is the wind-tunnel model. Similar to the free flight model, for the wind-tunnel model, the simulation starts with the aircraft initially unfolded. The difference here is that the wind-tunnel model is grounded to the base, and is not allowed to move freely in 3D space. This setup is adopted referring to wind-tunnel experiments, where a scaled-model of an aircraft is placed on a strut inside a wind-tunnel, and a freestream is passed through the aircraft. Sensors are generally placed on the strut where forces and moments in various directions are measured. By basing the model with a simple wind-tunnel experiment setup, forces and moments are measured by at the point where the strut is connected to the airframe. The purpose of creating this model is to obtain the stability derivatives of the Simscape model and compare them with another solver, which in this case, is AVL.

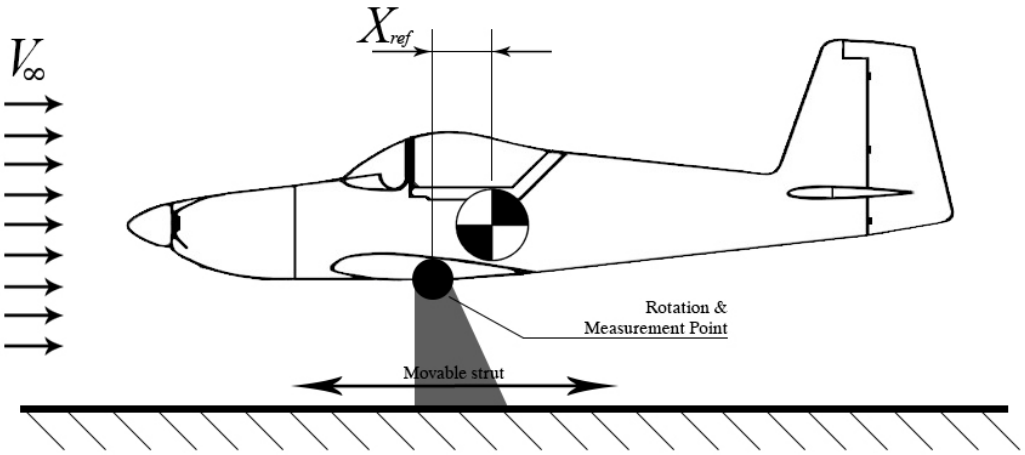

Figure 4.4: Illustration of the wind-tunnel model

Since there are two types of stability derivatives, where one can be measured by leaving the wind-tunnel

model in specified configuration and the other needs to be measured when the model is rotating at a specified rate, two types of models are constructed here. The static wind tunnel model is used to obtain the static stability derivatives of the aircraft, which are changes in non-dimensionalized forces and moments due to the variation of α and β. The second model is more tricky to construct as an imposed motion will need to be applied at the point where the aircraft is connected to the strut. Then, the same procedure to measure, non-dimensionalize and calculate the dynamic stability derivative is used.

As shown in Figure 4.4, the parameter X_{ref} is the distance between where the strut is placed on the model and the centre of gravity of the model. This value will later be varied during the validation process to also compare the trend of the stability derivative with changing X_{ref}.

4.3.3. Deployment Model

The deployment model is the main model created in this study. It includes not only the deployment dynamics of the aircraft, but also the initial condition of deployment which will be the parameters varied during the study, as explained in section 6.3. The simulation runs with the aircraft initially being folded and then unfolds after the specified delays and deployment duration as specified in Table 4.2. A 6-DOF joint is here used to define the relation between the airframe and the world axis and it is essential to use this joint here due to the limitations of the bushing joint described before.

For this model in particular, a simple control is included which helps the aircraft to pull-up. A simple proportional gain is used to convert the value of the flight path angle of the vehicle to the deflection of the elevator. The addition of this control is backed with experiences of the deployment, where without this control, most of the deployment assessed here will fail due to the excess in speed of the aircraft. Also, in practice, due to the already high speed generated in the two deployment scenarios evaluated in this study, the engine of the aircraft produces no force (is turned off) in the deployment model.

Another important thing to notice here is the minor difference between the modeling of the aerodynamics of the deployment model and the other model types. For the deployment model, before the aircraft unfolds its lifting surfaces, the lifting surfaces is not able to produce any aerodynamic forces. This is done by simple including a delay switch after the body sensor which reads the velocities experiences by each specific strip in the aircraft.

5

Model Validation

As with any numerical model created to predict physical phenomenons, a validation of the model created is a necessary step to assure that the results the model gives out is a good representation of what will happen in reality. In this study, the model of the Dash-X aircraft is created to predict the dynamics of the deployment of the vehicle. Although the study focuses on the deployment, the model validation of the vehicle is performed for a fully deployed version of the vehicle. This process is essential to proof that the aerodynamics of the aircraft modeled will be similar to that of the real aircraft.

This chapter focuses on the method of validation conducted in this study. Two validation methods are adopted. First, the wind-tunnel model will be used to extract information regarding the stability derivatives of the aircraft. This data is then compared with the result of an off-the-shelf aerodynamic solver. A description of the theory used to measure the stability derivatives in the Simscape Model is presented. Then, the model's response to basic control inputs are investigated to verify that the created model indeed behaves like a real aircraft. Secondly, the response of the Simscape model will also be compared with actual flight test data of the Dash-X aircraft. For this, the free-flight model of the aircraft will be used and the same control inputs will be applied to the model to check the resemblance and differences in responses between the Simscape model and the flight test data.

5.1. Validation with an Aerodynamic Solver

To compare the dynamics of an aircraft model between solvers, an agreement on what the variables to compare needs to be made beforehand. For this study, it is interesting to show that the aircraft modeled in Simscape will give the same result as the actual aircraft when an external force or input is applied to the model. For a dynamic system, the parameters that is able to describe the dynamic properties of the aircraft is its stiffness and damping values. In aircraft dynamics, these parameters are represented by the aircraft's stability derivatives, which explains how stiff the aircraft is when given a specific control input and how much damping the aircraft has to counteract the inputs. Thus, the stability derivative of the aircraft will be the parameters that is observed and compared in this study.

In this research AVL has been chosen to be the aerodynamic solver, with which the result of the Simscape model will be compared. AVL is able to compute the static and dynamic stability derivative of an aircraft model. This numerical solver is vortex-lattice based, and thus a division of the lifting surfaces is made beforehand. A cosine spacing law is also used to distribute the panels that divide the lifting surfaces in AVL. To perform the analysis in AVL, first a model of the aircraft is made in AVL. Information of the aircraft like planform and sectional airfoil parameters, as well as the geometric data of the aircraft is used to create the AVL model. An important thing to note here is that the same reference point is used in both models. This reference point defines where along the longitudinal axis of the aircraft the forces and moments are measured; thus it is critical to have the same point when comparing the data. However, to not only evaluate one set of

data, different reference point are used in this research and these different set of data will be compared later to show the differences or similarites in the trend of several major stability derivatives.

After obtaining the stability derivatives data from AVL, now the same values should be retrieved from the Simscape model. As said before, the model used here is the wind-tunnel model, where the aircraft is grounded to the world frame and the model experiences a headwind with varying angles. The method used to calculate the static stability derivatives slightly differs than the method used to calculate the dynamic stability derivatives, and thus different sub-type of the models are used. An explanation of these models have been explained in section 4.3.2.

$$C_{L_\alpha} = \frac{\partial C_L}{\partial \alpha} \qquad C_{D_\alpha} = \frac{\partial C_D}{\partial \alpha} \qquad C_{l_\alpha} = \frac{\partial C_l}{\partial \alpha} \qquad C_{m_\alpha} = \frac{\partial C_m}{\partial \alpha} \qquad C_{n_\alpha} = \frac{\partial C_n}{\partial \alpha} \tag{5.1}$$

$$C_{L_\beta} = \frac{\partial C_L}{\partial \beta} \qquad C_{D_\beta} = \frac{\partial C_D}{\partial \beta} \qquad C_{l_\beta} = \frac{\partial C_l}{\partial \beta} \qquad C_{m_\beta} = \frac{\partial C_m}{\partial \beta} \qquad C_{n_\beta} = \frac{\partial C_n}{\partial \beta} \tag{5.2}$$

Equations 5.1 and 5.2 shows the definitions of the static stability derivatives with respect to α and β. This equations becomes the basis of how the static stability values are acquired from the model. For example, Figure 5.1a shows the relationship of the lift coefficient and the angle of attack of a full aircraft. From this graph, the gradient of the curve is the static stability derivative C_{L_α}. The same is true for a graph relating the drag coefficient, the rolling moment coefficient and other coefficient of an aircraft.

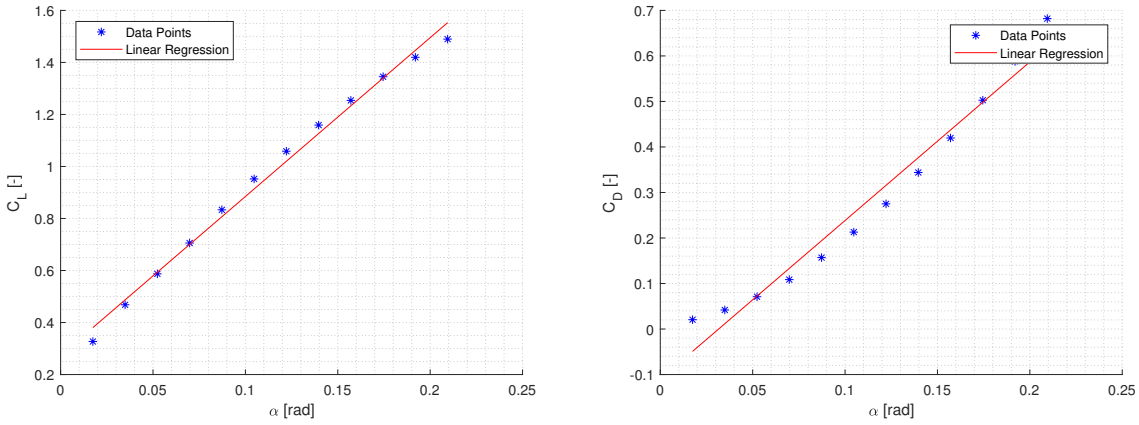

(a) (b)

Figure 5.1: Variation of (a) C_L & (b) C_n with α of the Simscape model

Basically, to obtain the static stability derivatives, the Simscape wind-tunnel model will be set at a specific angle of attack or sideslip angle and forces and moments are measured for that angle of attack or sideslip angle. These forces and moments are then non-dimensionalised and stored. The process is done for various angle of attack or sideslip angle and the results are then plotted in a graph. From the data obtained, a linear regression method is used to find the linear line that best fit the scatter of data points. By using linear regression, the linear line plotted to represent the data points has the least amount of error. This should then be a good representation of the data. The gradient of this line is then taken as the static stability derivatives. This process is shown in Figure 5.2 in the form of a flowchart.

As shown in Figure 5.1, not all of the data points can be well represented with the linear regression method. A very good approximation of the line can be seen in the C_L versus α curve. The representation of the C_D versus α curve with a linear line is however not as good as the C_L versus α curve. This means that with the current simple method of obtaining static stability, the value of C_{D_α} might not be as reliable as the data for C_{L_α}. The relation of C_D and α generally follows a higher order polynomial, and is therefore not easy to be represented with a linear curve. This is contrary to the relation between C_L and α below the stall point, which is easily represented with a linear curve.

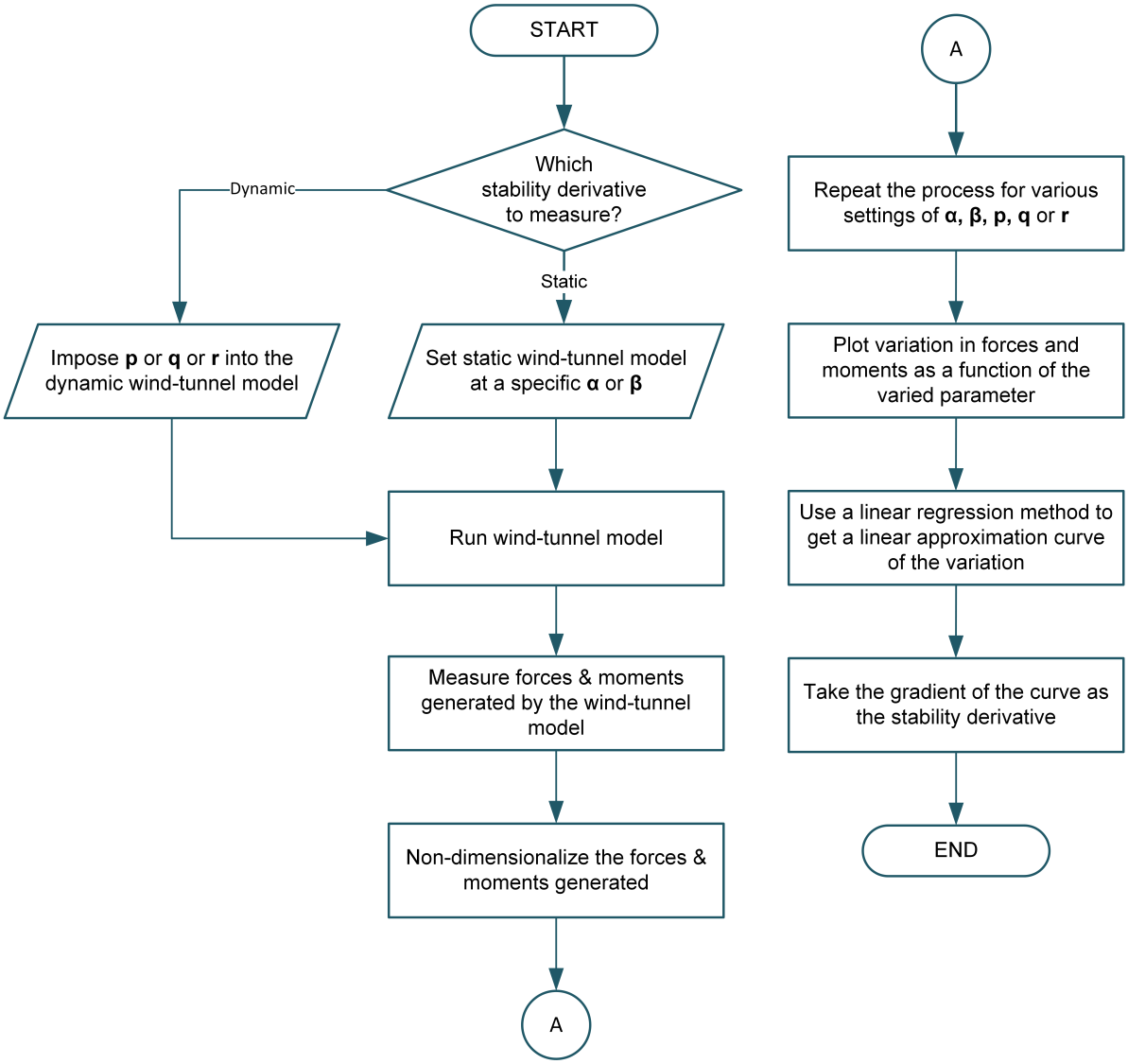

Figure 5.2: Method to obtain the static & dynamic stability derivatives from the Simscape model

$$C_{L_p} = \frac{\partial C_L}{\partial \frac{pb}{2V}} \quad C_{D_p} = \frac{\partial C_D}{\partial \frac{pb}{2V}} \quad C_{l_p} = \frac{\partial C_l}{\partial \frac{pb}{2V}} \quad C_{m_p} = \frac{\partial C_m}{\partial \frac{pb}{2V}} \quad C_{n_p} = \frac{\partial C_n}{\partial \frac{pb}{2V}} \tag{5.3}$$

$$C_{L_q} = \frac{\partial C_L}{\partial \frac{qc}{2V}} \quad C_{D_q} = \frac{\partial C_D}{\partial \frac{qc}{2V}} \quad C_{l_q} = \frac{\partial C_l}{\partial \frac{qc}{2V}} \quad C_{m_q} = \frac{\partial C_m}{\partial \frac{qc}{2V}} \quad C_{n_q} = \frac{\partial C_n}{\partial \frac{qc}{2V}} \tag{5.4}$$

$$C_{L_r} = \frac{\partial C_L}{\partial \frac{rb}{2V}} \quad C_{D_r} = \frac{\partial C_D}{\partial \frac{rb}{2V}} \quad C_{l_r} = \frac{\partial C_l}{\partial \frac{rb}{2V}} \quad C_{m_r} = \frac{\partial C_m}{\partial \frac{rb}{2V}} \quad C_{n_r} = \frac{\partial C_n}{\partial \frac{rb}{2V}} \tag{5.5}$$

The dynamic stability derivatives used in this study is defined in Equations 5.3 to 5.5 The calculation of the dynamic stability derivatives is similar to the static ones, but different in one single way. Instead of fixing the wind tunnel model at a fixed angle of attack with respect to the headwind, a constant rate angular motion is imposed to the model. The constant rate of angular motion is used to avoid the effect of inertial moment of the body as a response of the model due to the angular acceleration. However, due to the rotation of the vehicle, especially when pitching and yawing angular motion is imposed, the effect of the change in the model's angle of attack and sideslip angle may cause the readings to also have unwanted components. Therefore,

it is decided to measure the values of only the initial time step of the simulation, where the model has not change its position and thus, the forces and moments generated will only be due to the motion imposed. Then, the same procedure is done as the measurement of the static stability derivatives, where the forces and moments generated for every variation in magnitudes of angular rates imposed is plotted in a graph and the gradient of the plotted values are then taken as the dynamic stability derivatives. Figure 5.2 shows the process of obtaining the dynamics stability derivatives from the Simscape model.

For the validation process, several major stability derivatives are selected to be plotted and discussed. As stated before, several comparisons of these parameters are shown by changing the reference point along the longitudinal axis of the aircraft in both the AVL and the Simscape model. In this study, the C_{m_α}, C_{m_q}, C_{L_q}, which are the stability derivatives that varies with the changing of the reference points are taken to be compared.

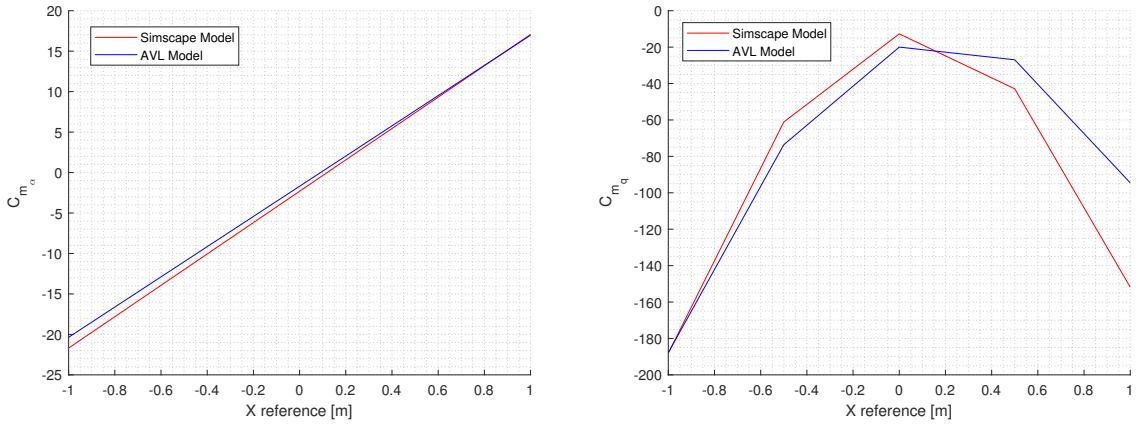

(a) (b)

Figure 5.3: Variation of (a) C_{m_α} & (b) C_{m_q} with changing reference point along the aircraft longitudinal axis

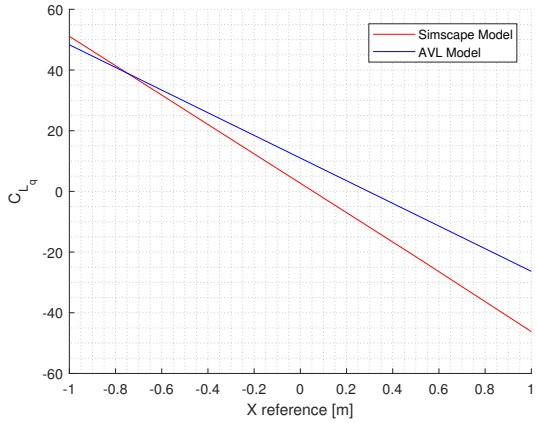

Figure 5.4: Variation of C_{L_q} with changing X_{ref}

Variations of the stability derivatives considered is shown in Figures 5.1 & 5.4. Differences in the trend the 3 graphs has are due to the limitations of each of the solver used. For instance AVL does not consider the profile drag of the lifting surfaces modeled in the model, whereas the Simscape model, basing its aerodynamic data from an open source wind-tunnel experiment [55] does incorporate the profile drag values of lifting surfaces. This is very visible in Figure 5.4, where the values of the dynamics stability derivative C_{L_q} drops at a rate that is higher than the AVL model. Although both graphs shows a similar trend of reduction with increasing X_{ref}, the rate by which these values drop are not alike. This is also observable in Figure 5.3, where although the trend are similar for both values, the rate by which the graph increases or decreases differs.

The Simscape model also does not consider interactions of lifting surface between as is done in AVL. This means that the downwash produced by the main wing that in practice influences the performance of the empennage lifting surfaces are not considered. This is a limitation of the Simscape model created in this study and causes the value of C_{m_α} measured from the Simscape model to generally be lower than the AVL model. A reason for this is the effectivity of the horizontal stabilizer of the Simscape model which is always higher due to the lack of modelling of the interactions between lifting surfaces. This, amplified with the fact that the tip loss effect of the lifting surfaces which is not modeled in the Simscape model, causes the the difference in the C_{m_α} and C_{m_q} values of both models.

5.2. Model Response to Basic Inputs

In this section, the model's response to various basic control inputs will be presented. The selected control input here is a quick step input (can also be regarded as an impulse input), and will be treated as inputs to the model in addition to the trim control deflection angles. Thus, the aircraft is first trimmed at a specific velocity and altitude, and then the external input in the form of a step input will be given in the elevator, aileron and the rudder of the aircraft. This step will be treated as a verification step of the model, to show how the model inherently behaves when given such control inputs.

Before checking the response of the model to external inputs control inputs, first an investigation on how the trim deflection angle of the elevator changes with airspeed is conducted. The created model is run multiple to obtain the values of the trim deflection angles and thrust required to maintain a steady level flight on the given airspeed. The trim elevator deflection angles for every airspeed is logged and plotted to show how the elevator deflection angle varies with increasing airspeed.

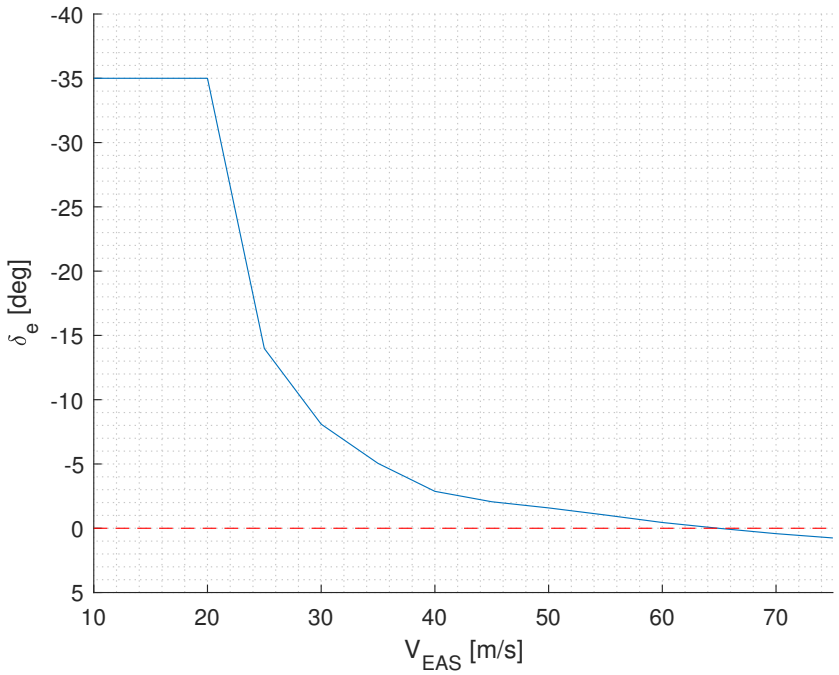

Figure 5.5: Variation of trim elevator deflection angle with airspeed of the Simscape model

Figure 5.5 shows this trend specifically. The purpose of conducting this test is to verify that the variation of the trim elevator deflection angle resembles of a normal aircraft, where with increasing altitude and speed, less deflection angle is required to be given to trim the aircraft. This test also shows that for the limited amount of thrust the aircraft has and the limited throw the elevator has, the aircraft can only go so slow before it stalls. At this point, the velocity by which the aircraft stalls is called the stall speed of the aircraft. From Figure 5.5, it can be said that the stall speed of the aircraft model is around 20 m/s. For speeds below 20 m/s, the elevator

angle goes to a constant value of 30 degrees. This is because of the upper limit of the elevator throw of the horizontal stabilizer, which is 30 degrees.

Indeed judging by the way the elevator changes with airspeed, the created model behaves as an aircraft should be. With increasing airspeed, the magnitude of the force generated due to the deflection of the control surface also rises. This means that for the same amount of deflection an elevator has, the forces at higher speeds is considerably higher, due to the quadratic relation of the aerodynamic forces with speed. Thus, a smaller amount of elevator deflection is sufficient to give the same counteracting pitching moment to the airframe, which prevents the aircraft from pitching up. From Figure 5.5, the elevator deflection trend also follows a quadratic trend and is asymptotic to a value of above the zero degree line. Increasing the airspeed further will only reveals that the change at higher speed will not be as significant as the change in lower speeds. At an airspeed value around 65 m/s, the sign of the elevator deflection angle switches from negative to positive. This indicates that at this point, the moment experience by the aircraft at its centre of gravity switches from a pitch down moment to a pitch up moment and thus, the elevator needs to compensate for this change.

After having an idea that the created model behaves as a real aircraft should behave, now step input will be given as additional inputs to the model to check how the model copes with sudden external inputs. First, the response of the aircraft to a step input in the elevator will be examined, followed by the model's response to step input on the aileron and the rudder. The Simscape model is run at a trim speed of 35 m/s and the step input is introduced 1 second after the simulation starts for 0.1 seconds. For all the step inputs introduced tom the model, a maximum control angle deflection is applied.

Response to Step Elevator Input

The variation of flight parameters as a response of the step input to the aircraft is presented in Appendix A of this report. As shown in Figure A.1, the flight path angle and airspeed of the vehicle varies after the introduction of the step input to the elevator. It can be clearly seen from Figure A.1a that at the moment the step input is introduced, the flight path angle jumps to a high value and suddenly drops before oscillating in a very lowly damped manner. This high jump is the short period mode of the aircraft, whereas the lowly damped gradually converging motion of the aircraft shows the phugoid motion of the aircraft. From this, it can be clearly seen that the model created is able to show the two longitudinal eigenmodes of an aircraft, which verifies the created model in this research. Due to the sudden introduction of a step input, the aircraft suddenly pitches up, and the airspeed suddenly falls. This is also denoted by the sudden spike in pitch rate generated by the maneuver in Figure A.3b. However, this spike is directly followed by an negative spike which is less in magnitude and during the phugoid motion, the pitch rates experienced by the aircraft is considerable less. Like the other longitudinal flight parameters, the angle of attack of the vehicle also spikes at the introduction of the step input.

On the contrary to the longitudinal parameters, the lateral and directional parameters of the flight varies as well, but with a much lower value. The deviation of the roll attitude and rates as well as the yaw attitudes and rates are very low compared to the pitch attitudes and rates. Although these values are rather small, they seem to not converge to a constant value like the pitch attitude and rate of the vehicle. This may very well be an indication that the aircraft considered here might not be stable in the spiral mode. However, this is not very visible when observing Figure A.6, which shows the aircraft trail of movement. In Figure A.6b, the red star indicates the starting point of the aircraft in the simulation. The altitude of the aircraft oscillates due to the phugoid motion and the aircraft moves in a fairly straight manner.

Response to Step Rudder Input

The graphs showing the changes in flight parameters due to the introduction of a step input in the aircraft's rudder is shown in Appendix A of this report. As the rudder is the control surface that is deflected, the yaw rate of the aircraft caries significantly higher compared to the other two angular rates of the vehicle. However, due to the fact that the lateral and directional axis of an aircraft is coupled, the introduction of a step input in the directional axis also has a considerable but not as significant effect on the vehicle's lateral axis. This is denoted by the variation in Figures A.10b and A.8b. The heading angle of the vehicle also quickly changes.

However, although the yaw rate varies greatly at the moment the step input is given to the aircraft, the yaw and roll rate of the vehicle quickly dampens out. Again, as noticed before, these values however does not converge to a constant value but rather continuously drops, which could be the indication of an unstable spiral mode.

This claim is again backed with the observation of Figure A.12, which shows the course of the aircraft movement in space. The deviation of the aircraft in the Y direction is far significant than the previous case. The altitude of the aircraft drops after the maneuver, but at very slow rates.

Response to Step Aileron Input

Like the previous two cases, the graphs showing the variation in the flight parameters due to the introduction of an aileron step input is presented in Appendix A. Judging by the way the aircraft moves after the introduction of the step input, the aircraft goes to a converging spiral, as shown in Figure A.18. The diameter of the spiral decreases in time, and the altitude of the vehicle also drops considerably. This is also shown with the general increasing value of the airspeed, although, in several points, decreases due to the orientation of the vehicle denoted by the flight path angle and pitch rates which oscillates as a response of the vehicle in the spiral motion.

The roll attitude of the aircraft settles at a specific value, since the aircraft is not corrected to fly in a straight manner again. However, the attitude keeps on decreasing even when very little roll rate is experienced by the vehicle. The roll experienced by the vehicle is very high in magnitude at the moment the step input is imposed on the vehicle, but dampens out very quickly. This is not the case with the pitch and yaw rates, where the values persist to change with time.

5.3. Validation with Flight Test Data

A model of an aircraft is said to be a good representation of the actual aircraft if the model is able to give similar responses as the actual aircraft, if the same control inputs are imposed in the model. By basing the validation process with the flight test data with the statement above, a process to compare the way the Simscape model behaves to the similar control inputs given to the actual aircraft during flight test is made.

Flight test data are generally noisy, and it is not rare that pinpointing a timeframe where the aircraft is steady before performing a maneuver is not an easy job. The aircraft considered in this research has performed several flight test and from the flight test data evaluated, the one where the aircraft performs a roll doublet maneuver will be considered here.

In principle, to test whether the model created will give similar responses as the actual aircraft during flight test, first, the time by which the maneuver of interest is conducted during the flight test will needs to be determined. The starting point here will be the time where the control inputs is started to be introduced to the aircraft. Generally, comparisons of model responses and flight test data should not be done for longer than 10 seconds due to the build up of error between the model responses. Any comparison longer than 10 seconds will leads to the results diverging and thus the result is not any more comparable. Thus, the flight test data to be considered is from the beginning of the maneuver until 10 seconds after maneuver. The selection of the maneuver starting point also defines what the initial condition of the simulation of the model will be. The initial condition here defines how the aircraft is oriented, at which speed and altitude the aircraft is flying as well as what the angular rates that the aircraft is experiencing are. These values are then treated as the ϕ_0, θ_0, ψ_0, V_0, h_0, p_0, q_0 and r_0 at the beginning of the simulation. Unfortunately, due to the limitations of data from the flight test, angular accelerations of the aircraft are not measured and thus this might effect the differences at the beginning of the simulation for the angular rates comparisons.

After setting the initial times as well as defining the initial condition of the simulation model, the next step is to trim the Simscape model at the initial altitude and speed. Once trimmed, the aircraft simulated will have trim control surfaces values. However, it is very unlikely that the trim control surfaces values of the actual aircraft and the Simscape model will be the same. A possible reason for this is the weight data of the

aircraft for the flight test might not be the same as for the model. In this study, the model is being simulated at maximum payload and the reduction of weight due to the burning of fuel is neglected. This may play a role in the difference in the responses of the aircraft. Due to this differences, the control surface inputs from the flight test data needs to be adjusted and multiplied by a gain, whose values are to be determined by a trial and error method. The equation used to adjust the control inputs from the flight test data to the Simscape model is expressed by Equations 5.6, 5.7 and 5.8. In the end, due to these differences, the final control surface inputs to be applied to the model is represented by Equations 5.6, 5.7 and 5.8. The simulation is then run for the amount of time specified. The adjusted flight test data inputs used here for the roll doublet maneuver is shown in Figure 5.6.

$$\delta_a = K_a \left[\delta_a - \delta_{a_t}\right]_{FT} + \left[\delta_{a_t}\right]_{Model} \tag{5.6}$$

$$\delta_e = K_e \left[\delta_e - \delta_{e_t}\right]_{FT} + \left[\delta_{e_t}\right]_{Model} \tag{5.7}$$

$$\delta_r = K_r \left[\delta_r - \delta_{r_t}\right]_{FT} + \left[\delta_{r_t}\right]_{Model} \tag{5.8}$$

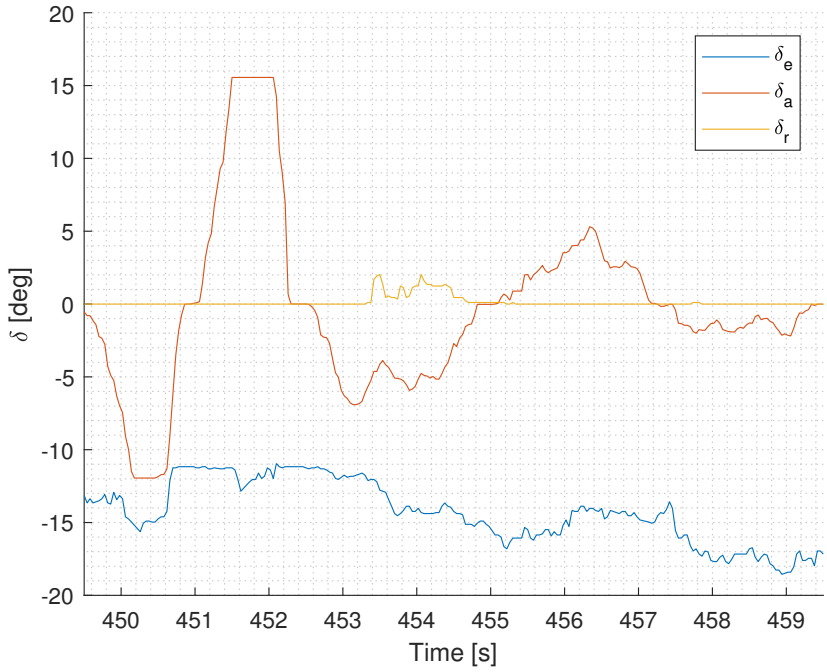

Figure 5.6: Adjusted elevator, aileron & rudder control inputs to the Simscape model which defines the roll doublet maneuver

As shown in Figure 5.6, to perform the roll doublet, an aileron deflection angle of around -12 degrees is first imposed to the model for around half a second and then directly followed by an aileron deflection of +15 degrees for around the same amount of time imposed to the Simscape model. The magnitudes of the inputs here are adjusted to the model from the original flight test data, but the time at which the controls are given are not changed. After the variation, the inputs of aileron for the remaining period is taken as well for consistency purposes. However, even this measure have been taken, the amount of error caused by the differences in the Simscape model's response and the actual flight test data is still going to pile up and causes the response of the aircraft to diverge after a certain amount of time. Other than the aileron inputs which is the major input for a roll doublet maneuver, the control inputs for the elevator and rudder are also taken and included as input signals to the Simscape model.

The comparisons between the roll attitude and roll rate of the Simscape model and the flight test data is shown in Figure 5.7. The original data of the roll rates from the flight test shows a lot of noise and thus a

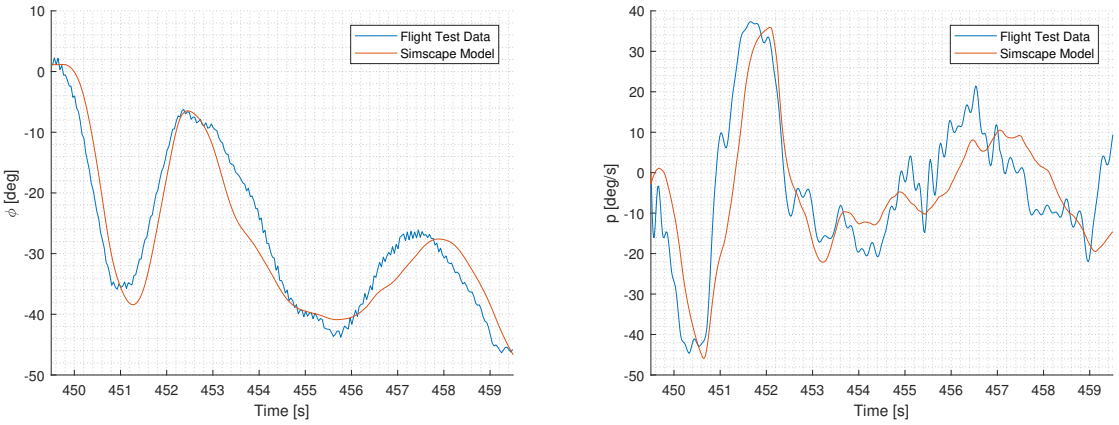

(a) (b)

Figure 5.7: Comparison between the (a) roll attitude & (b) roll rate response of the Simscape model and actual flight test data

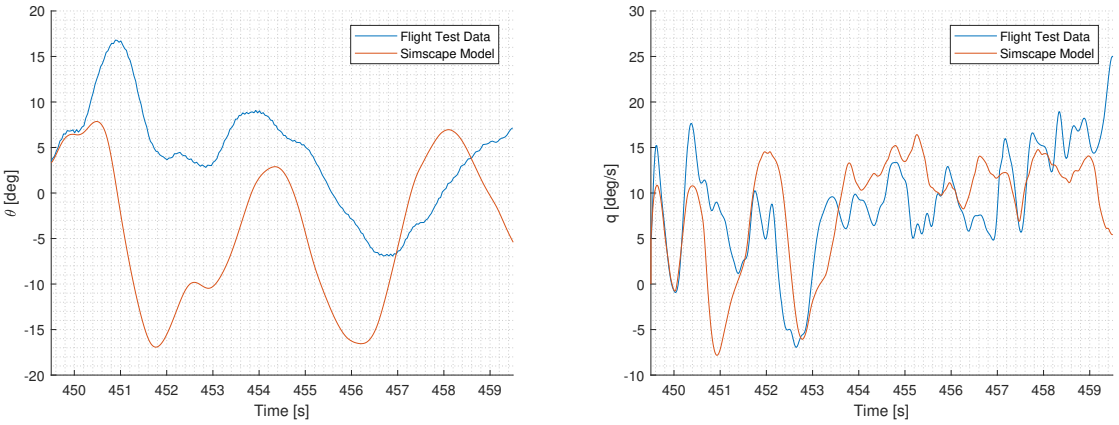

(a) (b)

Figure 5.8: Comparison between the (a) pitch attitude & (b) pitch rate response of the Simscape and actual flight test data

low-pass filter is used here to filter out the high frequency noise in the data. The instrument used to measure the rates during flight test is a gyroscope, as one of the modules in the built in IMU (Inertial Measurement Unit) of the flight control module. Such noises might be a result of the use of no damping between the flight control module and the airframe, and thus the frequency of the airframe during flight might also be captured in by the IMU. The comparison of the rates is then made between the Simscape model result and the filtered flight test roll rate data. Comparing with the flight test data, both the roll attitude and the roll rates of the aircraft shows good resemblance. This shows that the model created in Simscape is able to represent the dynamics of the actual aircraft. Considering the fidelity of the modeling of the aerodynamics of the Simscape model, the results presented here is considered to be very good. However observing the data closely reveals that the initial rate of the two data is not the same. A possible reason for this is that the angular acceleration of the aircraft at that specific point is not incorporated and imposed into the Simscape model. This actually is crucial information as this will determine in which direction the aircraft is actually rotating to due to the angular acceleration of the vehicle at that specific point. This is also shown by the slight difference in the time by which the roll attitude of the aircraft started changing. From Figure 5.7a, seeing the first few seconds of the two curves shows that the response of the Simscape model is falling behind the flight test data. This also might be the cause of the roll acceleration of the vehicle which is not available and not included in the Simscape model simulation.

Different to the comparisons of the roll and roll rates, the comparisons of the pitch and pitch rate of the

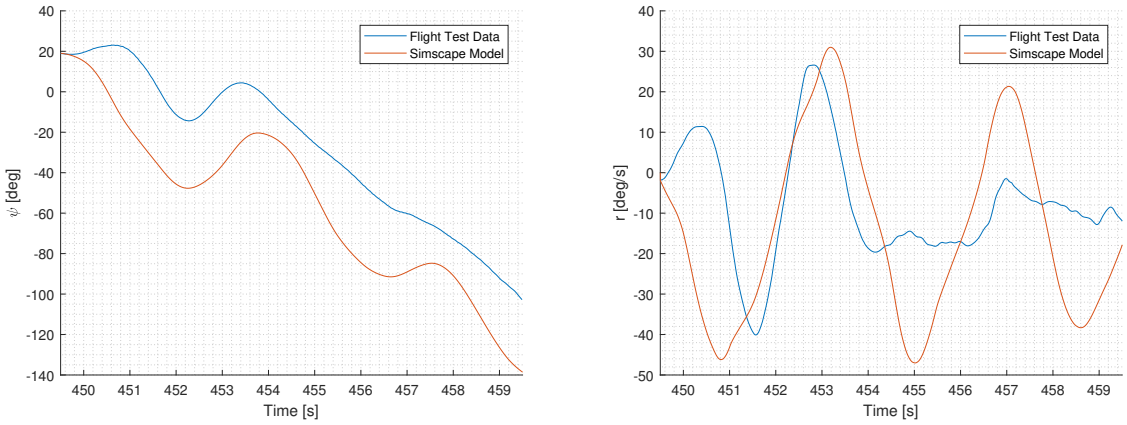

(a) (b)

Figure 5.9: Comparison between the (a) yaw attitude & (b) yaw rate response of the Simscape model and actual flight test data

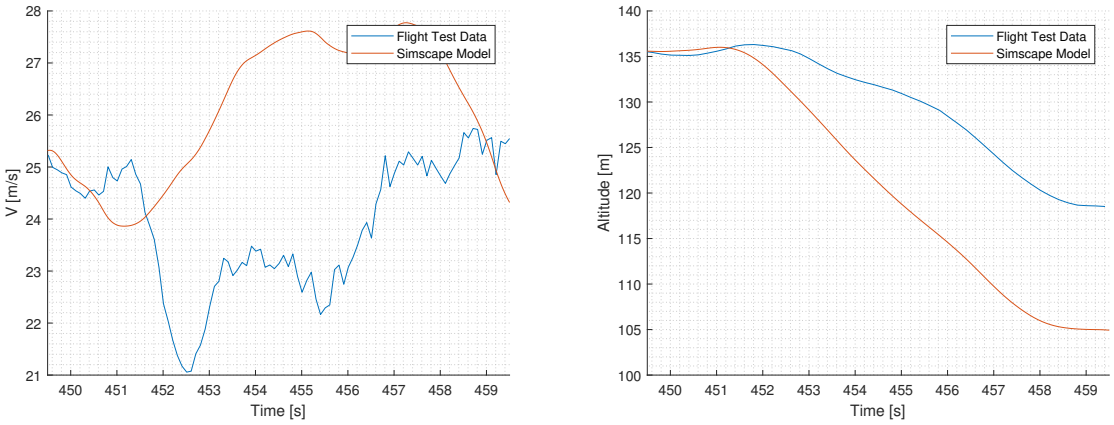

(a) (b)

Figure 5.10: Comparison between the (a) airspeed attitude & (b) altitude response of the Simscape model and actual flight test data

Simscape model and the flight test data does not show the same level of resemblance as the roll data. Again, for the rates, the data has been filtered with a low-pass filter due to the noise captured in the measurement. From Figure 5.8a, the pitch attitude of the vehicle is only for the first few seconds with the flight test data alike. The same can be seen in the pitch rate comparisons. Another observation is the magnitude of the pitch rate here due to the control surfaces inputs is not similar to the flight test data, depicted by the peaks of the pitch attitude during the introduction of the roll doublet maneuver. The damping of the aircraft from the pitch point of view is also not as high as the actual flight, where after the maneuver, the pitch attitude varies less than with the flight test data. However, the pitch rates of the Simscape model is much more varying than the pitch rate from the flight test.

The same can also be observed in the comparisons of the yaw and yaw rates. Although it begins at the same point due to the imposed initial condition of the yaw attitude, the yaw of the Simscape model goes to another direction as to the actual aircraft during flight test. The rates are also opposite in direction for both models. The Simscape model is first trimmed and the initial condition of the flight test is imposed into the model. This method of imposing a motion into a trimmed model without including the angular acceleration, as with the other 2 attitudes, could cause this difference. In reality, at the timeframe by which the flight test data is cut, the aircraft is nowhere near its trimmed condition. Instead, for the comparison here, a trimmed aircraft model is imposed by the initial condition of the determined point and the simulation is run. This may very well be the major cause of difference in the way the aircraft behaves in both the pitch and yaw axis. After the

maneuver, the trend of the yaw attitude similar to the flight test, although the values are not. In both cases, the aircraft then rotates to a more negative yaw attitude. The timing in which the yaw attitude of the aircraft increases and decreases are also comparable between the two model. The yaw damping of the Simscape model is also not similar to the actual aircraft, seen by the slow reduction of the yaw rate of the Simscape model as compared to the actual aircraft.

After comparing the three attitudes and rates of the Simscape model and the flight test data, now a comparison of the altitude and airspeed will be made. Figure 5.10 shows this very comparison. For the altitude, a GPS module as an extension to the flight control module is used and for the measurement of the airspeed, a digital airspeed sensor which was placed at the right wingtip is used. The airspeed values greatly differs after the maneuver. This is due to the drop in altitude as shown in Figure 5.10b which is much sooner in the Simscape model than the flight test. Throughout this study, the weight of the aircraft is also kept constant during the simulation runs and a maximum payload is used for all simulations. This assumption might also be the cause in difference between the attitudes and rates in the comparisons, especially for the longitudinal parameters of the aircraft as well as the airspeed and the altitude. Thus, the difference in the model's pitch attitude, pitch rates, airspeed and altitude might be influenced by this assumption made in this study.

6

Deployment Safety Assessment

After completing the first and second phases of the research, in this section the method the writer has taken to perform the third and final phase will be explained. As the title of the study is the deployment safety assessment of a deployable UAV, the research should in principle incorporate the evaluation of the safety of deployment. But what is actually defined as a safe deployment, what are the possible cases that may happen during the deployment of a morphing UAV and how will the safety of deployment be assessed? The answers to these questions will be presented in this chapter.

6.1. Assessment Method

In Section 2.5, we have decided that to assess the stability of the deployment, first a screening method will be performed. This screening method will reveals what are the parameters in the set of the deployments initial condition that have minor or no effect at all to the safety of the deployment, within the ranges considered in this research. In principle, there are several screening methods available in the literature that can be adopted here, but the simplest and most straightforward one is the one-at-a-time screening method by Morris[41].

$$d_i(x) = \frac{[y(x_1, x_2, x_3, ..., x_{i-1}, x_i + \Delta, x_{i+1}, ..., x_k) - y(x)]}{\Delta} \tag{6.1}$$

With Morris' one-at-a-time screening method, it is possible to understand which inputs have a high impact on the overall result of a simulation. The method is also able to predict whether interactions between parameters do exist. In essence, the method varies one parameter at a time in a specified range, whereas the other parameters of the inputs are kept constant. This means that if a combination of input parameters result in a failed deployment, the most likely explanation to the cause of failure is due to the change of the varied input or due to the interaction of the varied input with another parameter in the set. With this method, the changes in the output parameter is observed and quantified with respect to the change made by the varied parameter. In other words, a gradient (or termed "elementary effects" by Morris) is calculated which shows the effect the varied parameter has on the observed output parameter, as expressed in Equation 6.1 . Thus it is also necessary to specify which parameter in the output of the simulation that needs to be observed.

For the deployment safety assessment however, the parameter to be evaluated is the safety of deployment, which is a binary variable. The variable "safety" will only have 2 values, either "1" to denote that deployment have been successful or "0" to tell that the deployment had failed. This means that conventional one-at-a-time screening method will not be capable to get the degree of change of the observed output parameter due to a change in the input parameter. Thus a modification needs to be made on the method to make it suitable to be used in

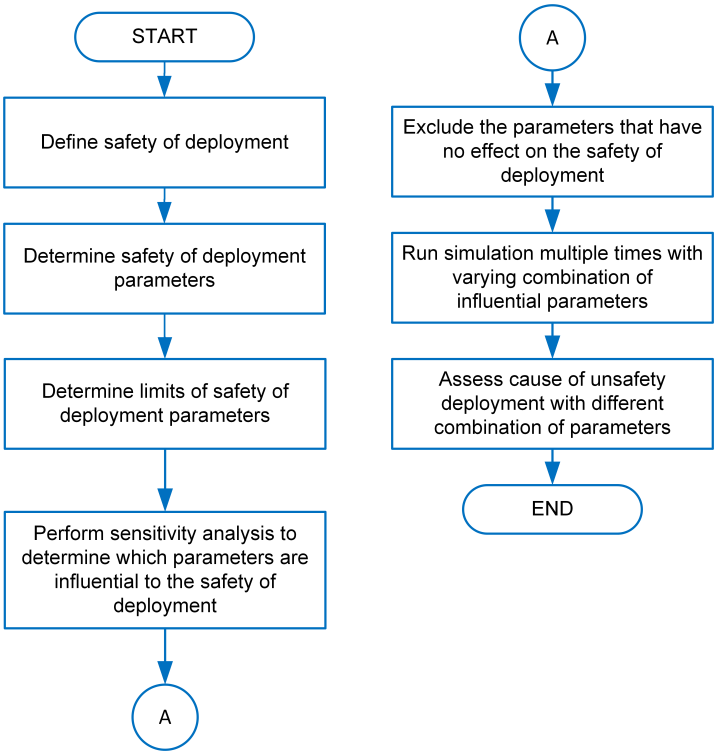

Figure 6.1: Deployment Safety Assessment Method Flowchart

In this study, a modified version of the one-at-a-time screening method is formulated which will be suitable to reveal the influential and non-influential parameters in a binary output system like this one. Instead of calculating the degree of change due to the variation of a parameter, the modified method calculates the amount of failed deployment in the specified range of input parameter. There is of course a possibility that when the range of input parameter is extended or narrowed, the result of the influential parameter might be different. Therefore, the definition of the range of input parameter needs to be universal, and encompasses a wide range of possible values. In other words, the screening method developed here is very sensitive to the range of input parameters and extreme care needs to be made when defining the input parameter range.

After being able to determine which input gives a big effect on the safety of deployment, the next step is to select these influential parameter (or exclude the uninfluential parameter) from the simulation. Three of the most influential parameter will be selected in this study so that the visualization in the form of a 3D graph can be made in the next chapter. With the range being specified previously, the three most influential parameter are varied and a the deployment is run multiple times with varying these parameters. Whether or not a deployment will be safe is thus determine by evaluating the safety deployment parameters. All in all, the process of assessing the deployment is described in the form of a flowchart in Figure 6.1.

6.2. Definition of Safe Deployment

Referring to the literature review performed before the start of this research, in this research, the definition of a safe deployment is as follows:

"A deployment is considered safe if none of the aircraft's structural or aerodynamic limits are surpassed and if the deployed aircraft goes to a controllable flight regime after the deployment"

From this definition, there are two different sections of the sentence that defines the safety of deployment. The first is related to the structural and aerodynamic limits of the aircraft. This structural part is pretty

straightforward, as exceeding the structural limits of an aircraft may cause the airframe to break during deployment. For this study, two parameters which defines the structural limits of the aircraft is taken, namely the never exceed speed of the aircraft (V_{NE}) and the load factor of the aircraft (n).

The aerodynamic limits meant in this statement is the stall angle of attack of the lifting surfaces. This is taken as a measure due to the fact that if the lifting surfaces that has a control surface is stalled, then the effectiveness of the lifting surface is greatly reduced. Due to this phenomenon, the stall angle of attack of the lifting surfaces is taken as the one of the limits in this study.

The second section of the definition of safety of deployment related to the controllability of the aircraft after the deployment. Basically, if an aircraft is able to regain control after the deployment when control is imposed, the deployment is said to be safe. A flight is classified as controllable if the angular rates of the aircraft converges after deployment, or the angular motion of the aircraft is damped in time. Due to this definition and from observations of the different results of different deployments in this study, the the safety of a deployment is classified into three different categories, from the perspective of controllability. To show an example for each category, the yaw rate of the vehicle considered here will be presented for the three different categories and differences will be pointed out. These examples are shown by Figures 6.2, 6.3 and 6.4.

The safety deployment parameters are shown in Table 6.1 along with what is the safety concern for the parameters are. After defining the parameters, upper and lower limits of the parameters will need to be set. This will later be treated as hard limits, that is, if in a simulation the values of one or more of these safety deployment parameters are crossed, the deployment is regarded as a failed deployment.

Safety Concern	Safety Deployment Parameters
Structural Limits	V_{NE}, n
Aerodynamic Limits	α_{MW}, α_{HT}, β_{VT}
Controllability	p, q, r

Table 6.1: Safety deployment parameters to be evaluated throughout the simulation

Deployment with Converging Rate Values

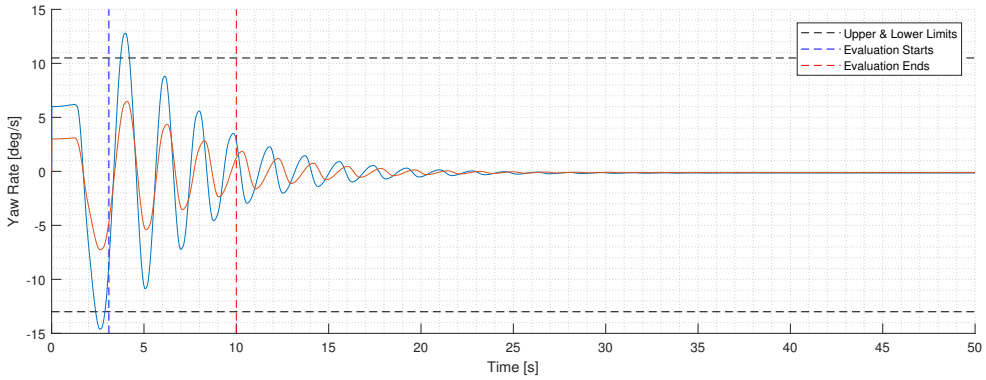

Figure 6.2: Example of deployments with converging rate values

If the rate values of the aircraft converges to a certain value after the deployment, the deployment will be classified as a safe one. This is a very general description, and thus needs to be narrowed down. Here, time as a variable is introduced. How long should the aircraft's rate values be allowed to oscillate, although a convergence pattern is seen will need to be determined. The time by which the safety deployment parameters starts to be evaluated also needs to be specified.

In this study, each simulation will be run for 10 seconds, which includes the deployment of the vehicle. The evaluation of the parameters defining the safety of deployment will start 1 second after the aircraft is fully deployed. Thus, referring to the aircraft's deployment sequence table (Table 4.2), this evaluation begins in the

3.1th second of the simulation. From this time on, if an observed safety deployment parameter crosses either the upper or lower limit of the parameter, the simulation will be stopped and deemed an unsafe one. On the other hand if from this point on none of the observed parameter crosses the safety deployment parameter limits, the simulation is deemed safe from the controllability perspective.

Figure 6.2 shows the variation of the yaw rate values as an example of a deployment which is controllable. Here, two graphs are shown and both of them converges in the end. However, the difference is that, due to the way the safety is defined in this paper, the red line is considered to be a safe deployment, whereas the blue line is not. This is because right after the start of the evaluation, the blue line crosses the upper limit of the safety deployment parameter and triggers the stopping of the simulation. Thus, the deployment is treated as an unsafe deployment. This type of unsafe deployment verdict is certainly possible in the assessment method defined in this study.

Deployment with Persisting Rate Values

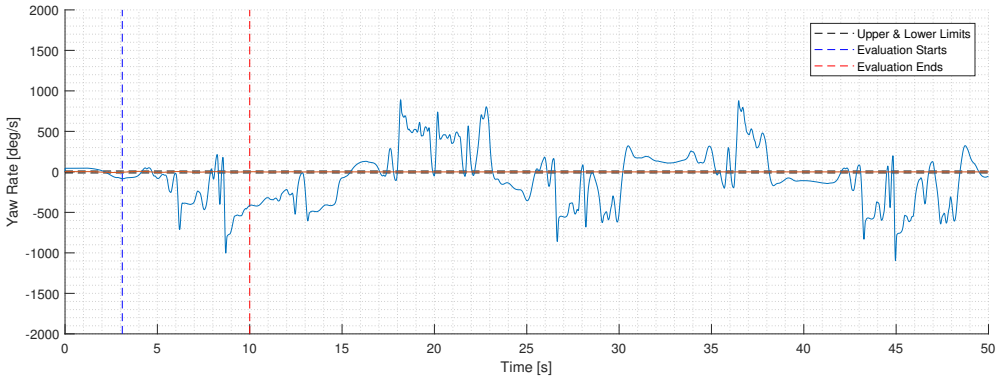

Figure 6.3: Example of a deployment with rate values that persists

In practice, it is also possible to have an aircraft whose rates oscillates and is underdamped. In such cases, the rate values of the aircraft will persist after the deployment. This can be troublesome if the oscillating rates are too high for the control surfaces to counter. On the other hand, if the values are able to be countered by the control surface, the deployment may be classified as a safe one.

Figure 6.3 shows an example of a yaw rate variation of a deployment that first diverges and reaches very high values, and then oscillates and is not underdamped even after leaving the simulation running for 50 seconds. Such a case is treated as a deployment with a rate value that persist. However, if we are only to observe the simulation from the time the evaluation begins to the time the evaluation starts, it is seen that the value of the yaw rate actually diverges from the initial value and reaches values up to around 1000 deg/s.

Deployment with Diverging Rate Values

The third category is one where the aircraft goes to an erratic motion and the rates of the aircraft goes to a value that is not able to be countered by the control surfaces. In such cases, the deployment is deemed unsafe. Figure 6.3 can be seen as a deployment with diverging rate values due to the fact that the rate values then increases from the initial rate values of the deployment. This is another way to look at this deployment case considering that the rates the aircraft experiences is far greater than the rate by which the deployment starts with. However, in other cases, it might also be the case that after a certain amount of time, the aircraft then regains speed due to the loss of altitude and the rate values converges. In this study however, since the evaluation of the safety deployment parameters begins at the 3.1th second of the simulation, these types of simulation will be deemed unsafe. Figure 6.4 shows the yaw rate variation of such a deployment, where the values are erratic at the beginning, but converges after a certain period. The deployment scenario here is of Scenario 1, which is a mid-air deployment of a UAV from a canister that is slowed down by parachute.

In short, the deployment of an aircraft is deemed safe or unsafe in this study if all of the safety deployment

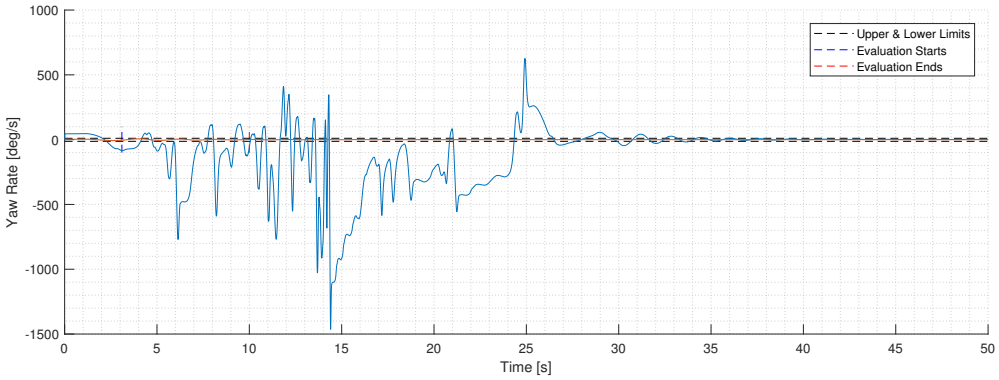

Figure 6.4: Example of a deployment with diverging rate values

parameters does not cross the specified limits. Theses includes the structural limits, the aerodynamic limits as well as the way the of the aircraft's motion develops over time. The concern from the controllability point of view is not the magnitudes of the rates, but more into the development of the rate values over time. However, due to limitations of this study, a restriction in rate values are imposed as hard limits since the beginning of the evaluation. Figure 6.5 shows an illustration of how all these classification falls in the safety deployment space. The goal here is to know where in the deployment space the aircraft is still safe to be deployed and when unsafe, what the cause of this unsafeness is.

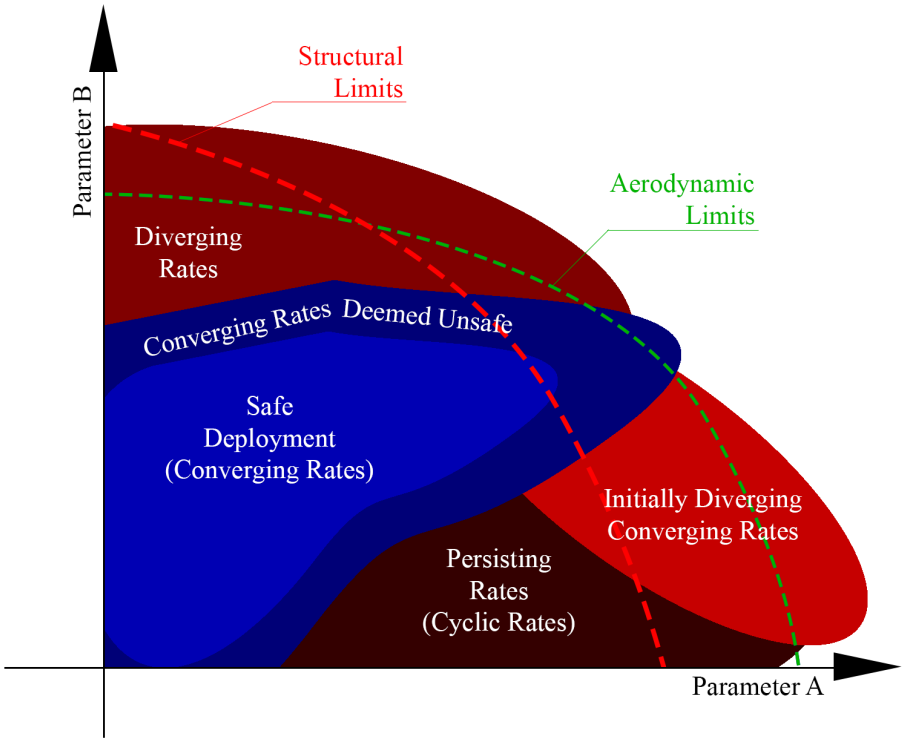

Figure 6.5: Illustration of different classification of zones in the deployment space

6.3. Simulation Input Parameters

For this study, the input parameters which will be varied defines the initial condition of the deployment. The input parameters used are case specific and unmeaningful inputs or a specific case is not included. For instance for the ground-to-air deployment, the initial altitude parameter is a non-varying parameter. Ranges of the input parameter used also varies between different deployment scenarios considering the nature of the deployment.

The included input parameters in this study consist of the launch speed, the initial attitude of the aircraft during deployment, the initial angular rates experienced by the aircraft caused by external factors such as wind or misalignment of deploying mechanism and the initial altitude by which the deployment takes place. Table 6.2 shows the different input parameters for the different deployment scenarios considered in this study.

	Scenario 1		Scenario 2		
Input Parameter	Lower Limit	Upper Limit	Lower Limit	Upper Limit	Unit
V_0	0	10	55	75	m/s
h_0	4000	8000	4000	8000	ft
ϕ_0	-	-	-45	45	deg
θ_0	-135	-45	0	45	deg
ψ_0	-45	45	-	-	deg
p_0	-28	28	-28	28	deg/s
q_0	-23	28	-23	28	deg/s
r_0	-13	10	-13	10	deg/s

Table 6.2: Ranges of Simulation Input Parameters

7

Results & Discussions

In this chapter, the result of the deployment safety assessment will be presented. First, results of the screening method applied to all three scenarios will be presented and followed by the discussion of the results for the three scenarios. For each scenario, an analyses of a single successful deployment will first be presented followed by the analyses of the safety deployment space obtained after performing the deployment safety assessment. Here, the different regions of deployments will also be discussed and example points representing a failed/successful deployment will also be discussed.

7.1. Results of the Screening Method

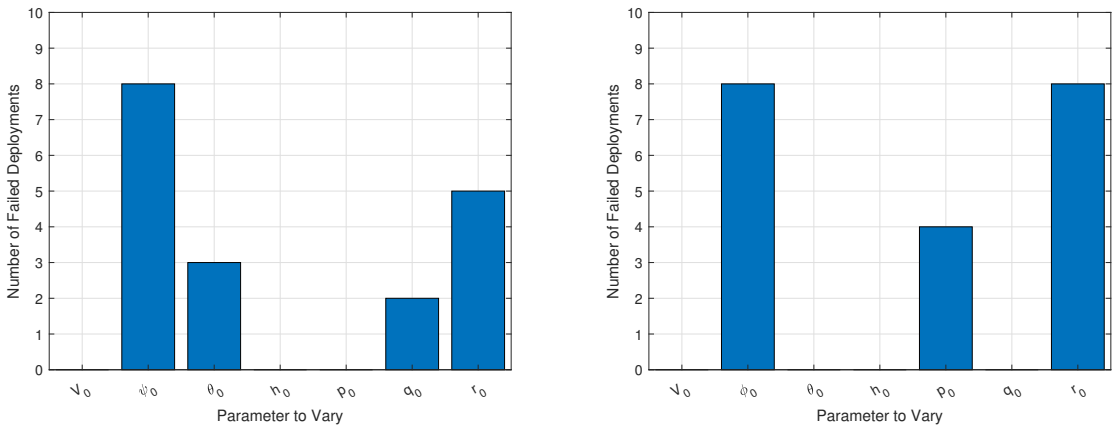

(a) (b)

Figure 7.1: Result of the screening method for (a) Scenario 1 & (b) Scenario 2

Figure 7.1b shows the result of the screening method for both scenarios assessed in this study. Running the deployment model in scenario one and changing varying one parameter at a time reveals that the influential deployment parameter for scenario 1 in the range specified are the initial yaw attitude, initial yaw rate and initial pitch attitude. The initial pitch rate also has an influence on the deployment safety within the ranges specified however since the number of failed deployments are less than the three other parameters, this value will not be treated as a highly influential parameter.

On the other hand, with the screening method, it is revealed that varying the launch speed, the initial altitude and the initial roll rate does not have any effect on the safety if deployment. In other words, no matter what

values are taken in the range specified, varying these parameters will not causes the deployment of scenario 1 to fail. Of course, by using the modified screening method, it is unknown how high a parameter might has a combined effect with another parameter to influence the safety of deployment. This is a limitation of the modified screening method used here.

From Figure 7.1a shows which variation of parameter causes the deployment of the aircraft to be jeopardized. It is understood here that initial roll attitude, initial roll rate and the initial yaw rates are the influential parameters that effect the safety of deployment. Other parameters however is not influential at all, at least from the default scenario 2 deployment specified.

With the screening method performed for both scenarios, the infuential parameters for each deployment scenario can be specified. Thus, in the next assessment method of both scenarios, only these parameters will be varied and the safety deployment space created will be a function of these parameters.

7.2. Scenario 1: Deployment from a Canister Slowed Down by a Parachute

7.2.1. Analysis of a Single Successful Deployment

In this scenario, the aircraft is initially contained inside a canister and is brought to altitude by means of a carrier aircraft. The aircraft then detaches the canister in a bomb dropping manner and upon descending, a parachute pops out of the canister to slow it down. After being slowed down, the canister opens, the UAV slides out of it, unfolds itself and goes to operation. For this case, a single successful deployment is presented. The input parameters used for this successful deployment is shown in Table 7.1.

Input Parameter	Value	Unit
V_0	5	m/s
θ_0	-90	v
h_0	6000	ft
ψ_0	0	deg
p_0	0	deg/s
q_0	0	deg/s
r_0	0	deg/s

Table 7.1: Input parameter values for a single successful deployment of Scenario 1

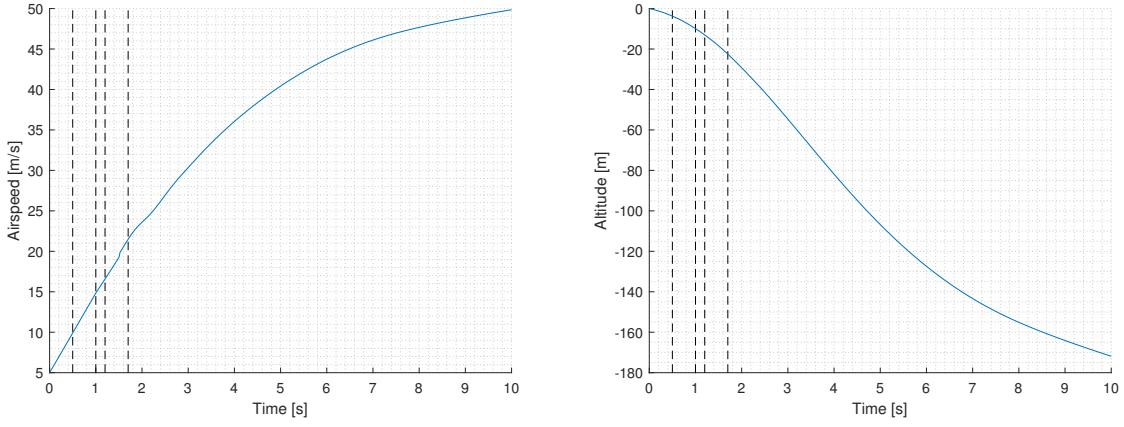

(a) (b)

Figure 7.2: Change in (a) airspeed & (b) altitude of deployment scenario 1

Because the deployment observed here is symmetric, that is, no lateral and directional input parameters have been used, only the variation of the parameters here will be observed. Figures 7.2 to 7.4 shows the changes

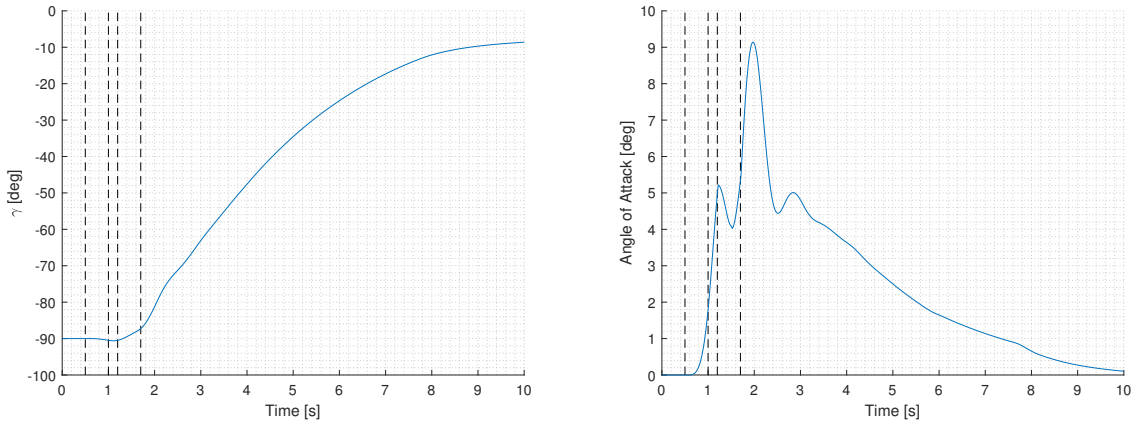

(a) (b)

Figure 7.3: Change in (a) flight path angle & (b) angle of attack of deployment scenario 1

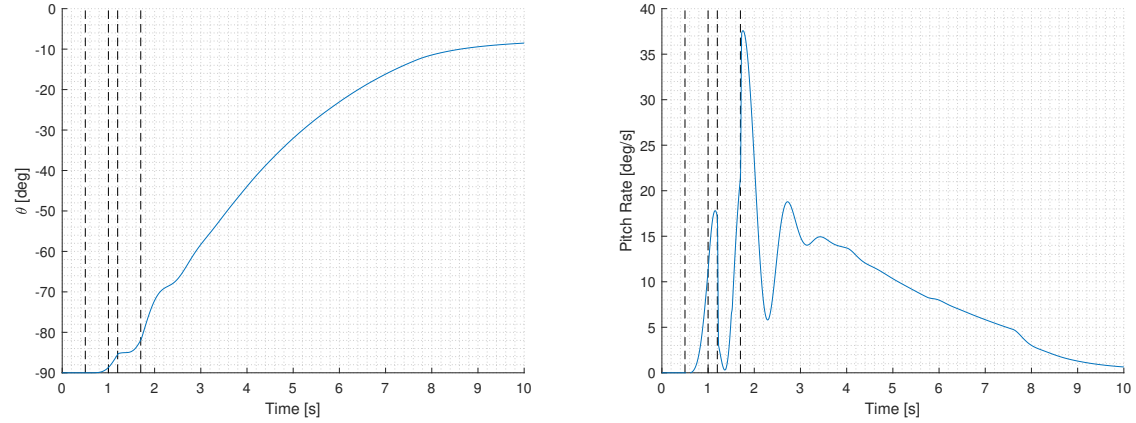

(a) (b)

Figure 7.4: Change in (a) pitch attitude & (b) pitch rate of deployment scenario 1

in flight parameters for a successful deployment of scenario 1. The first 4 vertical dash lines indicates when in time the deployment of the horizontal tail, main wing, vertical tail and telescopic of the main wing is respectively. Since the deployment observed here is a downward vertical deployment, the airspeed increases considerably as the altitude decreases. Not that the values displayed in Figure 7.2b is the change in altitude of the aircraft and not represent the actual values of the altitude. Figure 7.2 shows how the deployment of the lifting surfaces actually have very little effect on the changes in both these values.

This is not the case for the changes in the other 4 parameters, shown in Figures 7.3 to 7.4. Although the body velocity of the aircraft at which the lifting surfaces are deployed are relatively low, this still has an effect on the variation of the flight path angle of the vehicle. The simple pull up control used in the deployment model causes the flight path angle to increase with time. The value peaks at around -10 degrees, where the speed of the aircraft is not anymore able to compensate for the drag generated by the aircraft and thus, running the simulation longer will shows that the flight path angle will again drop. In reality, before this happens, the engine of the aircraft can be turned on and a more sophisticated control can be incorporated into the aircraft to prevent the flight path angle to again drop.

However, the parameter where the effect of the unfolding of the lifting surfaces are clearly visible are the angle of attack and the pitch rates. As can be seen, before the unfolding of the horizontal tail, both of these values are constant at 0. The moment the horizontal tail unfolds, the aircraft experiences a positive pitching moment due to the generation of aerodynamic forces at the rear part of the aircraft. The rise in the value is exponential

and is stopped when the main wing deploys. But the effect of the main wing is not instantly felt. Instead, at the moment the main wing is deployed, the angle of attack rise due to the horizontal tail introduction is still dominant. It is not until around the time the vertical tail is deployed, which is around the same time the main wing has completely been rotated, that that the rise in these two values are halted, and the values reduces instead. The rise of the values again right after the fourth vertical dash line is due to the extension of the main wing, which also causes the aircraft to pitch up. After the aircraft has been fully deployed, the values drops again and settles at a certain value. The reduction in the angle of attack and pitching moment values after the unfolding process is due to the pull-up control used here, which makes the aircraft always have a positive angle of attack and pitching moment. This will goes on unless the aircraft reaches a positive flight path angle, which is due to how the pull-up control is defined. These variations in the parameters due to the unfolding of the lifting surfaces are however less visible in the pitch attitude variation.

7.2.2. Deployment Safety Assessment Results

After understanding the influential parameters from the result of the screening method and the dynamics of the vehicle experienced during a successful deployment, in this section the influential parameters will be varied and different sets of these parameters will be used as inputs to the simulations. Multiple simulations will be run and a safety deployment space will be obtained, which shows which combination of these highly influential parameters will result in a safe deployment.

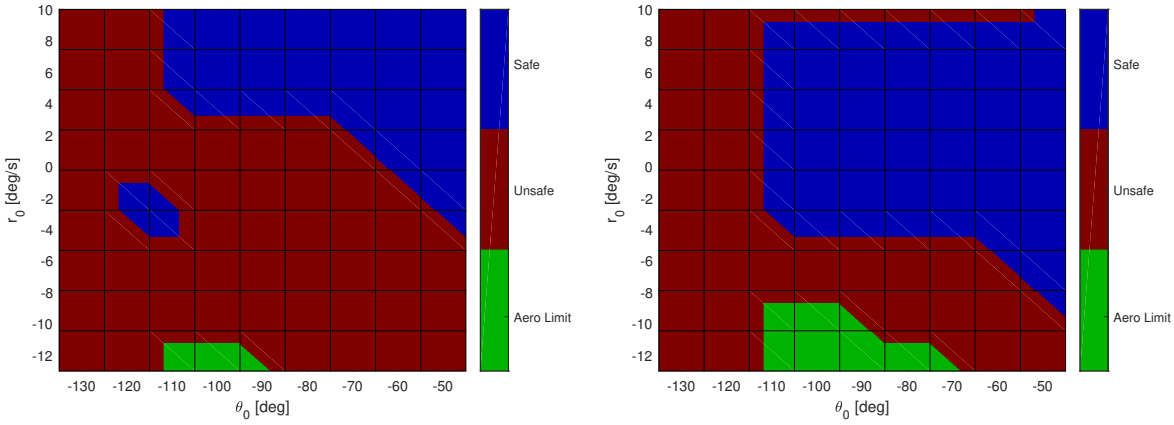

(a) (b)

Figure 7.5: Safety deployment space of scenario 1 for yaw attitude values of (a) -15 & (b) -5 degrees/s

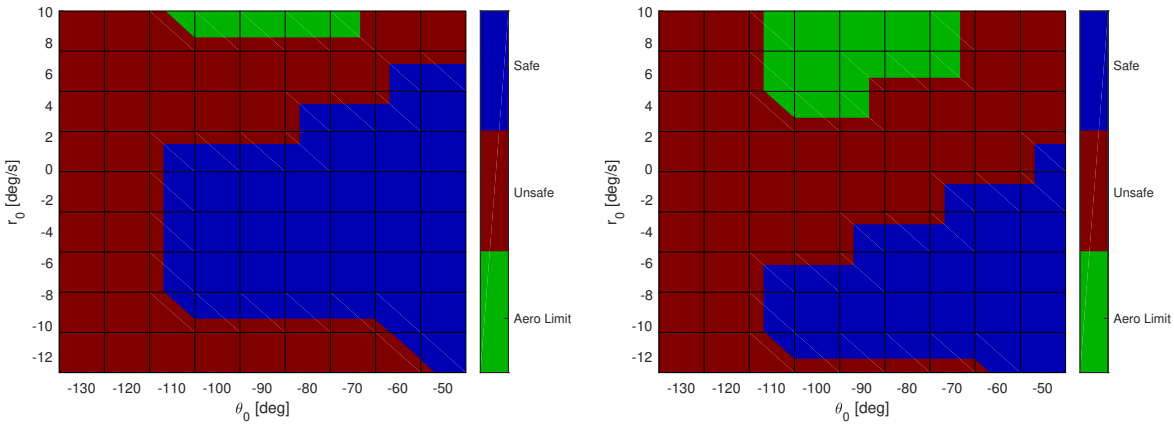

(a) (b)

Figure 7.6: Safety deployment space of scenario 1 for yaw attitude values of (a) 5 & (b) 15 degrees/s

Performing the simulation multiple times with varying combination of influential parameter gives out the safety deployment space as depicted in Figures 7.5 and 7.6. In these figures, the blue zone represents an area of successful deployment and the red zone shows the area of failed deployments. The green zone shows an unsafe deployment area where the aerodynamic limits of the aircraft causes the deployment to be deemed unsafe. An observation here is that an initial pitch attitude value lower than -105 never result in successful deployment, except for the one case in Figure 7.5a. In this deployment, the initial yaw attitude is -15 deg/s, the initial pitch attitude is -115 and the initial yaw rate is -2.5 deg/s.

Observing the change in the safety deployment space for the 4 figures also reveals that with increasing initial yaw attitude, the sliced safety deployment space tends to move downward in the graph. The area also reduces in size with increasing initial yaw attitude value. This shows that to have a successful deployment, an increase in the initial yaw attitude value needs to be compensated with the decrease in the initial yaw rate of the aircraft. This is intuitively correct, since a difference in sign of the initial yaw rate as compared to the initial yaw attitude will correct the aircraft orientation towards the ground, thus causing the aircraft to experience less sideslip and less drag. This allows the aircraft to descend in a cleaner manner as less oscillation will be experienced in the directional axis, and quicker speed increase will also be possible.

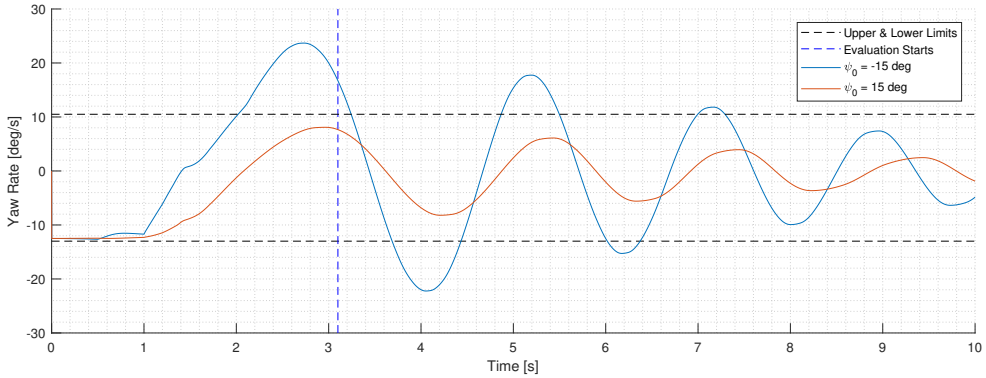

Figure 7.7: Comparison of yaw rate variation of deployments with different initial yaw attitudes

This phenomenon is clearly shown in Figure 7.7. For the variations in yaw rate of the deployment, the input parameters used are the same, except for the initial yaw attitudes. The deployment in this case is deemed unsafe, because the yaw rate values of the deployment is higher than the allowable value even at the beginning of the deployment. But seeing the trend, the yaw rate evidently converges in the end. Such a deployment then falls to the category converging rates, but deemed unsafe, as depicted by the dark green zone in Figure 6.5. The reason behind this is because in this study, the aircraft needs to already be controllable 1 second after it is completely unfolded. Thus, due to the cap defined, this deployment is considered unsafe.

Another zone of failed deployment that is worth mentioning is one where the value of the initial pitch attitude is lower than -105. In this zone, the pitching moment of the aircraft is so great due to the unconventional initial orientation of the vehicle during deployment that the vehicle actually experiences very high pitch rates. Another possible cause to the failure here is the use of the proportional gain to control the deflection of the aircraft, which causes the elevator to be fully deflected, thus creating a high pitching moment on the aircraft. With the increase in time, the aircraft losses altitude and increases speed and thus the increase in pitching moment generated is exponential. Figure 7.8 compares the angle of attack and pitching moment variation for two deployment with the same input parameters, except the initial pitch attitude values. The initial yaw rate here is 2.5 degrees/s and the initial yaw attitude is -5 degrees.

At the time the evaluation of the safety deployment parameters begins, the angle of attack of the body, which is the same as the angle of attack of the main wing and the horizontal tail (due to no interactions between bodies and lifting surfaces), is still within the allowable range. The pitch rate however, as predicted is the one parameter that causes the deployment to fail, since it triggers the upper limit of the allowable pitch rate. Again, in this case, the deployment is deemed unsafe not because the values of the rates are diverging, but rather because at the evaluation timeframe, the values of the pitch rate is still higher than the allowable value. This deployment again falls into the category converging rates, but deemed unsafe. Postponing the beginning

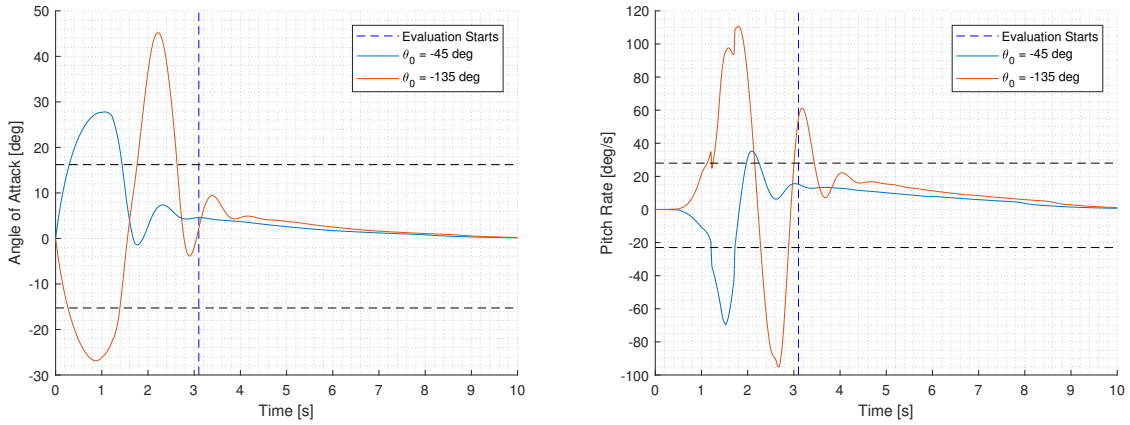

(a) (b)

Figure 7.8: Variation of (a) angle of attack & (b) pitching rate for deployment with different initial pitch attitude value

of the evaluation period may lead causes this deployment to be deemed safe.

For deployment scenario 1, with the ranges of input parameters defined in this study, no deployment falls into the category diverging rates. It is also understood that for all the combination of influential parameters used, none of the failed deployment is caused by the crossing of a structural deployment parameter. Hence, there are no regions of failed deployment due to structural limits in the safety deployment space. The whole spectrum of deployment which are deemed unsafe here are due to the cap defined in this study. In other words, if the cap is to be removed and the aircraft is allowed to be controllable at a later stage, all of the deployments will be safe. This means that to reach actual failed deployment zones in the deployment space, higher combination of values will have to be used. To illustrate this, an extra deployment case which is outside the input parameter range is simulated.

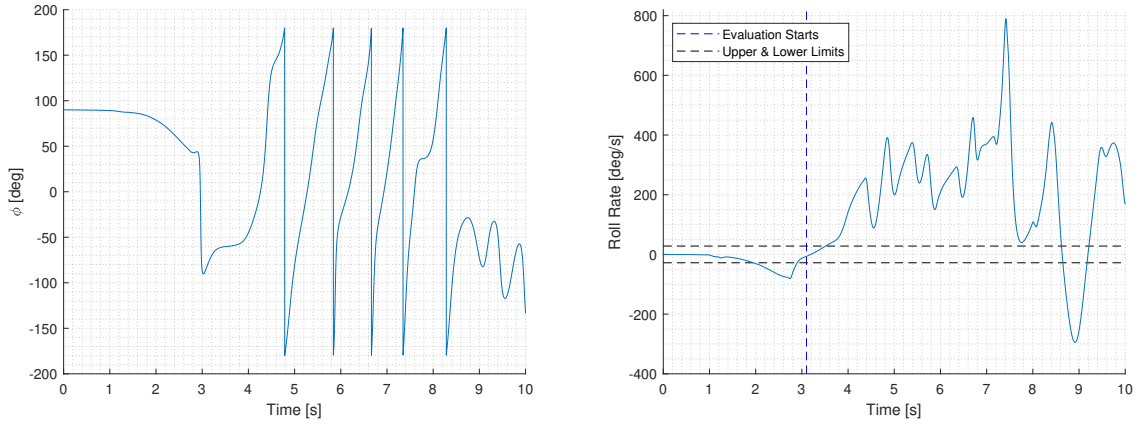

(a) (b)

Figure 7.9: Variation of (a) ϕ & (b) p for a deployment where the rates diverges

By using a value of -90 deg, -45 deg and -23.935 deg/s for the initial pitch attitude, initial yaw attitude and initial yaw rate respectively, a deployment classified as diverging rate is obtained. The initial deployment values above are taken so that the divergence is still observable and an understanding on what physical phenomenon is happening to the vehicle during the deployment can be explained. Taking higher values of yaw rates causes the deployment to diverge even further and the flight parameters later goes to extreme values. Although the initial deployment parameters used in this simulation specifically states that the initial pitch attitude and initial yaw attitude of the vehicle is -90 deg and -45 deg, but the values of these parameters starts at -45 deg in Figures 7.10a and 7.11a. This is because for this specific deployment scenario, the order by which

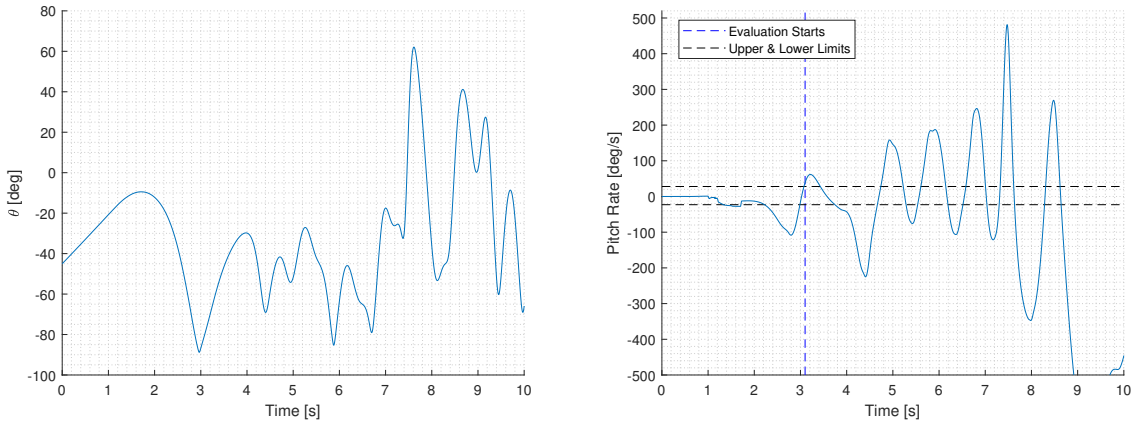

(a) (b)

Figure 7.10: Variation of (a) θ & (b) q for a deployment where the rates diverges

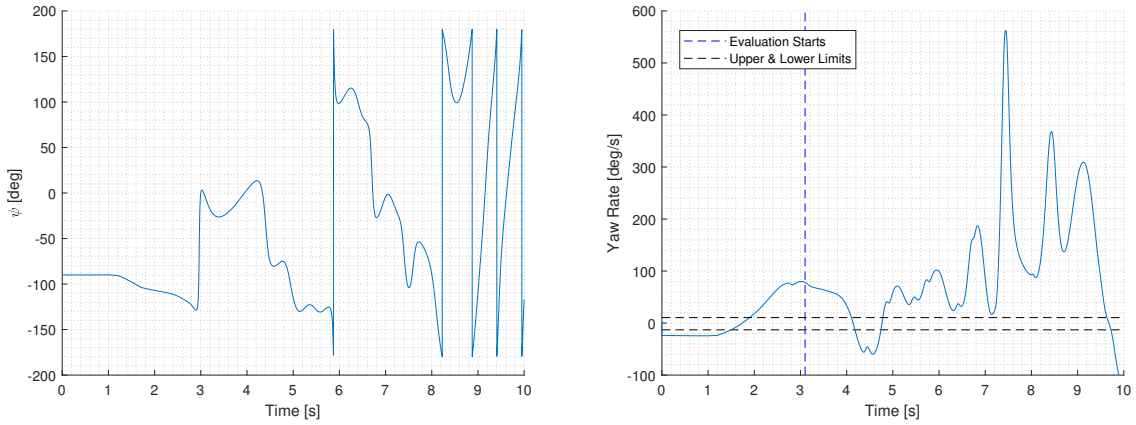

(a) (b)

Figure 7.11: Variation of (a) ψ & (b) r for a deployment where the rates diverges

the rotations of the vehicle at the beginning of the simulation is pitch-yaw-roll. A reason for not using the 3-2-1 rotation (yaw-pitch-roll) is to be able to simulate a condition where the aircraft is being rotated sideways at the beginning of the simulation, while still facing the ground due to the nature the deployment is defined.

For this deployment, the roll, pitch and yaw rates all diverge after the aircraft unfolds and the values jumps to considerable values, as shown in Figures 7.9b, 7.10b and 7.11b. It can be said that the time the deployment diverges, the values not only diverges at one axis of the vehicle, but on all the three rotational axis. Starting at the beginning of the simulation, the values for all the angular rates of the vehicle keeps on increasing until around the 7th second after the deployment, where the value drops for all the angular rates and then increases again before the end of the simulation. At this 7th second after the start of the deployment, the airspeed of the vehicle, which goes to a more or less steady value after the start of the evaluation, spikes for an instant and then oscillates again. But judging by the way the aircraft is oriented pitch-wise in this moment, the aircraft should actually loses speed since the pitch attitude of the aircraft is positive. The only possible explanation is that even though the aircraft is oriented upwards, the aircraft moves backwards and losses altitude with the nose of the aircraft still facing the sky. This is proven to be true when evaluating the X component of the body velocity, which is shown in Figure 7.13. This is again repeated between the 8th and 9th second, where the airspeed spikes, but the X component of the body velocity is negative. However, due to this phenomenon of moving backwards, the development of the rates of the aircraft which keeps on oscillating to higher values is in fact halted, which might be regarded as a stabilizing natural movement of

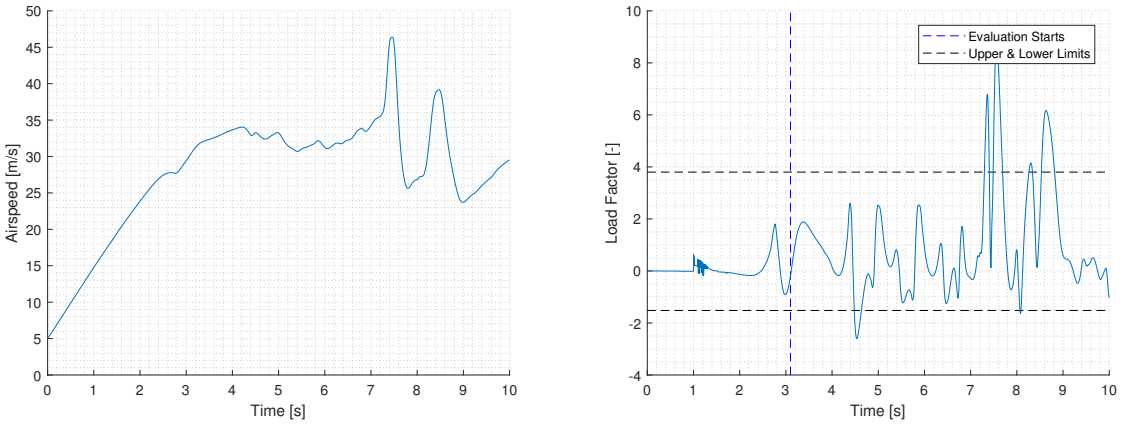

(a) (b)

Figure 7.12: Variation of (a) airspeed & (b) load factor for a deployment where the rates diverges

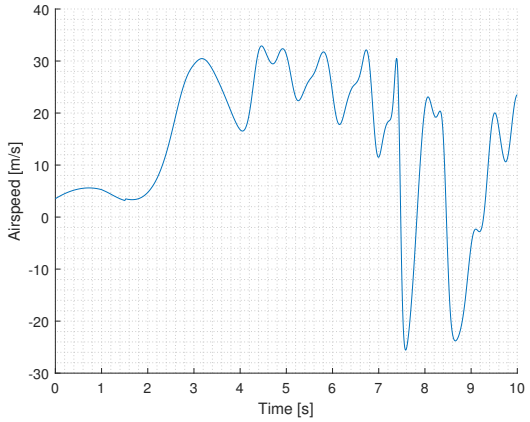

Figure 7.13: Variation of X component of the body velocity of the aircraft

the aircraft. In short, observing the way the aircraft behaves attitude-wise reveals that the aircraft starts with the deployment, goes on a continuous rotation (most visible in the roll and yaw attitude of the aircraft) and at the 7th second, the aircraft gains altitude although moving backwards and the development of the ever increasing rates of the aircraft comes to a stop.

Although may be regarded as a stabilizing natural occurrence of the aircraft, the moment the aircraft goes backwards, the load factor of the aircraft spikes multiple times and goes beyond the upper limit as shown in Figure 7.12b. This means that the aircraft's structural limits has been surpassed and thus, although previously regarded as a stabilizing phenomenon, it has other negative effects in the vehicle. All in all, for such a deployment, in which the aircraft rotates more than twice in a second in most of its rotational axis, the deployment is clearly unsafe. However, as an extra deployment case which is outside of the range specified, this deployment gives an overview of what a diverging deployment might look like.

7.3. Scenario 2: Deployment from Under the Wing of a Carrier Aircraft

7.3.1. Analysis of a Single Successful Deployment

For the second scenario, first an analysis on what actually happens when the aircraft is successfully deployed with this type of deployment scheme is conducted. The aircraft is detached from under the wing of a carrier

aircraft at an altitude, and thus the initial launch velocity, attitude as well as the rates experienced by the aircraft during deployment is directly related to the carrier aircraft speed, attitude and rates. For a successful deployment where none of the observed safety deployment parameters crosses the upper or lower limits, the initial deployment values as presented in Table 7.2 is used in the simulation.

Input Parameter	Value	Unit
V_0	55	m/s
θ_0	0	v
h_0	6000	ft
ψ_0	0	deg
p_0	0	deg/s
q_0	0	deg/s
r_0	0	deg/s

Table 7.2: Input parameter values for a single successful deployment of Scenario 2

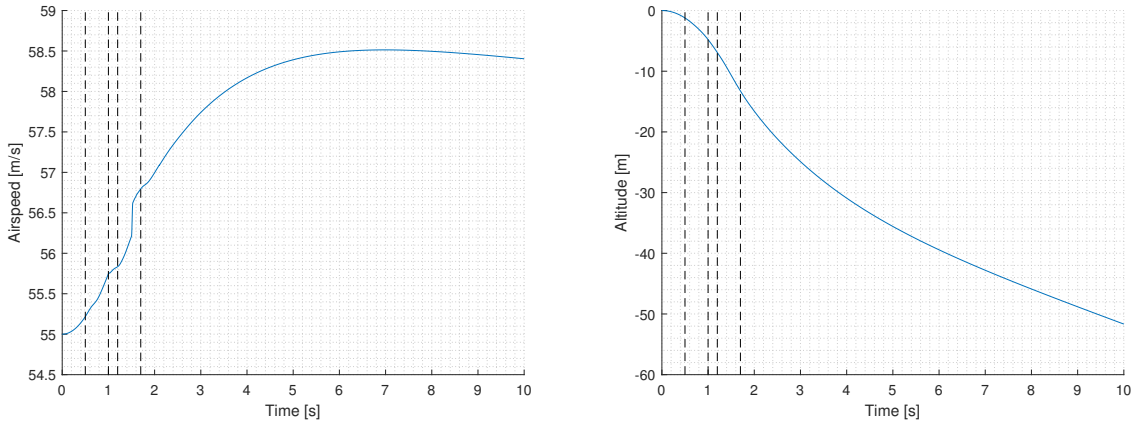

(a) (b)

Figure 7.14: Change in (a) airspeed & (b) altitude of deployment scenario 2

Again, for the case considered here, the deployment is symmetric, which means no lateral and directional initial condition parameters is used. Thus the focus of the analysis will be on the longitudinal dynamics of the vehicle during and after the deployment. The variation of the airspeed and altitude of the vehicle after the detachment from the carrier aircraft is shown in Figure 7.14. For Figures 7.14 to 7.16, the 4 vertical dash lines denotes the moment the horizontal tail starts to unfold, the main wing starts to rotates, the vertical tail starts to unfolds and the main wing's starts to extend itself in a telescopic manner. Throughout the deployment, the altitude of the aircraft decreases while the airspeed of increases. Observing the variation in airspeed shows that at the time the horizontal tail unfolds, the airspeed does not directly drops due to the act that the drag of the vehicle increases. This reduction in the rate the airspeed increases starts being visible after the main wing unfolds itself. Of course, the main wing, being a larger lifting surface will definitely contribute to a higher drag value than the horizontal tail when deployed. This increase in drag, which is directly proportional to the value of the angle of attack of the vehicle can also be seen from Figure 7.15b. From this figure, it can be seen that there is a slight lag in the time the trend of the angle of attack of the vehicle changes sign. From the time the vehicle detaches from the carrier aircraft to the moment the horizontal tail of the vehicle unfolds, the angle of attack increases steeply. However, slightly after the horizontal tail starts to unfold, the trend changes and the angle of attack of the vehicle started dropping, until the time the main wing unfolds. This is mainly due to the pull-up control imposed on the deployment model, which causes the deployment model to always want to reach a flight path angle value of zero. The angle of attack then oscillates until the extension of the main wing, where the value drops again before settling at a value slightly lower than zero.

The flight path angle varies very little in this deployment scheme. Since the initial condition of the deployment states that the vehicle is detached at an initial pitch attitude of zero degrees, the flight path also starts

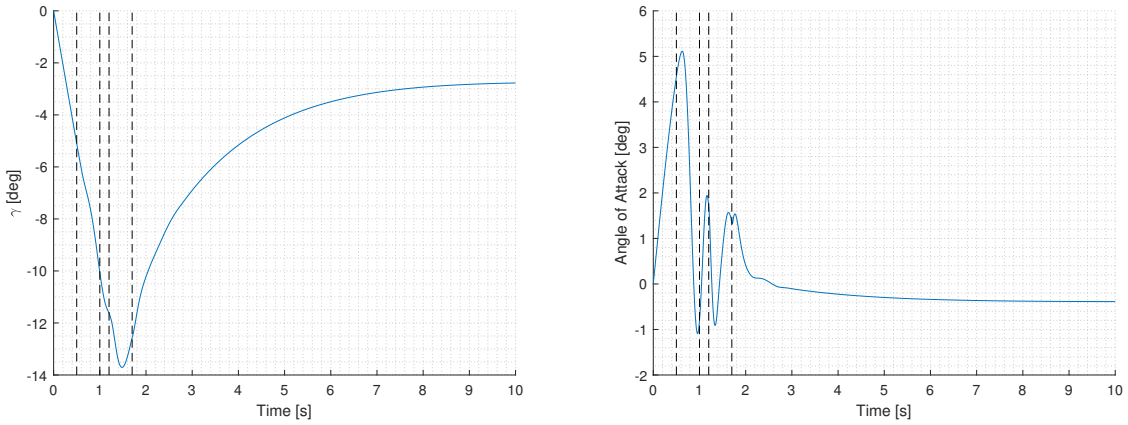

(a) (b)

Figure 7.15: Change in (a) γ & (b) α of deployment scenario 2

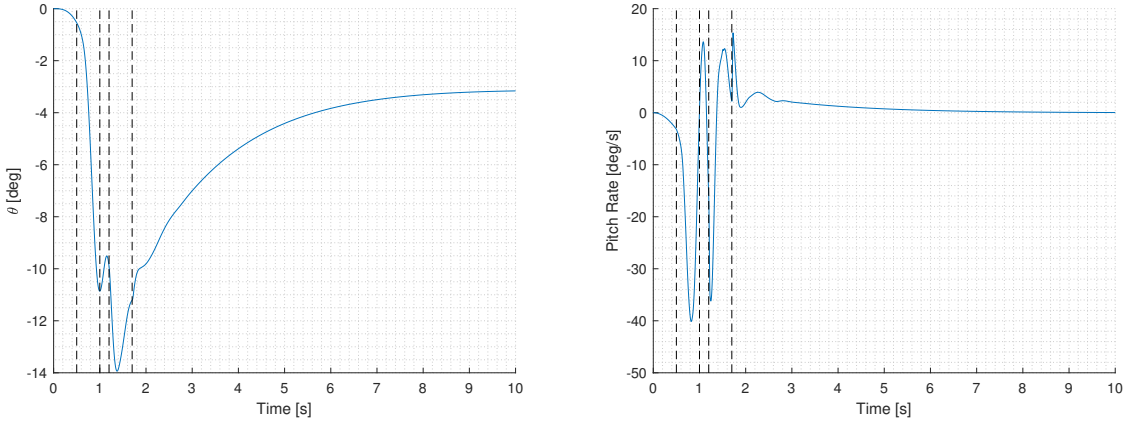

(a) (b)

Figure 7.16: Change in (a) θ & (b) q of deployment scenario 2

from this value. The flight path angle then drops and keeps on dropping until the time the horizontal tail, main wing and vertical tail are all fully deployed. The value also increases further with the extension of the main wing, where more lift is generated by the main wing which causes a more positive pitching moment to be experienced by the aircraft, in addition to the pull up control imposed on the elevator of the vehicle.

7.3.2. Deployment Safety Assessment Results

The same procedure of assessing the deployment safety of the deployable morphing UAV is performed for the second scenario. As determined before, the 3 influential deployment parameters for this scenario are the initial roll rate, initial yaw rate and the initial roll attitude of the aircraft during detachment from the carrier aircraft. Figures 7.17 and 7.18 shows the safety deployment space of the vehicle, within the initial deployment parameter range considered here. In addition to that, the aerodynamic limit of the aircraft which causes the deployment to fail is also highlighted in a separate zone in the figures below.

In the safety deployment space presented, the green zone indicate the aerodynamic limit of the aircraft. In other words, the evaluated deployment parameter triggered here that causes the simulation to stop and deemed unsafe are either the angle of attack of the main wing, angle of attack of the horizontal tail or the sideslip angle experiences by the vertical tail. Further investigation into the data reveals that all of the failures due to the aerodynamic limit are caused by the trigger of the sideslip angle of the vertical tail. As described

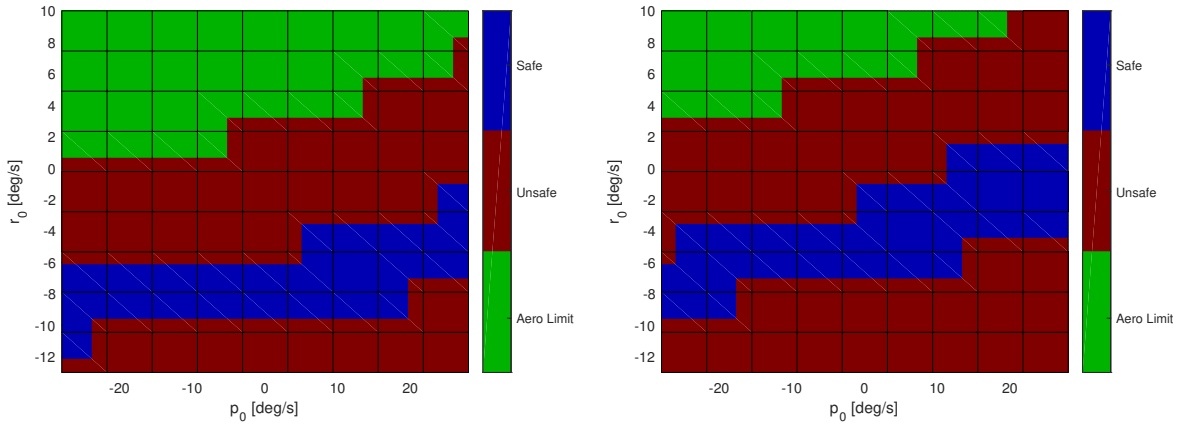

(a) (b)

Figure 7.17: Safety deployment space of scenario 1 for initial roll angle values of (a) -45 & (b) -25 degrees

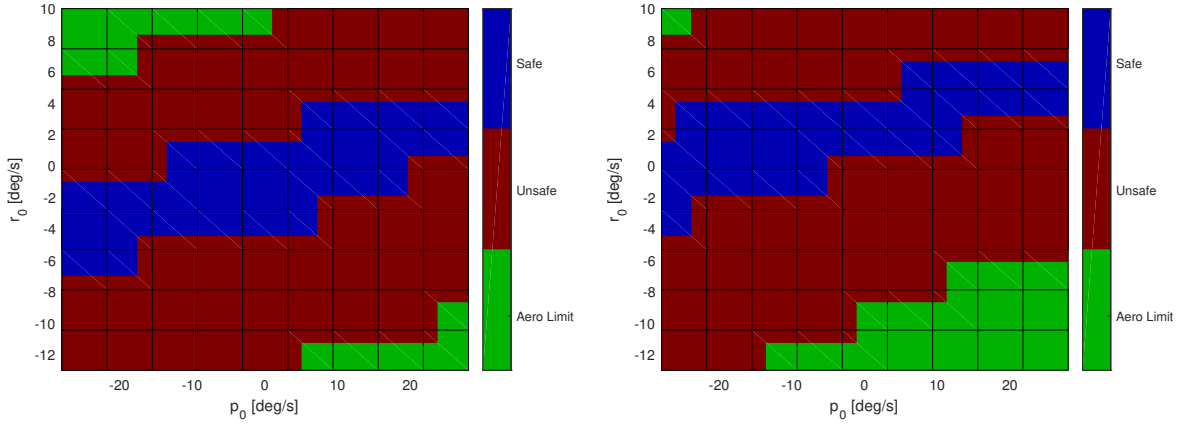

(a) (b)

Figure 7.18: Safety deployment space of scenario 1 for initial roll angle values of (a) -5 & (b) 15 degrees

before in the previous section, the airspeed of the vehicle increases at the beginning of the deployment, since it losses altitude. In the case that the deployment is symmetric as evaluated in the previous section, the lifting surface's stall limits which is considered as the aerodynamic limits will not be triggered. However, in the case that the aircraft has an initial lateral or directional rate or attitude, this increase in airspeed combined with the aircraft's condition which is rolling or yawing causes the sideslip angle of the vehicle to be higher than the allowable value. This higher value thus triggers either the upper or lower limit of the allowable sideslip angle of the vertical tail and causes the deployment to fail. It is of course very possible that in some of the unsuccessful deployment in the green zone, that not only the aerodynamic limits are triggered, but the limits of the rates of the aircraft is also triggered. Either way, the simulation is stopped ans is deemed unsafe.

A noticeable phenomenon in the safety deployment space is that to have a safe deployment, a combination of a more positive initial roll rate with a more positive initial yaw rate and vice versa is desirable. Also, a more positive initial roll rate and a more negative initial roll attitude also causes the deployment to be safe. This is because the difference in sign of the two deployment parameters here causes the misaligned attitude of the aircraft to be corrected by the initial rate.

In the 4 graphs provided to show the safety deployment space of this type of deployment, an increase in initial roll attitude of the aircraft means that the safety deployment space shifts upward. The graph is also quite symmetric when it shifts upward, with the green zone disappearing at the bottom and appearing at the top at high values of initial roll angle and vice versa. For all of the simulations run here, the safe deployment

zone is first bounded by an unsafe deployment zone and then comes the zone which states that the unsafe deployment is because the aerodynamic limits of the vehicle is surpassed. However, in this study, it is not possible to determine whether the deployment deemed unsafe and thus, several points will be taken and an investigation on what is actually happening during that failed deployment will be made.

It is known that the safety deployment space is symmetric for this deployment type, and thus taking a point above the blue zone will indirectly also explains what is happening during the deployment at the same point under the blue zone. In other words, if a plane is drawn to represent the blue zone and treated as a mirror plane, the dynamics of deployment at a point outside the blue zone will be similar to the dynamic of deployment at the mirrored point on the other side of the blue zone. Here, the deployment with the initial roll rate, initial yaw rate and initial roll attitude of 25 deg/s, 8 deg/s and -25 deg will be evaluated. The selection of these values is based on the furthest point from the safety deployment space of the vehicle which is still in the red region. It is decided that the evaluation will be done in the red region to investigate which type of unsafe deployment does this region represent when referring to Figure 6.5. When evaluating the unsafe deployment in the green zone, it is directly known that aerodynamic limits treated as hard limits are the ones being triggered and thus it is less interesting to investigate the unsafe deployment int he green zone than in the red zones.

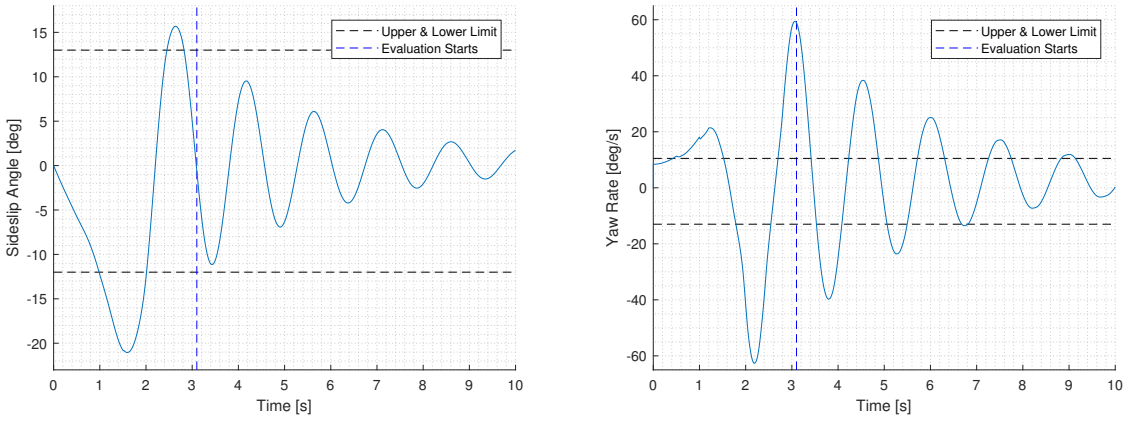

Figure 7.19: Variation in (a) β & (b) r of the vehicle during deployment scenario 2 ($p_0 = 25$deg/s, $r_0 = 8$deg/s, $\phi_0 = -25$deg)

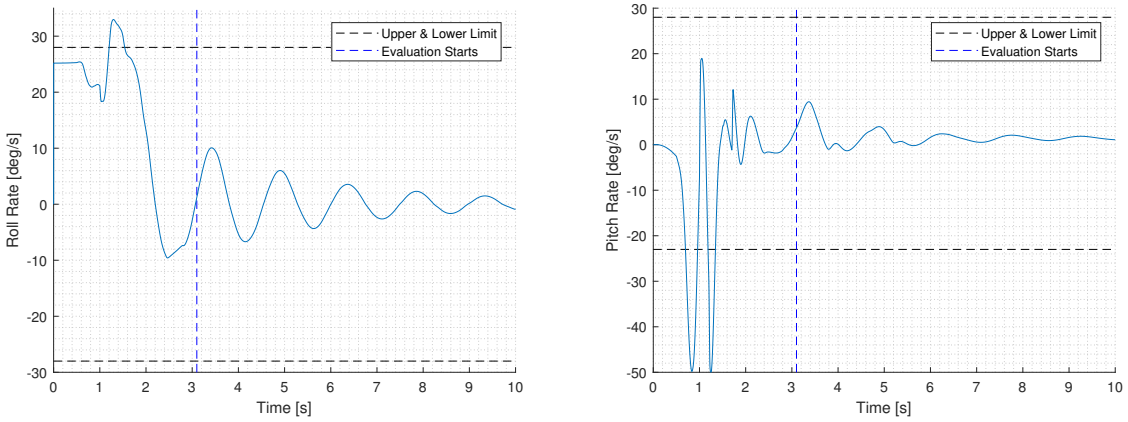

Figure 7.20: Variation in (a) p & (b) q of the vehicle during deployment scenario 2 ($p_0 = 25$deg/s, $r_0 = 8$deg/s, $\phi_0 = -25$deg)

Figures 7.19 and 7.20 shows the variation of the sideslip angle of the vehicle along with the rates of the vehicle for all the three axis. As stated before, the selected point in the unsafe deployment space of the vehicle is such

that it is as close as possible to the aerodynamic limit, but still hasn't triggered the aerodynamic limits of the vehicle. This is shown by Figure 7.19a, where after the starting point of the evaluation, the values of the vehicle sideslip angle is very close to the limit, but later converges and settles. The triggering evaluation parameter here is the yaw rate, which is still oscillating at values higher than the allowable limits. Thus, assessing the deployment with the method created in this study causes the simulation to be stopped and deemed unsafe. However, observing that the oscillation of the yaw rate is actually converging, this means that if the starting point of the evaluation will be postponed by several seconds, the deployment will be deemed safe. Hence, this concludes that this type of deployment falls into the category "converging rates deemed unsafe" based on Figure 6.5.

Unlike the yaw rate which causes this deployment to be deemed unsafe, the roll rate, although started in values which are very close to the upper limit, converges to the tolerable values after the evaluation starts. There exist a spike in the variation of the roll rate before the evaluation starts, and this is caused by the unfolding of the lifting surfaces of the aircraft. But this is quickly dampen by the aircraft's roll damping. The same is observed in the changes of the pith rate of the vehicle. The values goes outside the allowable limits before the evaluation starts, but then converges to allowable magnitudes after the evaluation starts. Hence the roll rate and pitch rate of the vehicle does not causes the deployment to be unsafe.

Another interesting observation from the safety deployment space of this deployment scheme is that none of the structural limit of the aircraft is triggered. Two parameters are taken as the evaluated parameters in this study, namely the never exceed speed of the vehicle and the load factor of the vehicle. This means that with the current range of initial deployment parameter, the structural limits of the vehicle is not triggered and from a structures point of view, all of the combination of the initial deployment parameters result in a safe deployment structure-wise. It can also be concluded that since none of the structural limits have been triggered in this deployment scheme, it is easier to trigger the other evaluated deployment parameters than the structural limits. Hence, the structural limit of the aircraft in such a deployment is way further than the range of initial deployment parameter specified here.

8

Conclusions & Recommendations

In this study, a method to assess the safety of deployment of a morphing UAV has been developed. The method is tested to check the safety of deployment of a test case aircraft, and tested in two different mid-air deployment schemes. From the observations of the results as well as the process the study is conducted, a lot of findings have been obtained from this study. In this chapter, the findings of this study which will be written as conclusions as well as the recommendations will be presented.

8.1. Conclusions

The study presented in this report has several main points that will be highlighted and conclusions which are as follows:

- A model of the test case aircraft have been created in this study by using the multibody dynamics approach. The result of the created model here is compared with the result of a corresponding model evaluated in an off-the-shelf aerodynamic solver. The values and trend of major longitudinal stability derivatives from the created model resembles the trend from an off-the-shelf aerodynamic solver when the longitudinal reference point of the model is varied. However, several differences exist which is mainly cased by the limitations of the created model and the off-the-shelf aerodynamic solver used itself. This comparison is treated as a validation step for the created model here. A second step to validate the created model is to test the response of the model with an actual flight test data. From this validation process, the response of the aircraft quite resembles the response of the real aircraft during flight testing, with some differences that is caused by the limitations of data provided. Thus, the model created in this study is said to be able to represent the dynamics of an actual aircraft during a steady level flight.
- To test how the model of the aircraft will behave to basic control inputs, the created model is tested by introducing the created model to a step input on all the three control surfaces of the aircraft. Here, the short period of the aircraft is visible and the phugoid motion of the vehicle dampens out in time. Upon introduction to a step input on the aileron and rudder, the aircraft goes to a spiral motion where the diameter of the spiral reduces in time. Thus, it is concluded that the aircraft considered in this study is inherently stable in its longitudinal axis, but has a slowly diverging spiral mode.
- To define the safety of deployment of a deployable morphing aircraft, in this study three different safety concerns are determined, which includes structural, aerodynamic and controllability of the aircraft. Flight parameters that relates to these three different safety concerns are then determined, which will be the parameters that will be constantly evaluated throughout every deployment simulation. Upper and lower limits of these parameters are determined. From this, the definition of a safe deployment is

derived, which states that a safe deployment is one where none of the aircraft's structural or aerodynamic limits are surpassed and one in which the deployed aircraft goes to a controllable flight regime after the deployment.

- From the definition of a safe deployment, several categories of deployment can be defined. These categories classifies the deployment based on whether the deployment is deemed safe or unsafe. More specifically in unsafe deployments, further classifications is made to determine what exactly causes the deployment to be unsafe. Figure 6.5 is created to illustrate the different types of deployment categories that may happen during a deployment.
- To assess the safety of deployment, a method is developed which consist of the selection of the influential parameters from the set of different initial deployment parameters for a deployment scenario. After identifying the influential parameters, multiple runs by using different combination of the influential parameters is done to obtain the safety deployment space for a specific deployment scenario. Two different scenarios are considered in this study and for both, the aircraft's initial lateral and directional attitudes and rates are highly influential to the safety of deployment in a deployment scheme. In other words, to perform a study on the safety of deployment of a deployable morphing aircraft, the lateral and directional axis of the vehicle needs to be addresses as their parameters are the ones that causes the most failed deployments. Thus a neglection on the modeling of the lateral and directional axis of the vehicle is an over simplification to the problem.
- For the deployment assessment of scenario 1, it is observed that the unsafe deployments shown in the simulated deployment space are falls into the category "converging rates deemed unsafe". This means that if the evaluation of the deployment parameters begins later, the deployment will be deemed safe since the values will converge to acceptable values. It is also understood that to see a deployment which falls into the category "diverging rates", a higher value of the initial deployment parameters need to be used, which is outside the range tested in this study.
- For deployment assessment of scenario 2, all of the unsafe deployments also falls into the category "converging deployment deemed unsafe". The reason behind this is also because of the cap imposed in this study, where the evaluation of the parameters starts 1 second after the aircraft unfolds completely. Higher values of the initial deployment parameters causes the aerodynamic limits of the aircraft to be surpassed. For all of the different combination of deployment parameters in scenario 2, none causes the structural limits of the aircraft to be surpassed. This means that the aerodynamic limit of the aircraft is easier surpassed as compared to the structural limits, which both are seen as hard limits in the safety definition of a deployable aircraft.

8.2. Recommendations

The study is completed in the limited amount of time allocated. However, there are still more to be done which can improve the result of this study. Below are a list of possible directions that can be taken for a follow-up or continuation of the study performed here:

- This study uses the Dash-X aircraft as the test case and since the aircraft's wingspan is not of great value, the lifting surface of the aircraft is considered to be rigid throughout the deployment. However, it is also interesting to use the method created here for long wingspans deployable morphing aircraft. For this, the assumption that the wing will stay rigid throughout the deployment will needs to be reevaluated and a new model of a flexible wing aircraft will needs to be created.
- The deployment space presented in this study is based on the range of varied initial deployment parameters determined. For the range of parameters determined, only unsafe deployments that fall to the category "converging rates deemed unsafe" are found. It is also found that by using values outside the range specified, unsafe deployments that fall to other categories can be seen. Thus, it is interesting to perform study that solely focuses on determining the range of input parameters for the simulation.
- Although this study defines the different categories of deployment, the method developed here is not able to automatically determine whether the unsafe deployment due to the controllability of the air-

craft falls into one of the defined categories. On the other hand, it is easy to determine when a deployment fails because the structural or aerodynamic limits of the aircraft is surpassed since these limits are treated as hard limits. However, since the assessment of the controllability of the aircraft is done by observing the trend of the vehicle at a specific timeframe, a more sophisticated method than just to define upper and lower limits of these values needs to be used. It is thus very interesting to focus a study that will be able to automatically categorize an unsafe deployment based on Figure 6.5.

- A modified one-at-a-time screening method is used in this study to reduce the number of parameters to be varied when performing multiple runs of the simulation. However this method is very sensitive to the range specified by the user. Therefore, other more advanced methods could be tested to cover the limitation of the method used here.
- The sequence of deployment for the aircraft is predefined in this study. A possible study is to check the impact the sequence of deployment has on the safety of deployment itself.

A

Model Response to Step Inputs

Response to Elevator Step Input

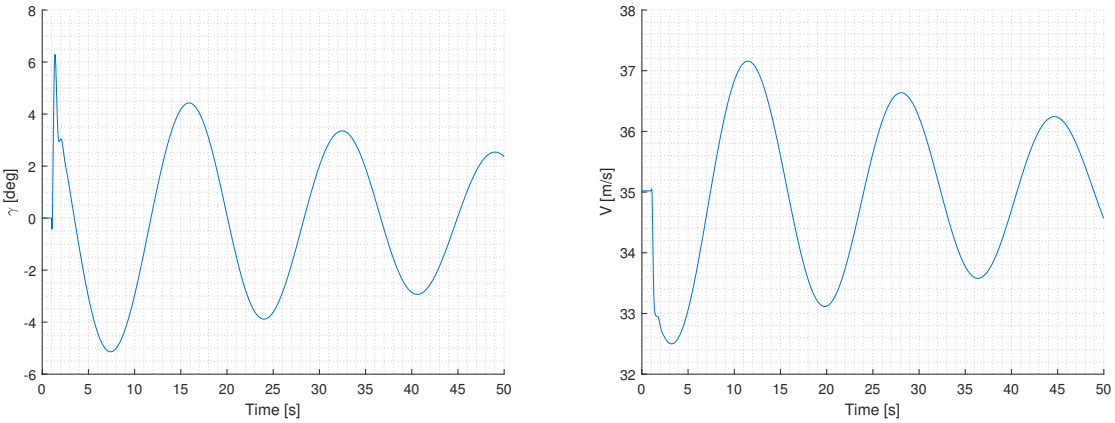

(a) (b)

Figure A.1: Change in (a) γ & (b) V as the model's response to elevator step input

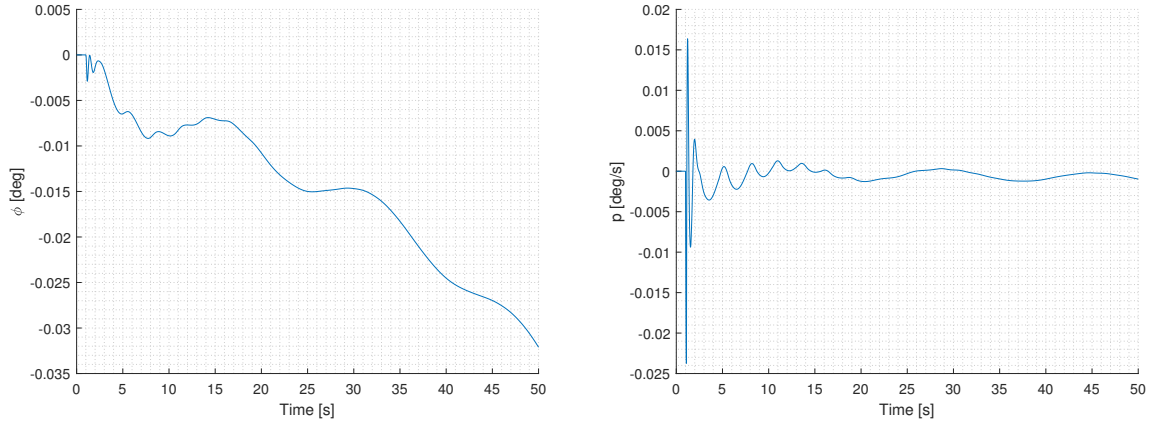

(a) (b)

Figure A.2: Change in (a) ϕ & (b) p as the model's response to elevator step input

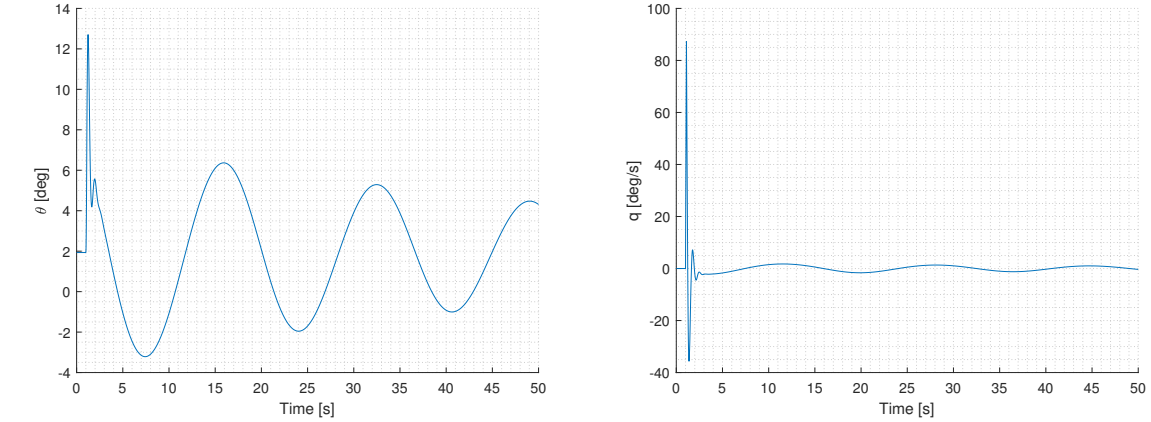

(a) (b)

Figure A.3: Change in (a) θ & (b) q as the model's response to elevator step input

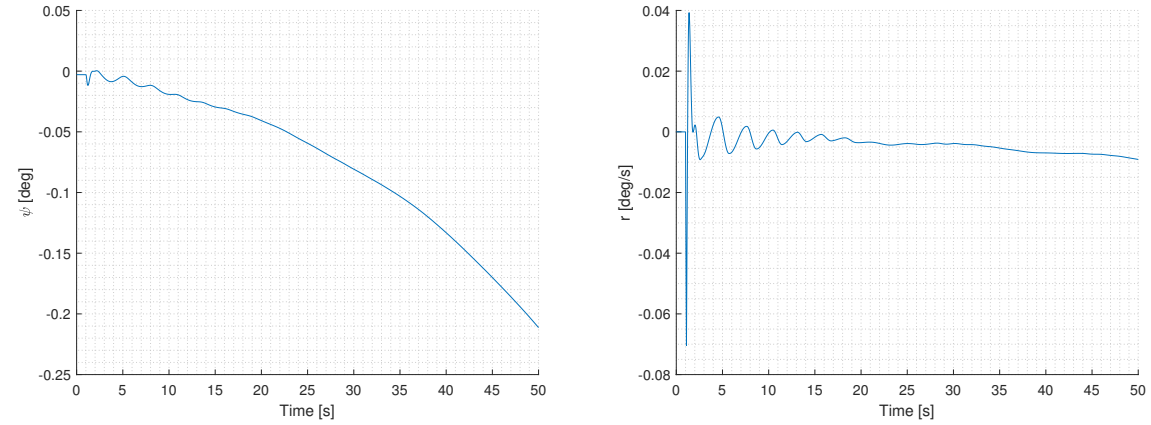

(a) (b)

Figure A.4: Change in (a) ψ & (b) r as the model's response to elevator step input

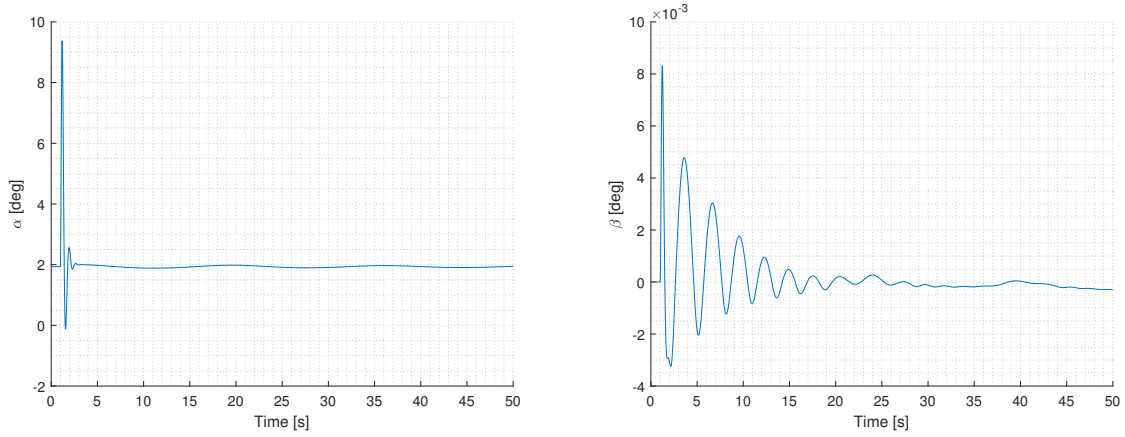

(a) (b)

Figure A.5: Change in (a) α & (b) β as the model's response to elevator step input

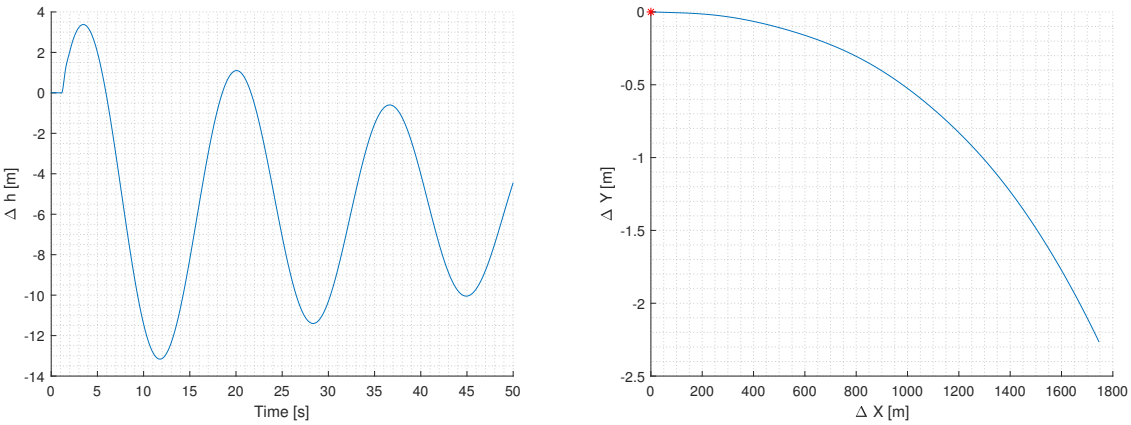

(a) (b)

Figure A.6: Flight path of model due to the introduction of a elevator step input

Response to Rudder Step Input

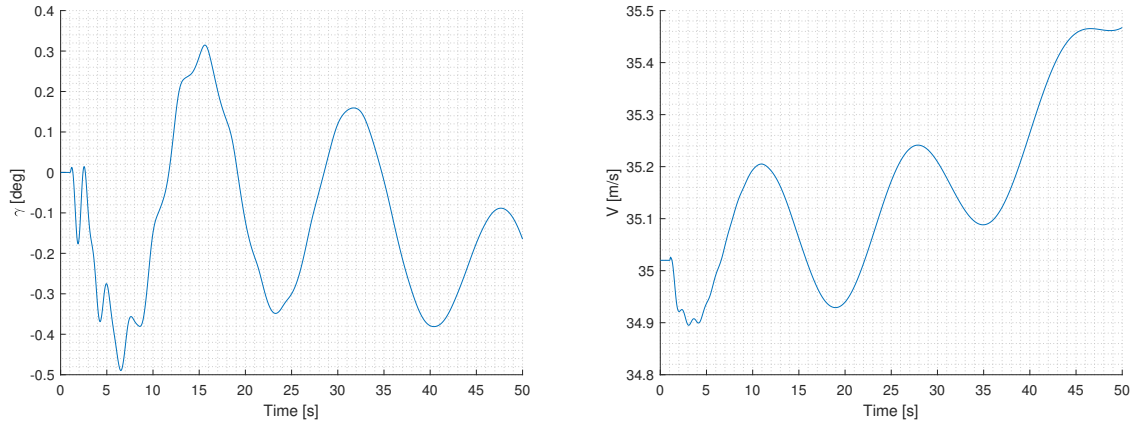

(a) (b)

Figure A.7: Change in (a) γ & (b) V as the model's response to rudder step input

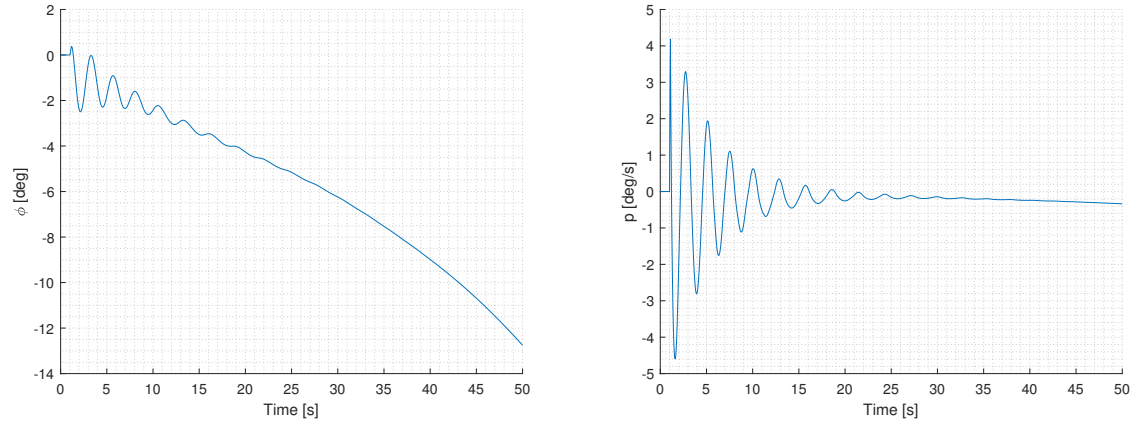

(a) (b)

Figure A.8: Change in (a) ϕ & (b) p as the model's response to rudder step input

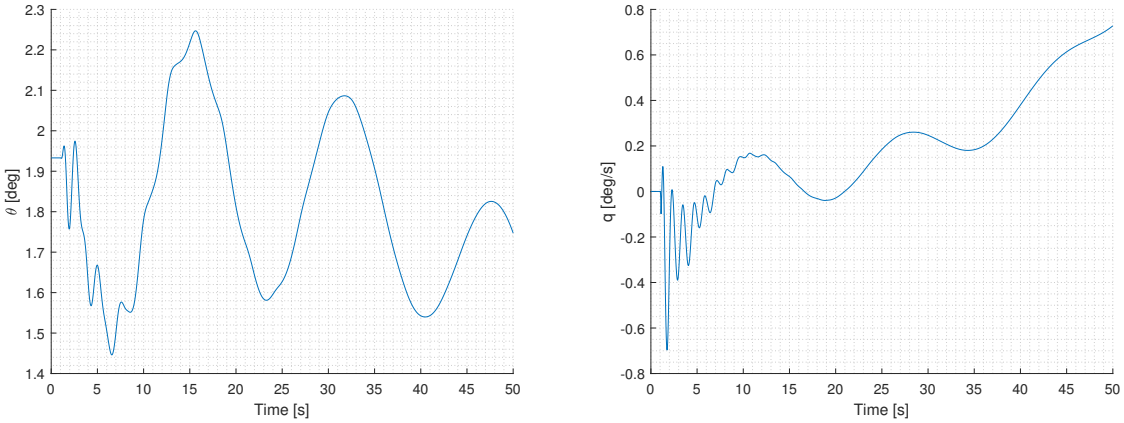

(a) (b)

Figure A.9: Change in (a) θ & (b) q as the model's response to rudder step input

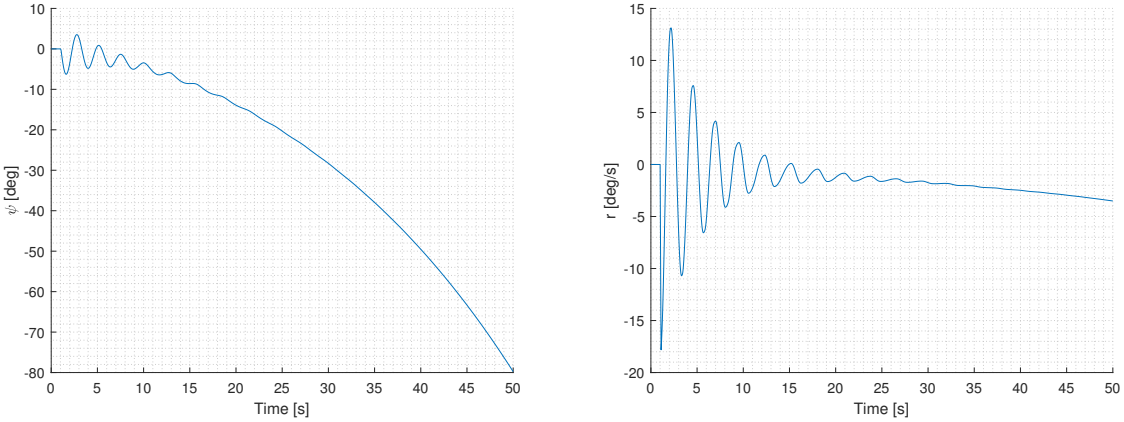

(a) (b)

Figure A.10: Change in (a) ψ & (b) r as the model's response to rudder step input

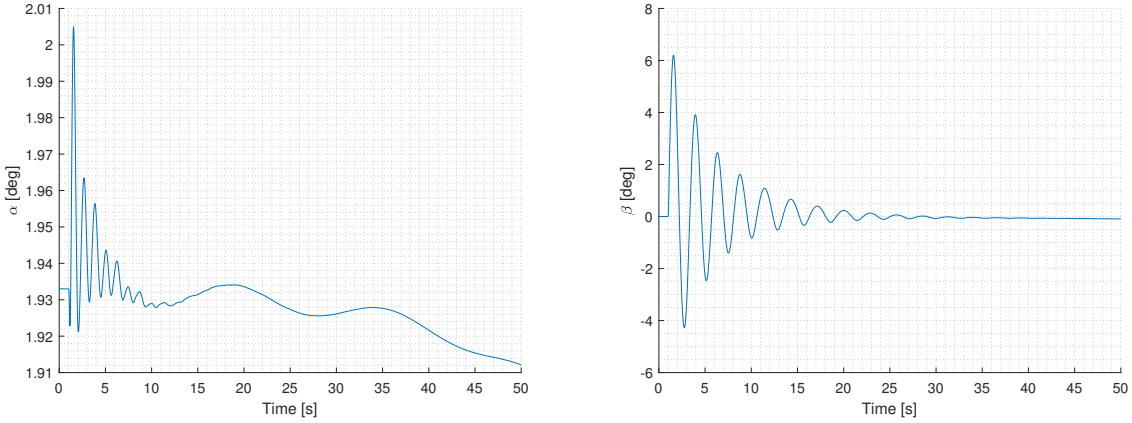

(a) (b)

Figure A.11: Change in (a) α & (b) β as the model's response to rudder step input

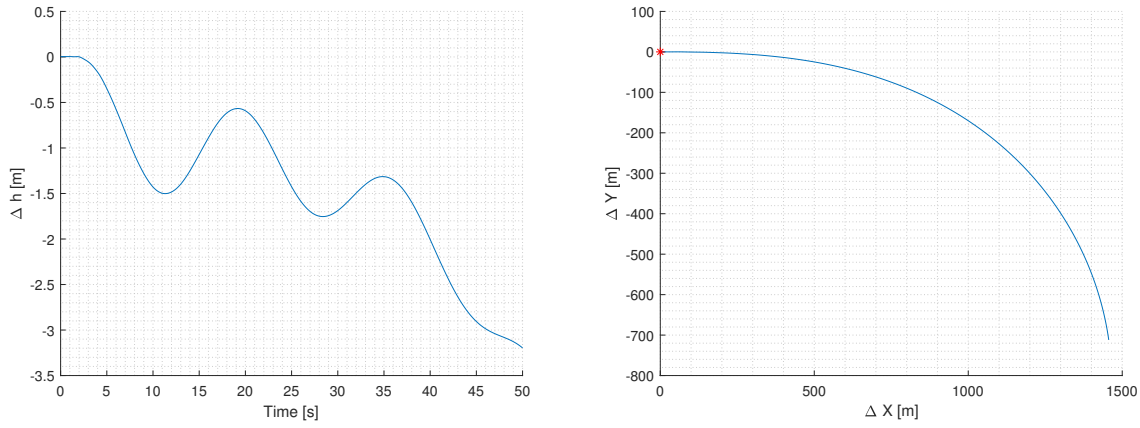

(a) (b)

Figure A.12: Flight path of model due to the introduction of a rudder step input

Response to Aileron Step Input

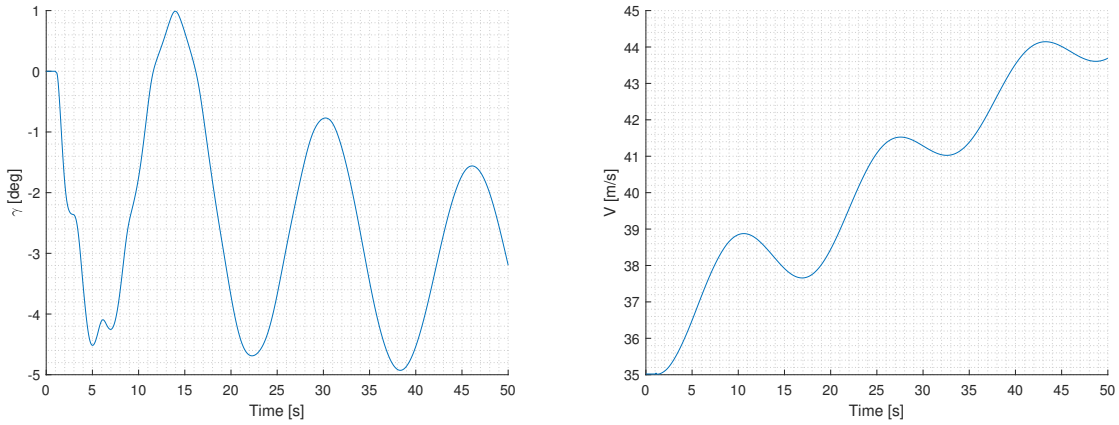

(a) (b)

Figure A.13: Change in (a) γ & (b) V as the model's response to rudder step input

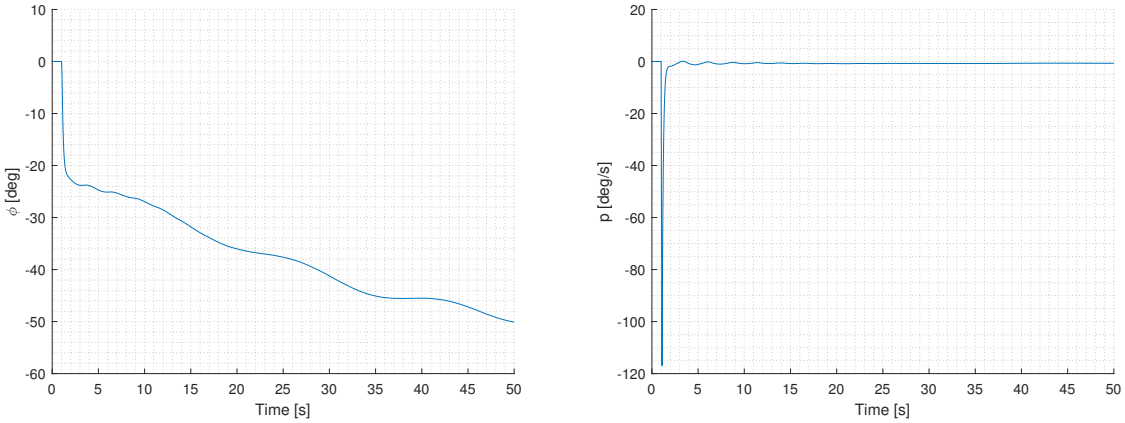

(a) (b)

Figure A.14: Change in (a) ϕ & (b) p as the model's response to rudder step input

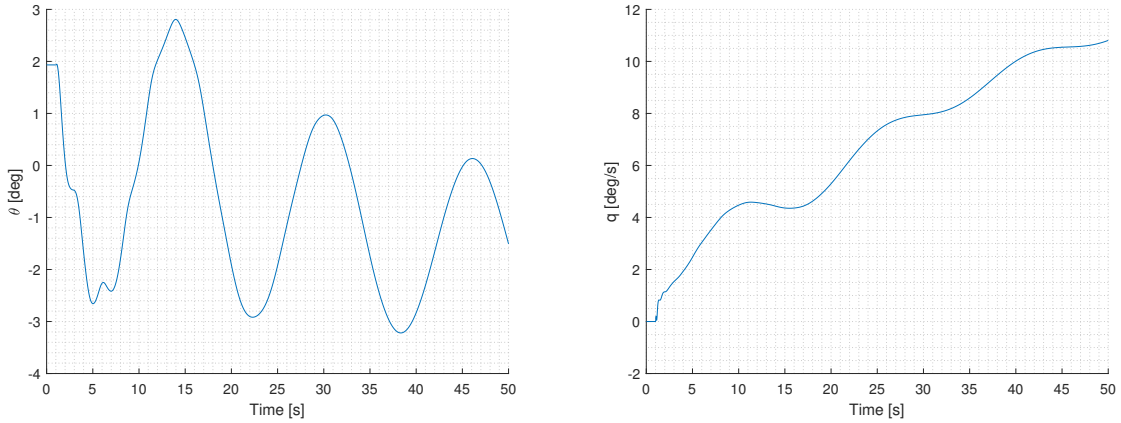

(a) (b)

Figure A.15: Change in (a) θ & (b) q as the model's response to rudder step input

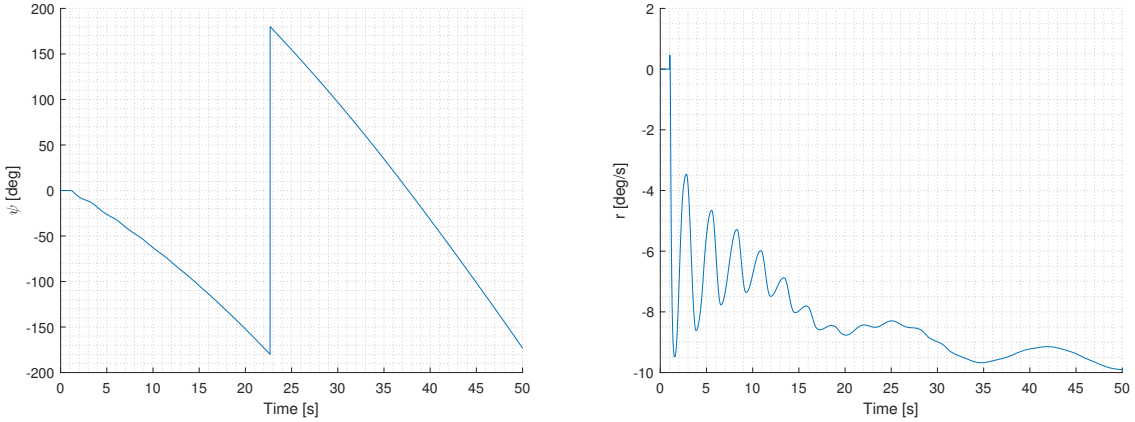

(a) (b)

Figure A.16: Change in (a) ψ & (b) r as the model's response to rudder step input

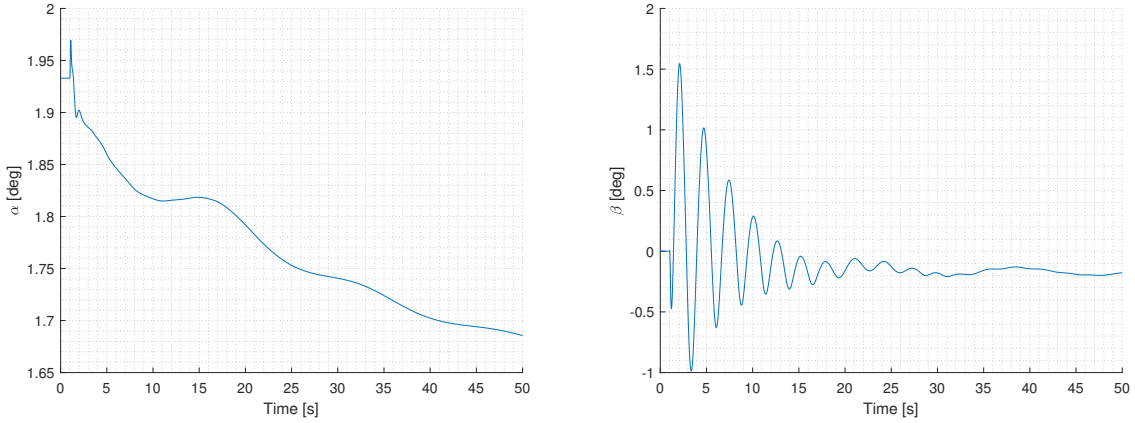

(a) (b)

Figure A.17: Change in (a) α & (b) β as the model's response to rudder step input

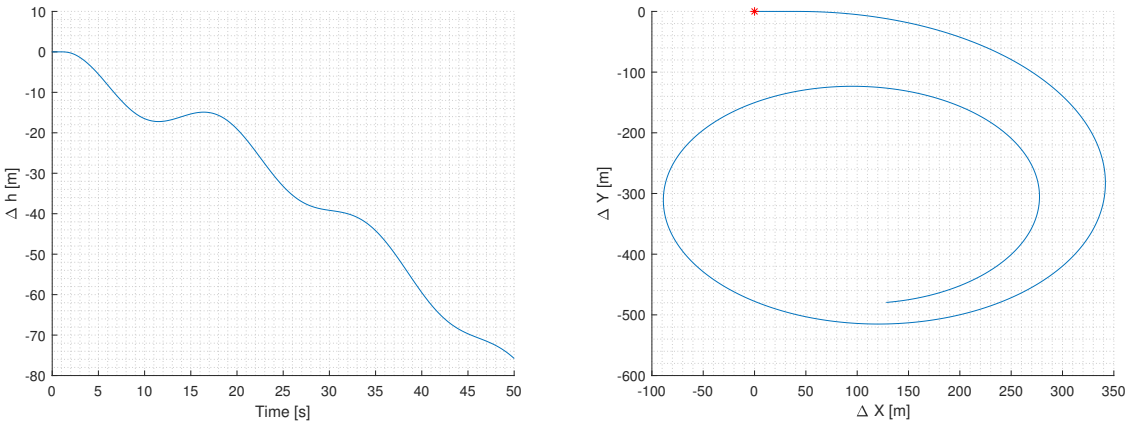

(a) (b)

Figure A.18: Flight path of model due to the introduction of a aileron step input

Bibliography

[1] M. J. H. Kraus, M. J. R. C. Pedersen Independent, M. N. Roberts Rolls, R. Plc, D. Mr, R. Sanderson, M. A. E. Sewell, . M. Douglas, L. Beach, C. Usa, and M. M. R. Smith, "ESDU 89008 NORMAL-FORCE-CURVE AND PITCHING-MOMENT-CURVE SLOPES OF FOREBODY-CYLINDER COMBINATIONS AT ZERO ANGLE OF ATTACK FOR MACH NUMBERS UP TO 5 CONTENTS," tech. rep.

[2] Z. Min, V. K. Kien, and L. J. Y. Richard, "Aircraft morphing wing concepts with radical geometry change," *IES Journal Part A: Civil and Structural Engineering*, 2010.

[3] C. S. Beaverstock, R. M. Ajaj, M. I. Friswell, W. G. Dettmer, R. De Breuker, and N. P. M. Werter, "Effect of Span-morphing on the Longitudinal Flight Stability and Control," pp. 2013–4993.

[4] J. D. Jacob and S. W. Smith, "Design Limitations of Deployable Wings for Small Low Altitude UAVs,"

[5] K. Fujita, S. Kanagawa, and J. H. Nagai, "Robustness analysis on aerial deployment motion of a Mars aircraft using multibody dynamics simulation: effects of wing-unfolding torque and timing," *The Aeronautical Journal*, vol. 121, no. 449, pp. 449–468, 2017.

[6] K. Fujita, T. Motoda, and H. Nagai, "Numerical Analysis for an Aerial Deployment Motion of a Folded-Wing Airplane,"

[7] R. D. Braun, H. S. Wright, M. A. Croom, J. S. Levine, and D. A. Spencer, "Design of the ARES Mars Airplane and Mission Architecture,"

[8] Grey Hautaluoma, "NASA Delays Mars Scout Mission to 2013," 2007.

[9] B. J. Kuchta, B. Spencer, and V. Hampton, "Aerodynamic and Flight Characteristics of Several Variable Geometry Entry Spacecraft During Subsonic Wing Deployment and Landing,"

[10] Mr. Scott Wierzbanowski, "Gremlins."

[11] "Rate of Change of Lift Coefficient With Co ntrol Deflection in Incompressible Two-Dimensional Flow, (A2) 0," tech. rep., IHS ESDU.

[12] "Slope of Lift Curve for Two-Dimensional Flow," tech. rep., IHS ESDU.

[13] J. An, M. Yan, W. Zhou, J. X. Sun, Z. Yanf, and C. Qiu, "Aircraft Dynamic Response to Variable Wing Sweep Geometry," vol. 25, no. 3, pp. 18–20, 1988.

[14] R. Shi and W. Wan, "Aircraft Engineering and Aerospace Technology: An International Journal Analysis of flight dynamics for large-scale morphing aircraft," *Aerospace Technology: An International Journal*, vol. 87, no. 1, pp. 38–44.

[15] Y. in, Q. Chuanren, and Y. hen, "The Dynamic Response of a Variable Sweep Aircraft In the Course of Changing Geometry,"

[16] F. Santoni and P. Gasbarri, "A Deployable Wing Airplane Supporting Human Landing on Martian Surface,"

[17] N. Prabhakar, R. J. Prazenica, S. Clyde, and M. Blvd, "Dynamic Analysis of a Variable-Span, Variable-Sweep Morphing UAV,"

[18] N. Prabhakar, R. Prazenica, S. Gudmundsson, and M. Balas, "Transient Dynamic Analysis and Control of a Morphing UAV,"

[19] Flight Level Engineering, "SURFACES."

[20] A. Niksch, J. Valasek, T. W. Strganac, and L. A. Carlson, "Six Degree of Freedom Dynamical Model of a Morphing Aircraft AIAA Atmospheric Flight Mechanics Conference,"

[21] K. Fujita, "A Parametric Study of the Deployable Wing Airplane for Mars Exploration,"

[22] K. Fujita, T. Motoda, and H. Nagai, "Dynamic Behaviour of Mars Airplane with Folded-Wing Deployment," *Trans. JSASS Aerospace Tech. Japan*, vol. 12, no. ists29, pp. 1–6, 2014.

[23] K. Fujita, H. Nagai, and A. Oyama, "Robust Aerial Deployment of Mars Airplane with Tilted Folding-Axis,"

[24] Fujita K, Hiroki Nagai, and Akira Oyama, "Effect of Yaw-Tilted Hinge Axis On Deployment Robustness of Mars Airplane," *ICAS 2016*, 2016.

[25] L. Tong and H. Ji, "Multi-body Dynamic Modelling and Roll Control of Asymmetric Variable Sweep Morphing Aircrafts*," 2013.

[26] A. Pons and F. Cirak, "Flight dynamics of a moving - wing aircraft,"

[27] M. Goman and A. Khrabrov, "State-space representation of aerodynamic characteristics of an aircraft at high angles of attack," *Journal of Aircraft*, 1994.

[28] J. Samareh, P. Chwalowski, L. Horta, D. Piatak, and A.-M. McGowan, "Integrated Aerodynamic/Structural/Dynamic Analyses of Aircrafts with Large Shape Changes," in *48th AIAA/ASME/ASCE/AHS/ASC Structures, Structural Dynamics, and Materials Conference*, 2007.

[29] "Aerologic CMARC."

[30] O. A. Bauchau, "Computational Schemes for Flexible, Non-linear Multi-body Systems," *Multibody System Dynamics, Volume 2*, vol. 2, pp. 169–225, 1998.

[31] J. H. S. Fincham, C. S. Beaverstock, A. B. Coles, L. L. Parsons, M. I. Friswell, and R. M. Ajaj, "Aerodynamic Forces on Morphing Wings During Span Extension,"

[32] H. Han, J. Hu, and Y. Yu, "Investigation of the Unsteady Aerodynamic Characteristics of an Unmanned Aerial Vehicle with Variable - Sweep Morphing," 2014.

[33] W. J. Vink, "Evaluation of Strip Theory and Doublet-Lattice Aerodynamics," 1998.

[34] K. Fujita, T. Motoda, and H. Naga, "Dynamic Behaviour of Mars Airplane with Folded-Wing Deployment," *Trans. JSASS Aerospace Tech. Japan*, vol. 12, no. ists29, pp. 1–6, 2014.

[35] Adin Dobkin, "Army tests helicopter-based, tube-launched UAVs," 2017.

[36] C. H. N. W. R. L. S. L. S. S. A. B. William R. Hurst, Thomas J. Star, "Design, Analysis and Testing of a Canister-Launched Mini-UAV," *AIAA 2005-7136*, 2005.

[37] Tamir Eshel, "AFSOC Gunships to Get Air-Launched UAVS for Operational Evaluation," 2016.

[38] P. Gnemmi and J. Haertig, "Concept of a Gun Launched Micro Air Vehicle," 2008.

[39] A. Stoica and I. Yaesh, "Jump Markovian-Based Control of Wing Deployment for an Uncrewed Air Vehicle," *Journal of Guidance, Control, and Dynamics IEEE Control Systems Magazine IEEE Trans-actions on Systems, Man,and Cybernetics*, vol. 25, no. 7, pp. 128–211, 2002.

[40] E. M. S. A. Saltelli, K. Chan, *Sensitivity Analysis*. West Sussex: Wiley, 1 ed., 2009.

[41] Max D. Morris, "Factorial Sampling Plans for Preliminary Computational Experiments," *Technometrics*, vol. 33, no. 2, 1991.

[42] Sarah C. Cotter, "A screening design for factorial experiments with interactions," *Biometrika*, vol. 66, no. 2, pp. 317–320, 1979.

[43] T. Andres, "Sampling methods and sensitivity analysis for large parameter sets," *Journal of Statistical Computation and Simulation*, 1997.

[44] Bert Bettonvil, "Sequential Bifurcation: The Design of a Factor Screening Method," 1989.

[45] Lee Hudson, "Northrop executive: Navy may incorporate new unmanned system for Growler Block II," 2017.

[46] B. Burgermeister, M. Arnold, and B. Esterl, "DAE time integration for real-time applications in multibody dynamics," in *ZAMM Zeitschrift fur Angewandte Mathematik und Mechanik*, 2006.

[47] R. E. Roberson, R. Schwertassek, S.-V. Berlin, H. N. London, and P. Tokyo, "Dynamies of Multibody Systems With 100 Figures,"

[48] Ahmed A. Shabana, *Dynamics of Multibody Systems*. Cambridge Univeristy Press, 2005.

[49] M. J. H. Kraus, M. J. R. C. Pedersen, M. A. E. Sewell, . M. Douglas, L. Beach, C. Usa, and M. M. R. Smith, "ESDU 89014 ESDU DATA ITEMS ESDU 89014 NORMAL FORCE, PITCHING MOMENT AND SIDE FORCE OF FOREBODY-CYLINDER COMBINATIONS FOR ANGLES OF ATTACK UP TO 90 DEGREES AND MACH NUMBERS UP TO 5 CONTENTS," tech. rep.

[50] K. Burgin, D. Choo, J. Pedersen, A. Sewell, M. Douglas Corp, L. Beach, and U. M. Smith, "ESDU 90034 ESDU DATA ITEMS ESDU 90034 COMPUTER PROGRAM FOR THE CALCULATION OF NORMAL FORCE AND PITCHING MOMENT OF FOREBODY-CYLINDER COMBINATIONS AT ANGLES OF ATTACK UP TO 90 DEGREES AND MACH NUMBERS UP TO 5, INCLUDING EFFECTS OF CONICAL BOAT-TAILING CONTENTS," tech. rep.

[51] M. J. R. C. Pedersen Independent, M. N. Roberts Rolls, R. Plc, D. Mr, R. Sanderson, M. A. E. Sewell, . M. Douglas, L. Beach, C. Usa, and M. M. R. Smith, "ESDU 87033 NORMAL FORCE AND PITCHING MOMENT OF CONICAL BOAT-TAILS CONTENTS," tech. rep.

[52] P. Jones, M. Rolls-Royce, D. D. Puyplat Aérospatiale, F. J. Spillman, J. Thomas, H. Vogel, and P. Sheppard, "THE PREPARATION OF THIS DATA ITEM SUBSONIC BASE DRAG OF CYLINDRICAL BODIES WITH CONICAL BOAT-TAILS CONTENTS," tech. rep.

[53] A. Hipp, P. Jones, J. Kloos, C. Member Saab-Scania, S. G. Lilley, M. Pike Rolls-Royce Ltd, D. D. Puyplat Aérospatiale, F. I. Rettie, B. Aerospace Company, U. J. Spillman, J. Thomas, and H. Vogel, "THE PREPARATION OF THIS DATA ITEM SUBSONIC PRESSURE DRAG OF CONICAL BOAT-TAILS CONTENTS," tech. rep.

[54] "U.S. Standard Atmosphere 1976," tech. rep., National Oceanic & Atmospheric Administration, National Aeronautics & Space Administration, United States Air Force, Washington D.C., 1976.

[55] I. H. Abbott and A. E. Von Doenhoff, "THEORY OF WING SECTIONS Including a Summary of Airfoil Data," tech. rep.